THE EFFECT OF MAGNETIC PINCH PRESSURE ON

BORON NITRIDE, CADMIUM SULFIDE, GRAPHITE, SILICA GLASS,

AND SOME OTHER MATERIALS

by

STEPHAN JAY BLESS

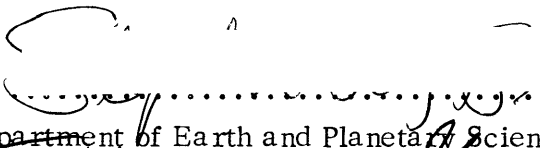S.B., Massachusetts Institute of Technology
(1965)

S.M., Massachusetts Institute of Technology
(1968)

SUBMITTED IN PARTIAL FULFILLMENT
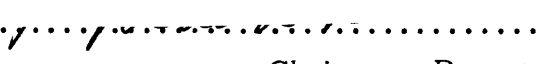OF THE REQUIREMENTS FOR THE
DEGREE OF DOCTOR OF
SCIENCE
at the
MASSACHUSETTS INSTITUTE OF
TECHNOLOGY
June, 1970

Signature of Author ....
Department of Earth and Planetary Sciences, May 21, 1970

Certified by .....
Thesis Supervisor

Accepted by ....
Chairman, Departmental Committee
on Graduate Students

ABSTRACT

We have developed a new method of high pressure production which uses a capacitor-discharge driven magnetic pinch. The pinch is capable of producing pressures greater than 500 kilobars, and is superior in several respects to other current high pressure techniques. Observed pinch effects include: production of the zincblende phase of boron nitride, production of hexagonal diamond from graphite, decomposition of mullite to alumina plus amorphous silica, and irreversible densification of powdered and solid silica glass. The resistance discontinuity sometimes seen in cadmium sulfide at 28 kilobars and the decomposition of albite to jadeite plus quartz did not occur. Some discrepancies between pinch results and those of conventional techniques can be explained by the heating which follows pinch pressure maximum. This latter condition can probably be eliminated by modification of the pinch apparatus.

TABLE OF CONTENTS

LIST OF SYMBOLS

A   Area, constant parameter

B   Magnetic flux density, constant parameter

C   Capacitance, heat capacity, constant parameter

C_o Capacitance of one capacitor = 15 μf

D   Constant parameter

d   diameter of spools, spacing of crystal planes in Angstroms

$\tilde{d}$ diameter of spools in mm

δ phase angle

E   voltage, Young's modulus

$\mathcal{E}$ emf

ϵ permittivity

I   current, X-ray intensity

K   bluk modulus, thermal conductivity

L   inductance

L_o inductance of one capacitor and spark gap

L_ℓ inductance of transmission line and sample

L_p inductance of aluminum plates

L_s inductance of sample

μ permeability

μ_o permeability of free space = $4\pi \times 10^{-7}$ h/m

N   number of capacitors

n   index of refraction

ν Poisson's ratio

ξ displacement

P	pressure, power
P_p	pinch pressure
Q	charge, thermal energy
R	resistance, gas constant
R_s	spool resistance
ρ	resistivity
ρ_m	mass density
r	radius
σ	stress, conductivity
Φ	magnetic flux
s	specific heat, skin depth
T	period, temperature
$\tilde{T}$	period in μsec
t	time
U	energy
V	voltage
$\tilde{V}$	voltage measured in kV
V_s	voltage across sample
V_L	voltage across series resistor
Z	impedance
ω	angluar frequency

Photo 1

Capacitor bank and transmission line.
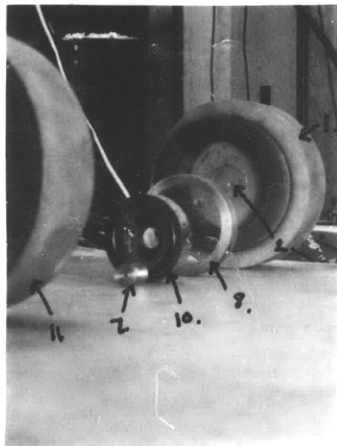
Photo 2

Sample assembly parts.

(Numbered items discussed in text.)
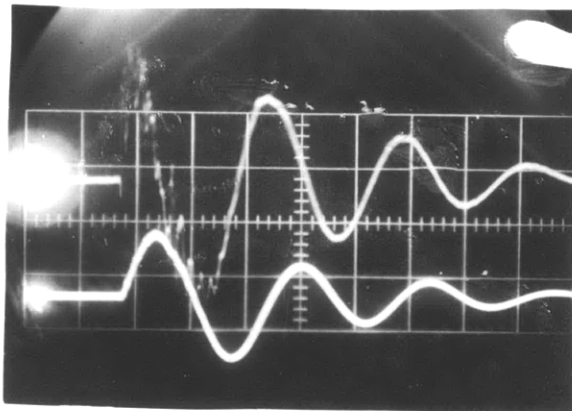
Photo 3

Typical oscillograph.

(For shot S6; N = 4, V = 14.5 kV)

Sweep is 2 usec/div.

Upper trace: Rogowski coil output, 200 V/div.

Lower trace: Integrator output, 40 V/div.
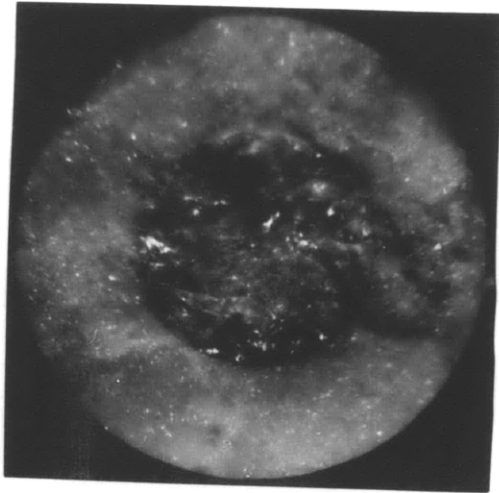
Photo 4 -

Cross section of fused
quartz rod, after pinch
and after copper spool
has been dissolved (shot T2)

Diameter of quartz rod is
.0303 inch. (Initial diameter
was .031 ± .0005 inch.)

Photo 5 -

Cross section of CdS sample after
pinch (shot E 24)
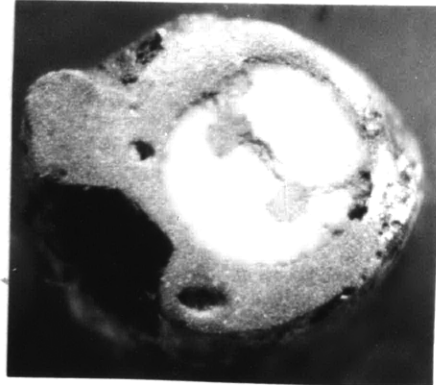
Photo 6 - Recovered fragments quenched from albite experiment A4
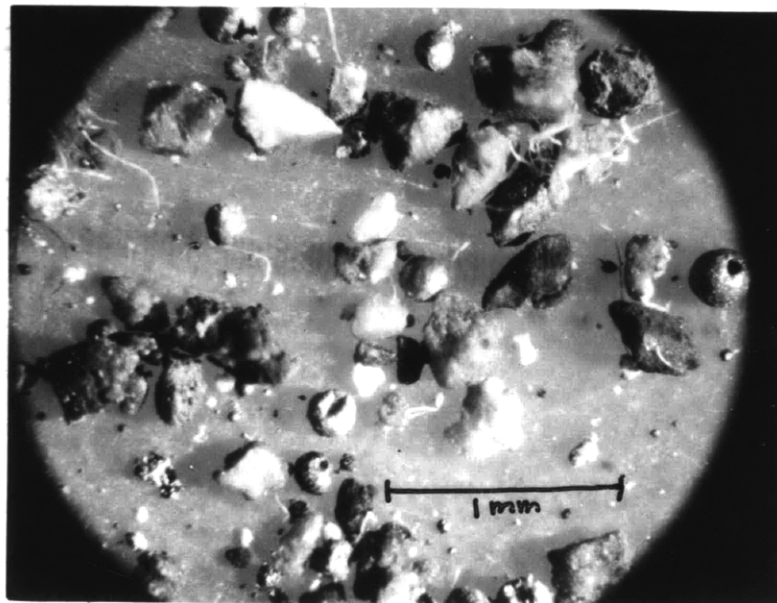
Photo 7 -

Comparison of new spool with
one of "little" damage (shot GQ2)
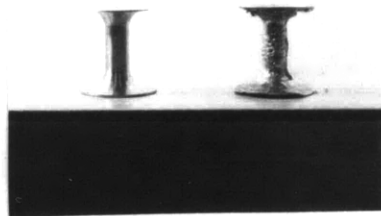
Photo 8 -

Comparison of new spool with
one of "great" damage (shot A2)
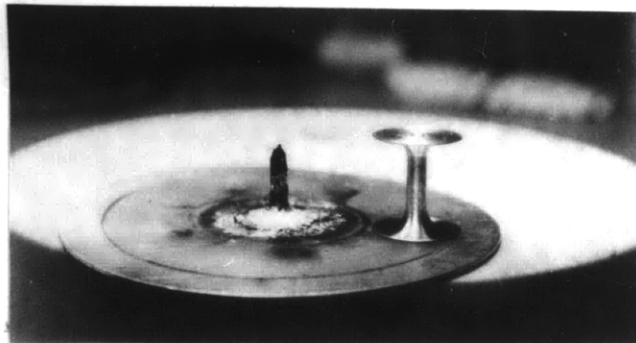
Photo 9-

Sample chamber after shot in
which spool was "destroyed"
(shot D2)
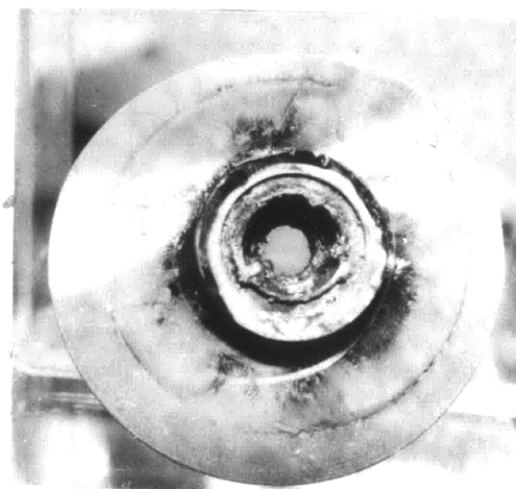
I. INTRODUCTION

1.1 Major Problems in High Pressure Geophysics

Much progress has been made in high pressure geophysics in the last decade. High pressure polymorphs of many minerals have been discovered, and the pressure dependence of elastic and thermodynamic parameters have been investigated. The purpose of this section is to point out several important questions which cannot be answered by current high pressure technology. These are problems concerning the structure and composition of the earth below about 500 kilometers. These are also the problems which we hope the development of magnetic pinch techniques will resolve.

1.11 Phase transitions in the mantle

Birch (1952) was the first to apply modern elastic theory and high

pressure experimental results to the study of the mantle. Using the appro-

priate seismic velocity-depth relationship available at that time, he deter-

mined that the velocity increase between 200 and 900 kilometers was not

consistent with a self-gravitating homogeneous medium; below that, to the

core, it was. He suggested that the velocity increase was due to the re-

duction of normal magnesium-silicates to denser oxide structures, a pre-

diction which has been verified by subsequent experimental results.
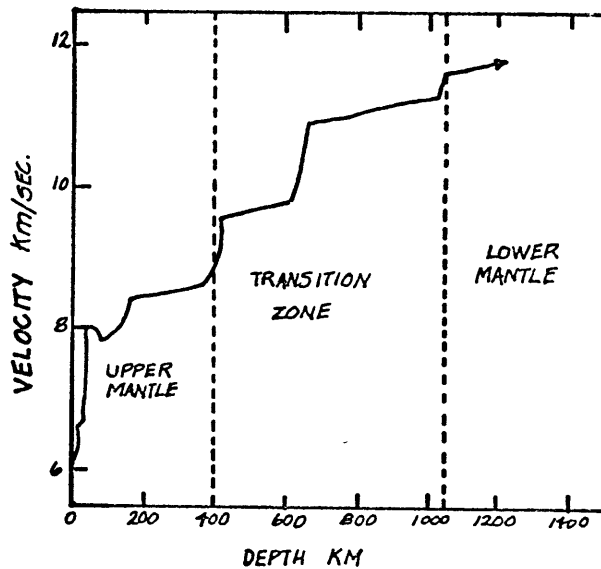
Fig. 1-1
Distribution of seismic
P wave velocities in
the outer 1200 kilo-
meters of the mantle.

(after Archambeau et.
al., 1969)

Figure 1-1 is an example of modern determinations of the seismic

velocity-depth function. It will be seen that in addition to the general

trends known to Birch, several clear discontinuities exist . At lower

depths, Toksoz et. al. (1967) have recently discovered additional sharp

increases at 700, 1200, and 1400 kilometers. McDonald's (1957)

derivation of the electrical conductivity of the mantle also implies a dis-continuity between 500 and 700 kilometers.

The lower mantle is believed to be largely composed of magnesium, silicon, and oxygen (see, for example, Ringwood, 1966). The common minerals composed of these elements are Mg_2SiO_4 (fosterite), $MgSiO_3$ (enstatite), MgO (periclase), and SiO_2 (quartz). It is very important to know how well the seismic and conductivity measurements can be explained by the high pressure properties of these minerals and their polymorphs.

The pressures occurring in the middle and lower mantle cannot be duplicated in present static apparatus, and shock wave techniques cannot be used because much overdriving is required to produce high pressure silicate polymorphs (see, for example, McQueen et. al., 1967). However, many high pressure properties of silicates can be inferred from study of germanate isomorphs (see, for example, Ringwood & Seabrook, 1962). Analogous high pressure phases form at power pressures in germanates because of the larger size of the germanium ion. Ringwood (1968) and others predict the following high pressure modifications of magnesium-silicates: Mg_2SiO_4 (spinel structure), $MgSiO_3$ (ilmenite structure), MgO (CsCl structure), $MgSiO_3$ (perovskite structure), Mg_2SiO_4 (Sr_2PbO_4 structure), and $Mg_3(MgSi)Si_3O_{12}$ (garnet structure). However, the P-T stability fields of these polymorphs have not been directly studied. Nor (except for shock wave analyses) have there been measurements of their elastic or electrical properties. Moreover, the entire concept of using germanate isomorphs to predict silicate phase transitions is made suspect by the recent discovery of a unique Mg_2SiO_4 structure which does not occur in Mg_2GeO_4 (Ringwood, 1970).

1.12 High pressure melting of geophysical materials

The study of melting phenomena is one of the few means available for estimating temperature in the interior of the earth. Let us designate T_o and T_i as the temperature at the upper and lower boundaries of the outer core (where the pressure is 1.4 and 3.2 megabars, respectively). Determination of the pressure dependence of melting for lower mantle consituents (such as MgO, SiO_2 or Al_2O_3) can place an upper limit on T_o. Determination of the fusion curves for probable core constituents (iron-silicon alloys) can place a lower limit on T_o and an upper limit on T_i. (If the fusion curve has a maximum, T_i may even be precisely determined.) The practical obstacles to this program are three-fold: (1) Fusion curves can only be empircally determined to a few hundred kilobars. (2) The methods used for extrapolation of fusion curves to higher pressures are of dubious validity. and (3) The actual composition of the earth is unkown.

Several studies of the melting of possible core materials have been carried out (for example, Sterrett et. al., 1965, Boyd & England, 1963, Strong, 1962), but no data has been taken above 200 kilobars. Ideally, melting could be studied at much higher pressures by using shock waves, but in practice, the onset of fusion is very difficult to detect because it has almost no effect on the PV hugoniot (see McQueen et. al., 1967, fig. 17a). Very seldom can the discontinuity in the u_s vrs. u_p hugoniot caused by fusion be resolved (see, for an example, Urlin, 1966).

There are several melting relations which may be used to extrapolate low pressure data to core conditions. Historically, the most important is the Simon equation, developed to describe the melting of helium (Simon, 1929):

$$\frac{P - P_o}{a} = \left(\frac{T}{T_o}\right)^c - 1 \qquad (1.1)$$

in which P_o and T_o are reference fusion curve coordinates, and a and c are adjustable constants. Kennedy (1970) has shown that this equation can only be expected to hold for solids which are bound by Van-der-Waals forces. For covalent solids (e.g. most minerals) , the Simon equation over estimates the melting temperature at high pressure.

The Lindemann melting law (see Roberts & Miller, 1951, for a simple derivation) is derived from the assumption that a solid melts when the amplitude of the thermal oscillations becomes a certain fraction of the interatomic spacing. Gilvarry (1955) has expressed the Lindemann law in the form

$$RT_m = \Omega K_m V_m \qquad (1.2)$$

where T_m, K_m, and V_m are evaluated at the melting point, R is the gas constant, and Ω is a constant which depends on Poisson's ratio and the nearest neighbor distance at melting. Gilvarry also showed that for γ_m (the Gruneisen contant of the solid at fusion) greater than 1/3 (which is always true at high temperature) T_m will be a monotonic-increasing function of pressure. Although the Gilvarry formulation of the Lindemann law works rather well for many metals (Knopoff, 1970), it can never predict the fusion curve maxima which have been discovered in several others (Newton, 1966, fig. 21).

Krout and Kennedy (1966) and Kennedy (1970) have observed that

$$T_m = T_o (1 + C \frac{\Delta V}{V})$$

for most metals and silicates. (Here $\Delta V/V$ is the relative compression

at fusion, and C is an adjustable constant.) Gilvarry (1966) has shown that this

relationship is an approximation to (1.2) which ignores terms of the order

$(V_o - V_m)^2$. Therefore, it should not be used for extensive extrapolations.

In summary, neither equation (1.1) nor equation (1.2) can be used

to predict melting deep within the earth without some input of data obtained

under extreme pressure. Nor can they describe melting of solid solutions,

in which eutectic effects can dramatically lower melting temperatures

(Newton, 1966).

1.13 Electrical properties of the core

Another area of importance is the study of the electrical properties

of materials likely to compose the earth's fluid core. The variables re-

quired for hydrodynamic analysis of motions in the core are density,

conductivity, permeability, and viscosity. The dynamic processes

possible in the core are largely determined by the value of the magnetic

Reynolds number

(thickness) x $\sigma \mu$

and certain dimensionless scaling parameters (see, for example, Hide,

1966). Yet, at the present time, no relevant experimental data for these

parameters has been obtained.

1.2 Role of the Magnetic Pinch

1.21 Limitations of static pressure devices

Truly hydrostatic pressures (in which the pressure transmitting medium is a fluid) are only possible well below 50 kilobars. All solid media devices suffer from stress anisotropy, which can be very large. Pressure can be calibrated by means of known phase transitions or compressibilities to an accuracy of a few percent; temperature under pressure can be measured with thermocouples, but the errors are not known (see, for example, Strong, 1962). Most existing equipment is designed to operate below 100 kilobars. There are a few laboratories where uniaxial pressures to 200 kilobars and temperatures to 1000 °C can be produced (Ringwood & Major, 1966, Akimoto & Ida, 1966 , Bundy, 1965), but volume cannot be measured as a function of pressure, and structure determinations must be done with quenched materials. Those laboratories which can produce pressures of 200 kilobars and obtain X-ray patterns under pressure must operate near room temperature. (Bassett, 1967, Drickamer, 1966).

1.22 Limitations of shock wave techniques

Production of intense shock waves in solids can result in transient pressures as high as five megabars (Doran & Linde, 1966). However, the duration of the pressure pulse is a small fraction of a microsecond, and the strain is one-dimensional. (See Rice et. al., 1958, for an introductory discussion of shock wave production and analysis.) Shock wave experiments require rather expensive facilities, so only a few authors have been active

in this field. Analyses of shock data have yielded high pressure equation of state, electrical, and optical parameters; most of the geophysical results are discussed by Ahrens et. al.(1969). However, there are serious ambiguities concerning the application of shock wave data to the study of the earth. The difficulties in interpretation fall into three catagories:

(1) The elementary fluid theory and jump conditions used to derive hugoniots may be wrong (Fowles et. al., 1970). (2) All of the various algorithms for reducing shock hugoniots to isothermal or adiabatic data (for example, Ahrens et. al., 1970, Munson & Barker, 1966, McQueen & Marsh, 1967, Duvall & Fowles, 1963) require assumptions about the pressure dependence of the Gruneisen constant, hydrostatic stress, and constitutive relations which are not well substantiated. (3) Phase changes which require more than simple displacement of atoms may not have time to occur (such as olivine to spinel), or may not occur at the equilibrium pressure (such as graphite to diamond).

Fig. 1-2

Magnetic Pinch geometry
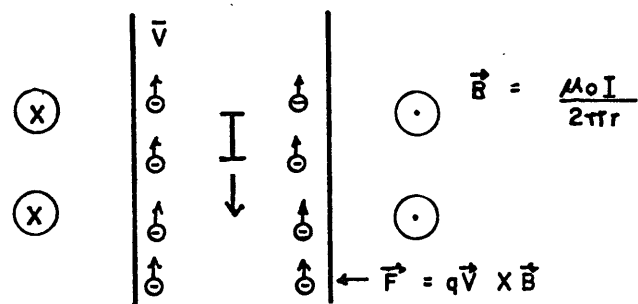
$$\vec{B} = \frac{\mu_0 I}{2\pi r}$$

$$\vec{F} = q\vec{V} \times \vec{B}$$

1.23 The magnetic pinch device

The geometry of the magnetic pinch effect is illustrated in figure 1-2. A large current is established in a straight conductor. A magnetic field

$$B = \frac{\mu_o I}{2\pi r}$$

is set up around the conductor. The field exerts a force

$$\vec{F} = q\, \vec{v} \times \vec{B}$$

on the current carrying electrons. Thus the electrons experience a pressure equal to the magnetic pressure

$$P = \frac{B^2}{2\mu_o} \ .$$

Since the electrons are bound to the atoms, the pressure is felt by the solid material. In practice, the current is supplied by discharge of a high energy low inductance capacitor bank. The linear conductor is a hollow cylinder, and the material to be studied is placed inside.

1.24 Previous pinch research

Only Bitter et. al. (1967) and Bless (1968, 1969) have reported application of a magnetic pinch to high pressure research. They found that:

a) Magnetic pinch pressure could produce the ,,\` = phase transition in iron, which at room temperature occurs at 130 kilobars.

b) The ability of solid rods to survive destruction by the pinch current was enhanced by radial reinforcement. This suggested that the principle mechanism of failure (aside from simple melting) was development of instabilities which mechanically broke the conductor.

c) The energy which is deposited in the sample being pinched was always much less than the energy stored in the capacitor bank.

d) High pressure polymorphs of quartz could not be recovered from pinch experiments on fused quartz.

1.25 Advantages of the magnetic pinch

At its present stage of development, the pinch offers little advantage over conventional high pressure techniques. However, looking foward to the solution of what appear to be straightfoward technical problems, we can forcast that the pinch will:

a) Allow measurements of elastic and electrical properties at pressures of one megabar.

b) Compress materials adiabatically, with well defined P-T conditions.

c) Allow more accurate pressure determination than shock waves, since the pressure is a simple function of the current.

d) Greatly reduce the cost of high pressure experiments.

1.3 Production of Megagauss Magnetic Fields

1.31 Exploding wires and plasma confinement

The technology which permits construction of ultra-low inductance high energy capacitors has only been in existence for about ten years (see, for example, Frungel, 1965). Two traditional research areas where capacitor discharge techniques have found application are plasma pinch effects and electrically exploded wires. Neither of these efforts are directed toward producing kilobar pressures in solids. Rather, plasma confinement requires pressures of a few hundred bars containling volumes of many cubic centimeters. Exploding wire studies emphasize maximum energy input (primarily for explosive detonation). Bless (1968) reviews the research results in these two fields and lists an extensive bibliography.

1.32 Production of megagauss magnetic fields by chemical explosives

Fig. 1-3

The relation between magnetic field and pressure.

(After Bitter, 1965)
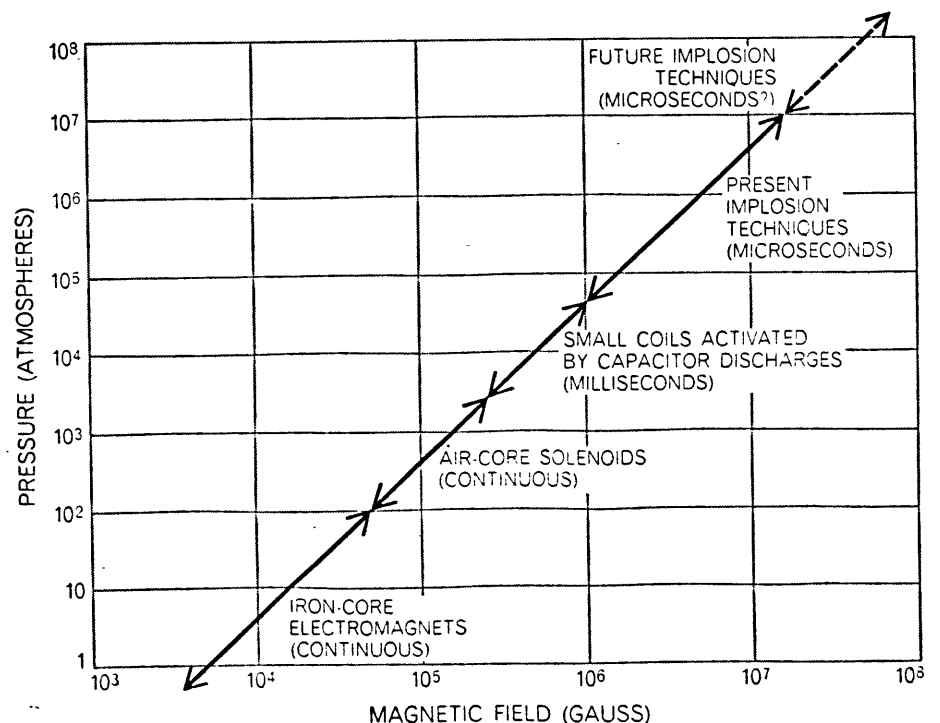
Francis Bitter (1965, 1967) was the first to point out the possible

application of ultra-high magnetic fields to high pressure research.

Figure 1-3 illustrates the relationship between magnetic flux density

and pressure. Although considerable progress has been made in the

laboratory production of megagauss magnetic fields, with the exception

of the author's work, no practical application has been attempted. How-

ever, many of the technical problems encountered in high magnetic field

production carry over to the pinch work discussed in this paper.

METAL CYLINDER
TO CONTAIN FLUX

RING OF EXPLOSIVE

COIL TO PRODUCE
INITIAL MAGNETIC FIELD

Figure 1-4 Typical geometry for flux compression by explosives.
(After Bitter, 1965)

Figure 1-4 shows the geometry for explosive flux compression. A

magnetic field of typically 100 KG is established inside a seamless cylinder

(called a liner) with a typical radius of 5 cm. This is accomplished by

capacitor discharge, typically about 100 kilojoules with a time constant of 10^{-3} seconds. The field diffuses into the liner in the characteristic time

$$T = \mu_o rd/2\rho \quad \text{(Latal, 1966)}$$
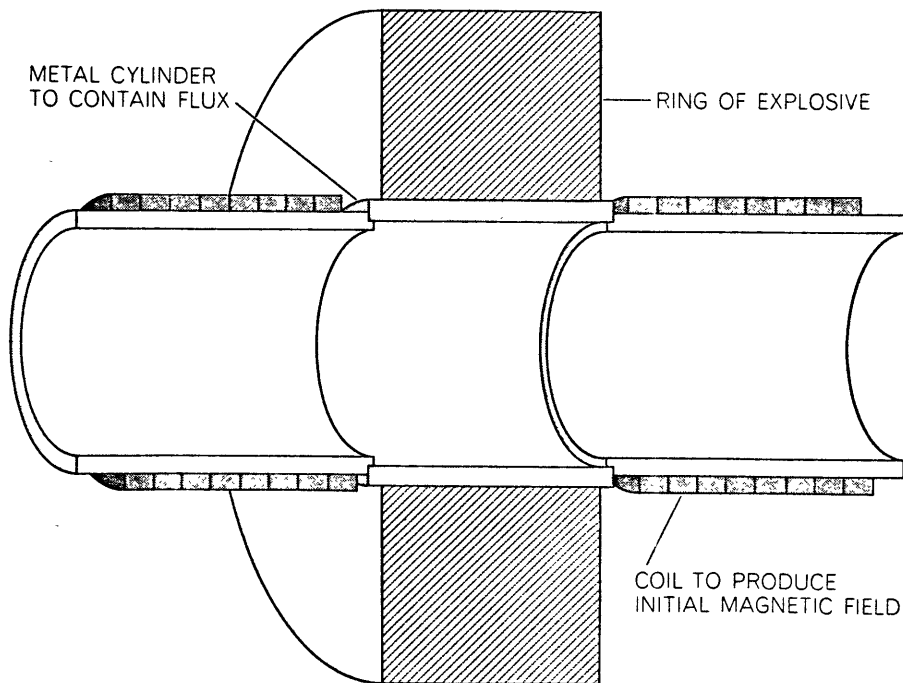
where r = liner radius, d = liner thickness, ρ = liner resistivity, and $\mu_o = 4 \pi \times 10^{-7}$ h/m. The liner is compressed by explosives, trapping the "seed" field inside. The maximum field reported by this technique is 10 MG (Besançon, 1967). Keeler (1970) is presently adapting this type of apparatus to high pressure research.

The maximum compression occurs when the magnetic pressure in the liner equals the pressure of the chemical explosive. The maximum attainable field will depend on the properties of the liner material, viz. the increase in liner resistivity and its equation of state. Eventually, joule heating of the liner will convert it to a plasma; then the resistivity decreases as the 2/3 power of temperature. Unfortunately, the differential equations linking these phenemena have not been solved for the general case (see, for example, Herlach, 1968). Lewin and Smith (1964) obtained an approximate solution, which applied to Fowler's (1960) experiment predicts that the final pressure coefficient of resistivity of the liner (copper) was not greater than 1/200th its usual value. The final P-T conditions were approximately 2×10^5 °K and 8 megabars.

1.33 Production of megagauss magnetic fields by capacitor discharge

Two methods of producing megagauss magnetic fields by capacitor discharge have been tried. The first, developed by Cnare (1966), utilized electromagnetic compression of a cylindrical aluminum foil. The foil was placed inside a single turn coil connected to a 130 kilojoule capacitor bank.

Sufficient flux leaked through the aluminum foil before implosion that a peak field of over 2 MG was produced within it. The theory of the "Cnare Effect" has been developed by Latal (1967). Further experimental work has been done by Guillot (1968).

The other means of producing high magnetic fields by capacitor discharge is to use a single turn coil. Shearer (1969) has been the principle investigator of this method. The maximum field he has obtained is about 3 MG. X-ray photographs of the massive copper coil during the discharge showed a compression of about 10% (in linear dimension), suggesting a shock pressure of about 200 kilobars. He calculated the interaction of the field with the metal wall and predicted that a shock type discontinuity would appear after the pressure wave had travelled about 4mm into the copper. Shearer also observed that under some conditions the surface of the wall moved into the high field region because of the rapid heating due to skin effect.

II. APPARATUS

2.1 Discharge Circuit

2.11 The capacitor bank

The large currents required to produce high pinch pressure were obtained by discharging a high energy low-inductance capacitor bank. The basic arrangement of the capacitors was similar to that described by Bless (1968). There were eight Tobe Deutschmann model ESC-248A capacitors. Each was 15 μf, 20 kV, 3000 joules, making a total of 120 μf and 24 kilojoules. They were arranged around an octagonal transmission line, designed for low inductance. Photo 1 shows this equipment. Any combination of the capacitors could be fired at one time; however, the lowest voltage at which simultaneity was obtained was 14 kV.

Figure 2-1 is a sketch of the capacitor and trigger circuits. The capacitor power supply was located outside of the instrument cage, in order to avoid ground loops. The charging voltage was pre-set, and the operator enclosed himself in the shielded instrument cage (which was also armoured with plywood). The highest charging voltage that could be used was 40 kV, otherwise there was danger of arcing across switch A. The "outside meter" could be read from inside the cage. When the bank voltage reached the desired value, the oscilloscopes were triggered. A gate pulse from one of the scopes was used to initiate the pulse sequence that resulted in firing of the spark gaps. Residual charge on the capacitors could be drained by activating a 10 megaohm dump relay in the power supply. If the sample was destroyed, it was necessary to close switch B for this operation. When not

DOUBLE SCREEN INSTRUMENT ROOM
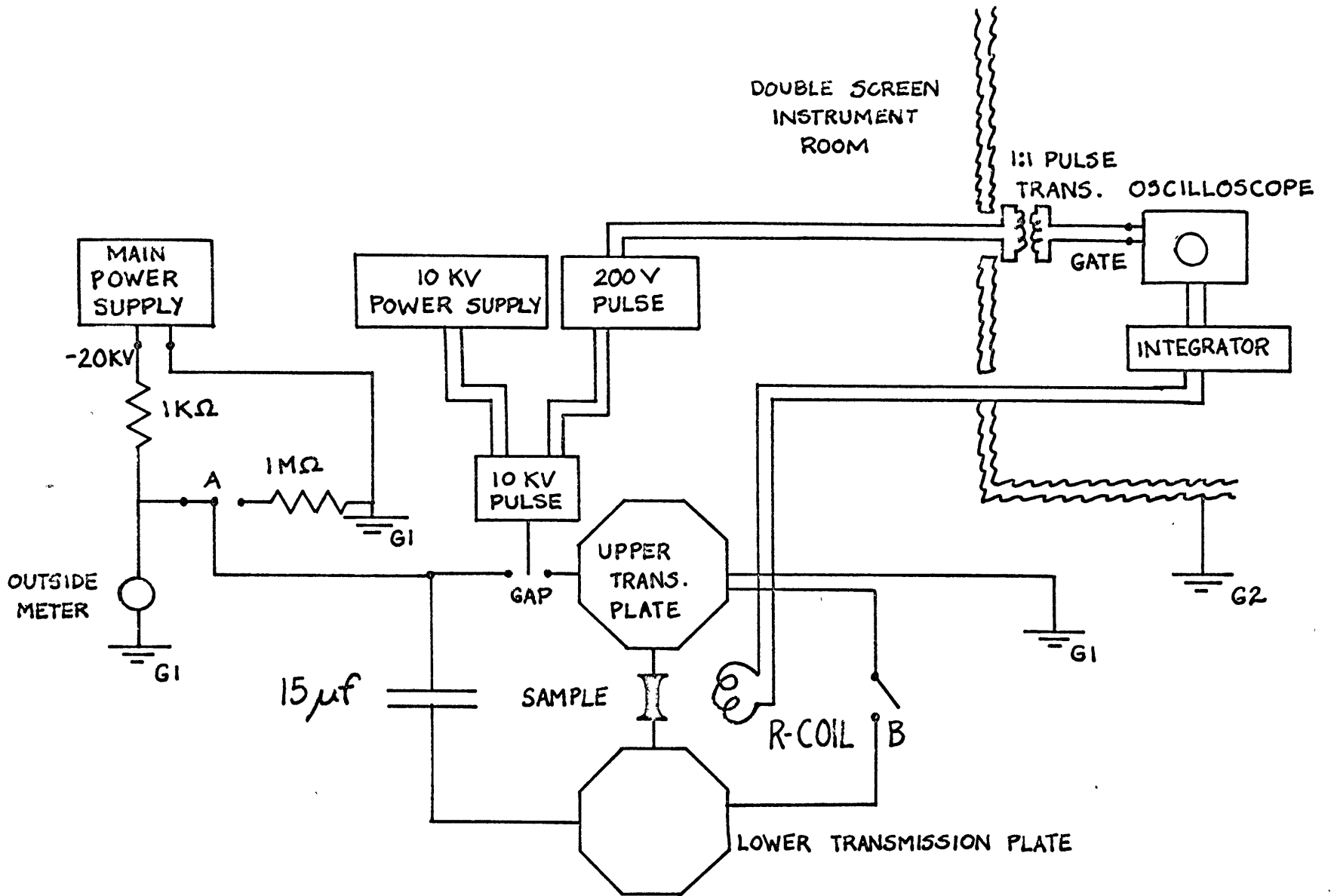
FIG. 2-1 CIRCUIT DIAGRAM, SHOWING ONE OF EIGHT CAPACITORS. SWITCHES ARE IN CHARGING POSITIONS. G1 IS APPARATUS GROUND. G2 IS INSTRUMENT GROUND

FIG. 2-2

SAMPLE   ASSEMBLY
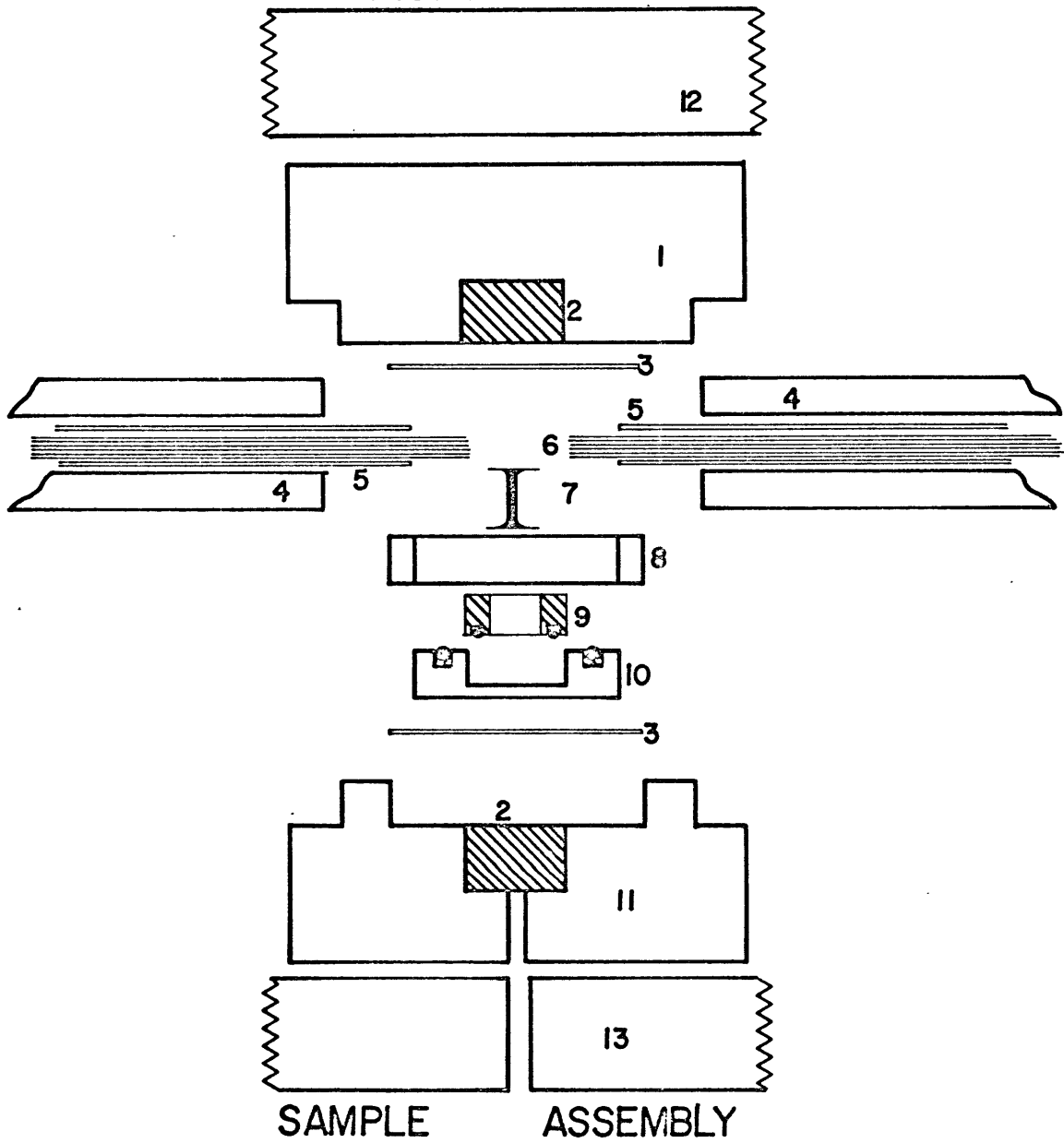
in use, switch A was connected to a 1 megaohm bleed resistor. As an extra precaution, each capacitor was checked for zero charge with a grounding pole after every shot. Power supply ground (G1 in figure 2-1) was a cold water pipe, while instrument ground (G2 in figure 2-1) was an electrical conduit. There was never a direct connection between the two.

2.12 Sample design

The current which produced the magnetic pinch was carried by copper spools, like the one shown in photo 2. The shaft diameter was almost always .115 inches (2.92 mm); the length was .545 inches. The spools had a .065 inch (1.65 mm) diameter hole along their axes. Usually, the centers of the spools were fitted with insulating tubes which contained the materials to be studied. In this paper, the word "sample" refers to the contents of the copper spools.

The spools were connected across the two octagonal transmission plates by the sample assembly, shown in photo 2 and figure 2-2. The important parts are numbered:

1) Upper phenolic clamp block.

2) Steel impact block to absorb recoil of spools.

3) .020 inch thick copper discs, which made connection to the spool.

4) 3/8 inch thick center of aluminum transmission plates.

5) .010 inch copper connecting sheets.

6) Six .010 inch mylar insulating sheets.

7) Copper spool which contains sample. The spool was often encased in epoxy.

8) Copper conducting ring (inner diameter = 2 inches).

9) Steel <u>guard ring</u>, to contain material thrown off spool; O-ring seal-spring on bottom. The guard ring was often shimmed on the bottom to insure a good blast seal on top.

10) Phenolic <u>insulating ring</u>, with O-ring seal on top.

11) <u>Lower clamp block</u>, with 1/8 inch hole which could be used to hook up experiments inside the spool (for which purpose a hole was drilled in the lower impact block).

12) <u>upper anvil</u>, which threaded into top of aluminum plate structure (see photo 1).

13) <u>lower anvil</u>.

A relatively large amount of time was required to keep the sample assembly in good condition. Generally, shots producing less than about 50 kilobars caused little damage. During shots of 50 to 200 kilobars, much of the copper spool melted, the epoxy coating on the spool was partially pulverized, and the blast and soot degraded the mylar insulating sheets. After approximately every other such shot, the lower-most mylar sheet had to be replaced, in order to be certain that the insulating ring O-ring made a good seal. After about five shots, all the mylar sheets and copper connecting sheets had to be replaced. Shots producing over 200 kilobars often did great damage, for unless the tolerances were extremely tight, hot gases and ejected material tore the top copper sheet and cracked the mylar. Pressure waves from these shots often expanded the guard ring by more than .010 inch, and excavated holes up to 1/4 inch deep in the impact blocks. Sometimes, the clamp blocks even cracked.

At the present time, one person can replace the insulating sheets in about 90 minutes. This is an improvement over the time required at our last report (Bless, 1968), when half a day was required by two people. The reduction resulted from several modifications in the plate design which simplified parting the center sections of the aluminum plates.

The average time required to set up, perform, and repair after a 100 kilobar shot was about four hours. Including manufacturing charges for samples and spare parts (and excluding the value of the experimenter's time), the cost per 100 kilobar shot was about $10. The initial cost of the capacitor bank and power supply was about $6000.

2.13 Computation of maximum current

The charge stored in the capacitors is

$$Q = N C_o V. \tag{2.1}$$

N can be varied from 1 to 8, $C_o = 15 \mu f$, and V can be varied from 14 to 20 kV. (N, V, C_o, and Q are defined in the list of symbols.) The maximum value of Q is 2.4 coulombs. The maximum energy, given by

$$U = \frac{1}{2} N C_o V^2 \tag{2.2}$$

is 24 kilojoules, or 5760 calories (gram).

The current which flows through the copper spools is

$$I(t) = dQ/dt.$$

For a decaying oscillatory discharge (see, for example, Harnwell, 1949, p. 458)

$$Q = \frac{Q_o}{\sqrt{\frac{R^2 C}{4L} - 1}} \; e^{-Rt/2L} \; \sinh \sqrt{R^2/4L^2 - 1/LC} \; t \; . \tag{2.4}$$

For the limit $R \to 0$, equation (2.4) becomes

$$Q = Q_o \cos \omega_o t \qquad (2.5)$$

where

$$\omega_o = 1/\sqrt{LC}, \quad \text{and} \quad Q_o = N C_o V \qquad (2.6)$$

In our experiment, R is a function of time and is not zero. For the less stringent condition $R^2 < 4L/C$, equation (2.4) becomes

$$Q = \frac{Q_o}{\sqrt{1 - \frac{R^2 C}{4L}}} \, e^{-Rt/2L} \, \sin\left(\sqrt{\frac{1}{LC} - \frac{R^2}{4L^2}} \; t + \delta\right) \qquad (2.7)$$

$$\delta = \arctan\sqrt{\frac{4L}{R^2 C} - 1} \qquad (2.8)$$

It is difficult to evaluate the term $(4L/R^2 C)$ because the resistance of the copper spool and spark gaps changes as the current flows. A rough estimate can be made by examining a typical current record. For example, in figure 2-7b, with $N = 2$ and $V = 17$ kV, the amplitude decay gives

$$\frac{2L}{R} \cong 16 \; \mu sec. \qquad (2.9)$$

From the period:

$$T \cong 2\pi \sqrt{LC} \cong 4.5 \times 10^{-6} \; sec \qquad (2.10)$$

or

$$\sqrt{LC} \cong .717 \times 10^{-6} \; sec . \qquad (2.11)$$

Putting equations (2.9) and (2.11) together gives

$$4L/R^2 C = (2L/R)^2 (1/\sqrt{LC})^2 \cong 500.$$

Therefore, for purposes of calculating discharge current we may use the approximation

$$I = -\omega_0 Q_0 \sin \omega t . \qquad (2.12)$$

The maximum of I occurs at $t = \dfrac{\pi}{2} \sqrt{LC}$, and is

$$I^{(max)} = Q_0/\sqrt{LC} . \qquad (2.13)$$

Writing $T = \dfrac{2\pi}{\sqrt{LC}} = \tilde{T}$ μsec, $V = \tilde{V}$ kV, and combining 2.1 with 2.13 gives

$$I^{(max)} = \frac{2\pi N C_0 V}{T} = 94.2 \times 10^3 \frac{N \tilde{V}}{\tilde{T}} . \qquad (2.14)$$

2.14 Calculation of circuit inductance

N units
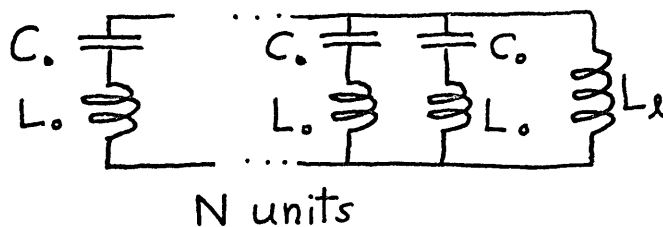
Fig. 2-3

Circuit for computation of effective inductance

Figure 2-3 represents the circuit which must be analysed to compute the effective inductance. If Q is the charge on a capacitor C_0, Kirchoff's rule for this circuit is:

$$\frac{Q}{C_o} - L_o \frac{d^2Q}{dt^2} - N \frac{d^2Q}{dt^2} L_{\ell} = 0$$

$$Q - C_o(L_o + NL_{\ell}) \frac{d^2Q}{dt^2} = 0$$

$$Q = Q_o \cos \omega t$$

$$\omega = 1/\sqrt{C_o(L_o + NL_{\ell})} = 1/\sqrt{C_o L} \qquad (2.15)$$

where

$$L = L_o + NL_{\ell} \qquad (2.16)$$

L_o = the inductance of a capacitor and spark gap

L_{ℓ} = the inductance of the transmission lines and sample

In Bless (1968) it is calculated that

$$L_o = 11.7 \text{ nanohenries}. \qquad (2.17)$$

Since

$$L = \Phi/I, \quad B = \mu_o I/2\pi r, \text{ and } \Phi = \iint \vec{B} \cdot \vec{dS},$$

we can write L_{ℓ} as the sum of two terms,

$$L_{\ell} = L_p + L_s,$$

where L_p is the contribution to L_{ℓ} from the flux contained between the transmission lines, and L_s the the inductance from the flux contained in the sample assembly. In Bless (1968) it is also calculated that

$$L_p = .747 \text{ nanohenries} \qquad (2.18)$$

Fig. 2-4

Geometry for calculation

of contribution to the inductance

of the copper spools.
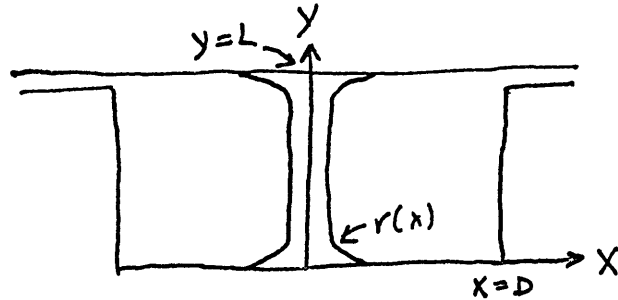
Figure 2-4 is a simplified drawing of the interior of the sample

assembly. Using the coordinates defined there, we write the enclosed flux as

$$\Phi = \int_0^L \int_{r(x)}^D \frac{\mu_0 I}{2\pi x} \, dy \, dx \qquad (2.19)$$

This integral was evaluated by dividing the curved portions of r(x) into three

steps; its value was 6.54 I. Therefore,

$$L_s = 6.54 \text{ nanohenries}, \qquad (2.20)$$

for a 2.92mm diameter spool.

From equations 2.6, 2.16, 2.17, 2.18, and 2.20, the total inductance

for a discharge of N capacitors is

$$L = 11.7 + N(7.29) \text{ nanohenries}. \qquad (2.21)$$

For example,

L = 67 nanohenries when N = 8.

The theoretical disc harge periods, calculated from

$$T = 2\pi\sqrt{C_0(L_0 + NL_s)} \qquad (2.22)$$

are listed below:

N = 1   T = 3.4 μsec

N = 2   T = 3.94 μsec

N = 4   T = 4.92 μsec

N = 6   T = 5.72 μsec

N = 8   T = 5.85 μsec.

Appendix A1 gives all the observed values of T. The agreement is fair at low voltages and good at high voltages. The dependence of T on voltage arises because the spark gaps have less resistance and inductance at high voltages.

According to this analysis, the maximum current which can be produced in a 2.92 mm diameter spool is given by equation (2.14) with $\tilde{T}$ = 5.85, N = 8, and $\tilde{V}$ = 20; e.g.

$$I^{(max)} = 8.44 \times 10^6 \text{ amperes.} \tag{2.23}$$

2.15 Measurement of the current

In order to measure the pinch current, a Rogowski coil was made by lacing flat copper ribbon through one of the mylar insulating sheets. Figure 2-5 shows the coil geometry. The ribbon was .005 inch by 1/16 inch. The cross section of the coil was 1 1/2 inch by .010 inch, or $9.67 \times 10^{-6} m^2$. There were 60 turns, and the mean distance from the center of the copper spools was 14 1/2 inches (.362 m). It was wound back through itself to reduce sensitivity to azimuthal current inhomogeneities.

Fig. 2-5

Rogowski coil geometry
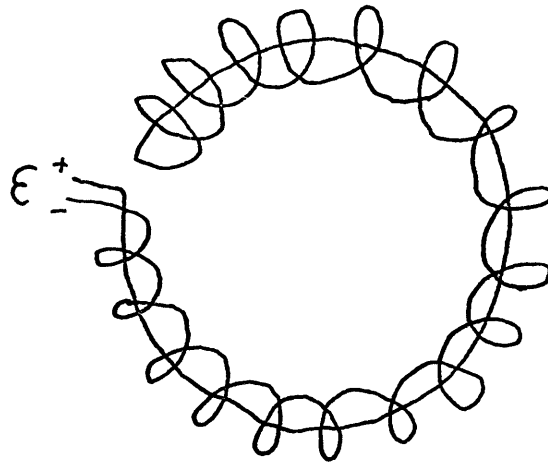
The voltage induced in the Rogowski coil is readily calculated

from Maxwell's relation:

$$\oint \vec{\mathcal{E}} \cdot \vec{dr} = \iint \frac{\partial \vec{B}}{\partial t} \cdot \vec{dS} .$$

Here,

$$\mathcal{E} = nA \frac{dB}{dt}$$

where $\mathcal{E}$ is the total emf induced in the coil, n is the number of turns, and

A is the toroidal cross sectional area. Since

$$B = \frac{\mu_o I}{2\pi r} = \frac{\mu_o \, \omega \, N C_o \, V \sin \omega t}{2\pi r} ,$$

$$\mathcal{E} = \frac{\mu_o \, A n N \omega^2 \, C_o \, V \sin \omega t}{2\pi r} . \tag{2.24}$$

Equation (2.24) is evalued for $V = \tilde{V}\,kV$, $2\pi/\omega = \tilde{T}\,\mu sec$:

$$\mathcal{E}^{(max)} = 190 \, \frac{N \tilde{V}}{\tilde{T}^2} . \tag{2.25}$$

The Rogowski coil was connected to an RC integrator, for which

$R_i = 330 \; \Omega$, and $C_i = .01 \, \mu f$. In this circuit, the self inductance of the

Rogowski coil can be ignored, for it is only (approximately)

$$L_R \cong \mu_o \frac{N^2 A^2}{(\text{length})} \approx 19 \text{ nanohenries,}$$

and

$$4L_R/R_i^2 C_i \simeq 7 \times 10^{-13}.$$
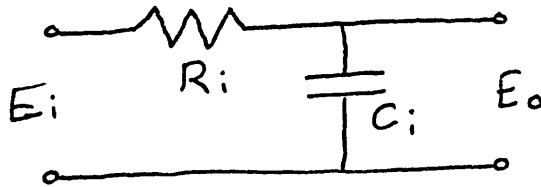
Fig. 2-6

RC integrator

For $R_i >> 1/\omega C_i$, the output of an RC integrator (using complex notation) is

$$E_o = 1/ j\omega C_i$$

$$I = E_i/R_i$$

$$E_o = E_i/ j\omega C_i R_i = \int E_i \, dt ,$$

if E_i can be written as a Fourrier sum. The critical period of the integrator was

$$T_c = 2\pi C_i R_i = 20.8 \ \mu sec.$$

Notice that the integrator also discriminates against high frequencies, thus filtering out much of the noise. An oscillator was used to test the high frequency response of the integrator; it failed above 7 MHz.

Let Y be the attenuation of the integrator,

$$Y = E_o/E_i = T/2\pi C_i R_i = \tilde{T}/ 20.8 . \qquad (2.26)$$

Combining equations (2.26) and (2.25) gives

$$E_o = 9.13 \ N\tilde{V}/\tilde{T} . \qquad (2.27)$$

The current (equation 2.14) is

$$I = 94.2 \times 10^3 \frac{N \tilde{V}}{\tilde{T}} \quad . \tag{2.14}$$

Thus,

$$I \text{ (amperes)} = 1.03 \times 10^4 \, E_o \text{ (volts)} . \tag{2.28}$$

This equation relates the current in the copper spools to the voltage output of the Rogowski coil/integrator circuit.

Typical records of Rogowski coil voltages are shown in figure 2-7 and photo 3. Unfortunately, the magnitude of the first integrated voltage peak is anomalous, for it fails the test

$$\int_0^{T/2} I \, dt = Q_o' = N C_o V .$$

Reference to the unintegrated voltages reveals there is a great deal of noise in the first half cycle. The low integrated first maximum must result from failure of the integrator to properly integrate through that noise.

Since good data for the first current maximum cannot be obtained directly from the recorded Rogowski coil output, we calculated $I^{(max)}$ from the recorded periods. We took T to be twice the interval between the first (positive) and second (negative) current maxima. (Sometimes, the first maximum was very poorly defined; in those cases, the period was taken as twice the interval between the second and third current maxima.) $I^{(max)}$ is calculated from equation 2.14, using the measured values of $\tilde{T}$.

Figure 2-7   Some examples of Rogowski coil and integrator signals (traced from oscillographs).

a) 1 Capacitor, 15 kV.   Upper trace: Rogowski coil output, 200 V/cm.   Lower trace: Integrator output, 20 V/cm.

b) 2 Capacitors, 17 kV.   Upper trace: Rogowski coil output, 200 V/cm.   Lower trace: Integrator output, 50 V/cm.

a)

b)
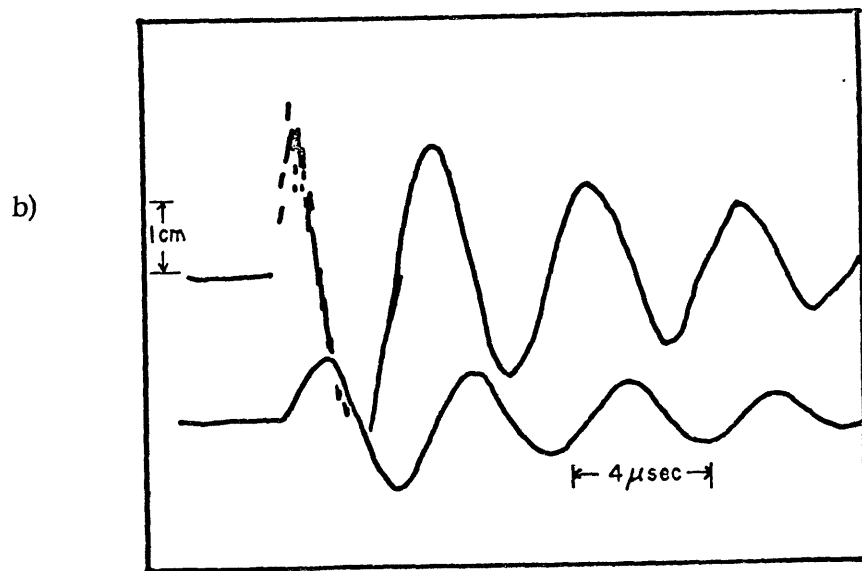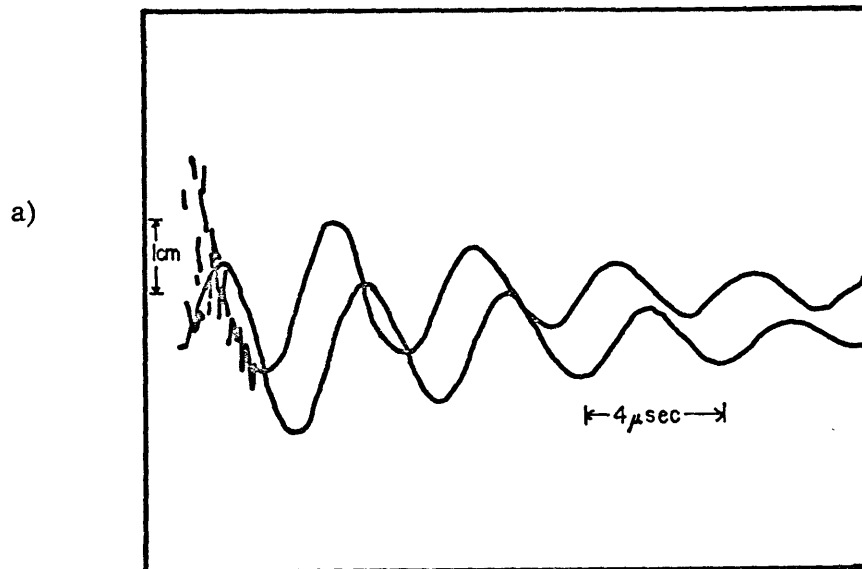
2.2 Effects of the Pinch

2.21 Production of high pressures

The magnetic pressure is

$$P = \frac{B^2}{2\mu_o} .$$

The field produced by the current, I, in the copper spool is

$$B = \frac{\mu_o I}{2\pi r} .$$

Thus,

$$P = \frac{\mu_o I^2}{8\pi^2 r^2} . \tag{2.29}$$

Substituting d = 2r and the value for $I^{(max)}$ in equation (2.14),

$$P^{(max)} = \frac{2\mu_o N^2 C_o^2 V^2}{\pi^2 T^2 d^2} \tag{2.30}$$

or

$$P^{(max)} = 5.66 \frac{N^2 \tilde{V}^2}{\tilde{d}^2 \tilde{T}^2} \equiv P_p . \tag{2.31}$$

Throughout this paper, the term "pinch pressure" refers to P_p in equation (2.31). P_p is a convenient quantity because it is easily evaluated from measured parameters, and it comes from equation (2.29), which is an exact expression for the magnetic pressure at the surface of the spool. However, except for the case of zero current penetration, equation (2.29) is not a rigorous expression for the pressure inside the spool. An exact calculation of the pressure inside the spool is impossible because the radial variation of resistivity is not known. It is shown in appendix A4 that due to current penetration, the sample pressure will be between 10 to 100 percent greater than P_p.

FIG. 2-8 PINCH PRESSURE WHICH CAN BE PRODUCED IN
STANDARD SPOOL OF DIAMETER 2.92mm., CALCULATED FROM

$$P_p = \frac{2\mu_o N^2 C_o^2 V^2}{\pi^2 T^2 d^2} \quad \text{AND} \quad T = \sqrt{C_o(L_o + NL_\ell)}$$

WITH V VARIED FROM 14 → 20 KV

N
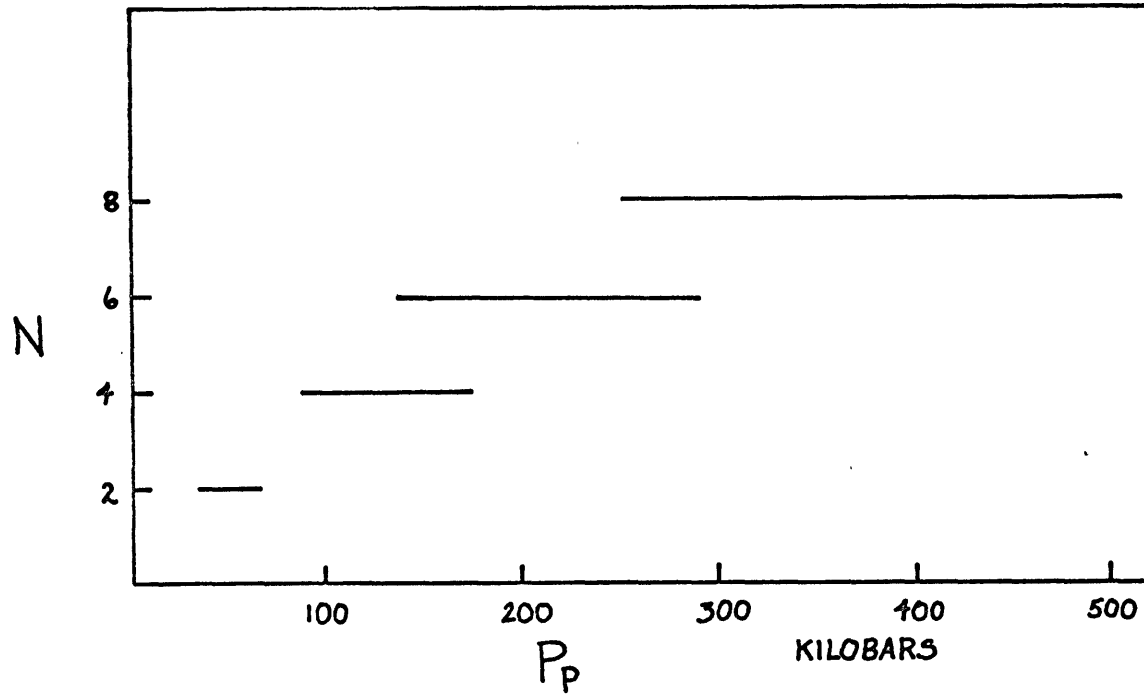
P_p KILOBARS

The greatest value of P_p produced in a 2.92 mm diameter spool was in shot D1. There $N = 8$, and $\tilde{V} = 16$. The measured period was 6 μsec, thus P_p (from equation 2.31) was 300 kilobars. Figure 3-8 shows the maximum pressures obtainable in 2.92 mm diameter spools for various values of N.

It is interesting to note the behavior of P_p as the radius of the spool becomes very small:

$$P_p \propto I^2 \propto \frac{1}{T^2 r^2}$$

but

$$T^2 \propto L \propto \ln\left(\frac{1}{r}\right)$$

Thus

$$P_p \propto \frac{1}{r^2 \ln\frac{1}{r}} \to \infty \quad \text{as} \quad r \to 0.$$

This argument will fail, of course, because T will start to depend strongly on the spool resistance when r gets very small. Specifically, Pp will increase as shown above until

$$R^2 \approx \frac{4L}{C},$$

or

$$\frac{\rho \ell^2}{\pi^2 r^4} \approx \frac{2\mu_o}{\pi C} \ln \frac{D}{r} \tag{2.32}$$

where ρ and ℓ are the resistivity and length of the sample, $C = NC_o$, and D is as defined in figure 2-4. Equation (2.32) is solved graphically on the next page.
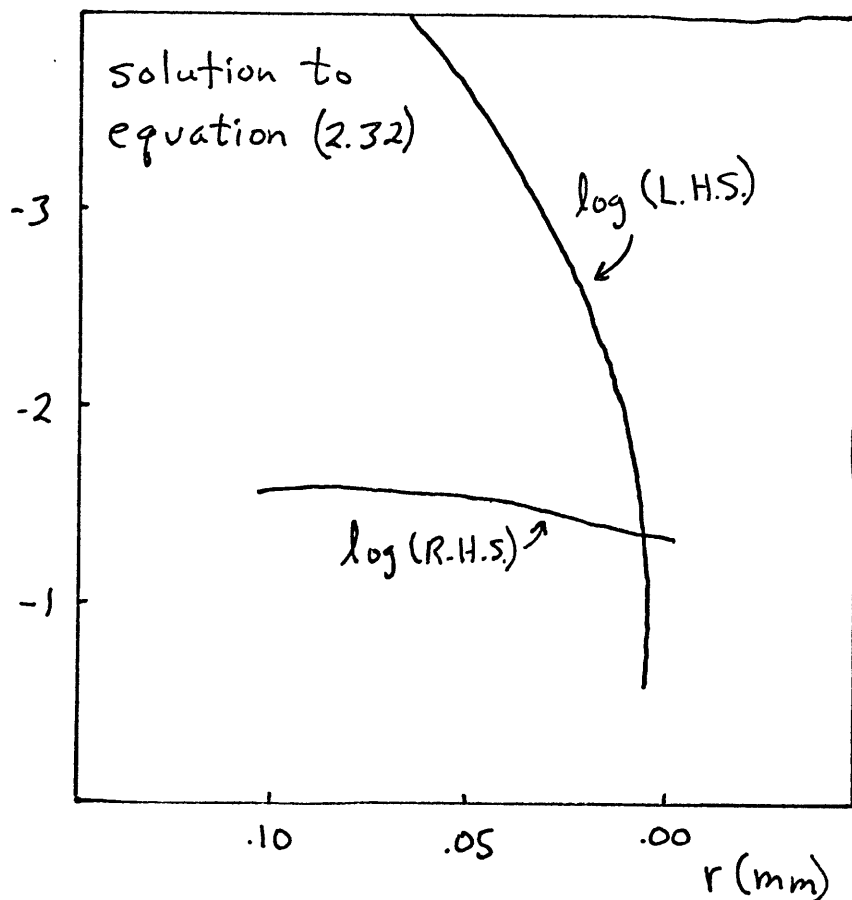
The equality in equation (2.32) holds when $r \approx 10^{-2}$ mm. For this value, $L \approx 12.5 \times 10^{-7}$ h, $T \approx 77$ μsec, and equation (2.31) yields 600 Megabars! Needless to say, this pressure is not usuable for studying effects in solids, since a spool of .02 mm diameter is too small to instrument. Looking ahead to the next section, we can calculate the energy required to vaporize a .02mm diameter spool by multiplying the value given in figure 2-10 by $10^{-2}/(2.92)^2$. Doing so, and comparing the result with figure 2-9, shows that the discharge producing 600 Megabars will impart to the spool over 1000 times the energy required to vaporize it.

The precision with which P_p can be computed is given by

$$\frac{\Delta P_p}{P_p} = \sqrt{2\left[\left(\frac{\Delta V}{V}\right)^2 + \left(\frac{\Delta d}{d}\right)^2 + \left(\frac{\Delta T}{T}\right)^2 + \left(\frac{\Delta C}{C}\right)^2\right]} \quad (2.33)$$

V was usually read to ± .1 kV. The outside meter was calibrated with a Hewlit Packard VTM Model 412A and a Calibration Standard Corporation 1000:1 Precision High Voltage Divider. d was machined to ± .0005 inch, and T could usually be read to ± .2 μsec. C_o was checked with a General Radio impedance bridge to be ± 1 μf. For common values of V and T (15kV and 5 μsec), equation (2.33) becomes

$$\frac{\Delta P_p}{P_p} = 10^{-2} \times \sqrt{.88 + .38 + 32 + 88} = .11 \quad (2.34)$$

2.22 Melting of the copper spools

In experiments which produced pinch pressures greater than about 100 kilobars, the copper spools were usually completely destroyed. That is, except for the end-flanges, nothing of the spools could be recognized in the debris remaining in the guard ring after the experiment. The purpose of this section is to calculate the rate at which energy is deposited in the spools, and to compare it with the heat content of the spools at elevated temperature. Appendix A2 reviews all the pertinent observational data in this area. The conclusions of the two sections agree very well.

The rate at which energy is deposited into the spools is given by $R_s I^2$, where R_s is the resistance of the spools. R_s can be calculated from the restivity ρ by means of the equation:

$$R_s = \frac{\rho \ell}{\pi s (2r - s)} \quad (2.35)$$

where ℓ is the length of the spool, r is its radius, and s is the skin depth, given by

$$s = \sqrt{\frac{T\rho}{\pi\mu_o}} \quad .$$

A typical value of s is .2 mm. R_s in equation (2.35) is relatively insensitive to changes in ρ, since

$$R_s \propto \frac{\rho}{s^2} \propto 1 \; .$$

Equation (2.35) has been evaluated for two extremes of ρ, the normal value of 2×10^{-8} Ω - m and 10^{-6} Ω - m which Bennett et. al. (1964) obtained for the resistivity of liquid copper near vaporization in an exploding wire. The extremes of R_s thus generated were 1.7×10^{-4} Ω and 1.96×10^{-4} Ω.

The energy absorbed by the sample is

$$Q(t') = \int_0^{t'} R_s I^2 \; dt \; .$$

The current is

$$I = I_o \, e^{-Rt/2L} \, \sin(2\pi t/T) \; . \tag{2.36}$$

So that

$$I^2 = I_o^2 \, e^{-Rt/L} \, \sin^2(2\pi t/T) \; ,$$

and

$$Q(t') = \int_0^{t'} R_s I_o^2 \, e^{-Rt/L} \, \sin^2(2\pi t/T) \; dt$$

$$= \frac{R_s I_o^2}{\frac{R^2}{L^2} + \frac{16\pi^2}{T^2}} \; e^{-Rt/L} \left[\frac{8\pi^2 L}{T^2 R} - \frac{R}{L} \sin^2(2\pi t/T) \right.$$

$$\left. - \frac{2\pi}{T} \sin(4\pi t/T) \right]_0^{t'}$$

$$Q(t') = \frac{8\pi^2 I_o^2 L \ (R_s/R)}{T^2 \ (R^2/L^2 + 16\pi^2/T^2)} \ (1 - e^{-Rt'/L}),$$

for $t' = nT/2$. Reducing further:

$$Q(t) \cong \frac{1}{2} L I_o^2 \ \frac{R_s}{R} \ (1 - e^{-Rt/L})$$

$$\cong N C_o V^2 \ (1 - e^{-Rt/L}) \ \frac{R_s}{R} \ . \tag{2.37}$$

In equation (2.37), R_s is the resistance of the sample, and R is the total resistance of the circuit.

We can measure R from the decay of the current. According to equation (2.36), the amplitude ratio of the first and second current peaks (separated by T/2) is

$$\frac{I_1}{I_2} = e^{RT/4L} \ ,$$

or,

$$R = \frac{4L}{T} \ \log \ (I_1/I_2) \ . \tag{2.38}$$

R in equation (2.38) was computed by using equation (2.14) to calculate I_1 and equation (2.28) to calculate I_2. The data were taken from several shots in which V = 15 kV and the oscilloscope records were clear enough to allow all relevant quantities to be read to within 10%. The results are given on the next page:

shot	I_1(units of 10^6 amps)	R (units of 10^{-3} Ω)
S2	.705	21.9
T2	1.04	10.9
Tl	.974	8.76
Sl	.763	26.4
T3	1.41	8.67
Gl	1.36	9.2

For most cases, R is in the range $15 \pm 7 \times 10^{-3}$ Ω. Using a mean value

of $R_s = 1.8 \times 10^{-4}$ Ω, the ratio R_s/R will usually fall in the interval

$$R_s/R = (1.2 \pm .4) \times 10^{-2}.$$

Figure 2-9 is a graph of

$$Q_o = \frac{1}{2} \frac{R_s}{R} N C_o V^2$$

evaluated for $R_s/R = .012$ and various N.

The copper spool shafts are heated according to the relation

$$T = Q/MC \qquad\qquad (2.40)$$

where M is the mass of the spool hafts and C is the heat capacity of copper.

For copper at STP, C = .092 cal/gm-°C. For the spool shafts, M = .165 gm.

Thus,

$$1/MC = 65.7 \ °C/cal.$$

Kelly (1960) gives the heat content of copper up to 2800 °K. From

his data, the heat content (in gram calories) of the spool shafts is plotted in

figure 2-10. Added to it is the heat of vaporization of the shafts, computed
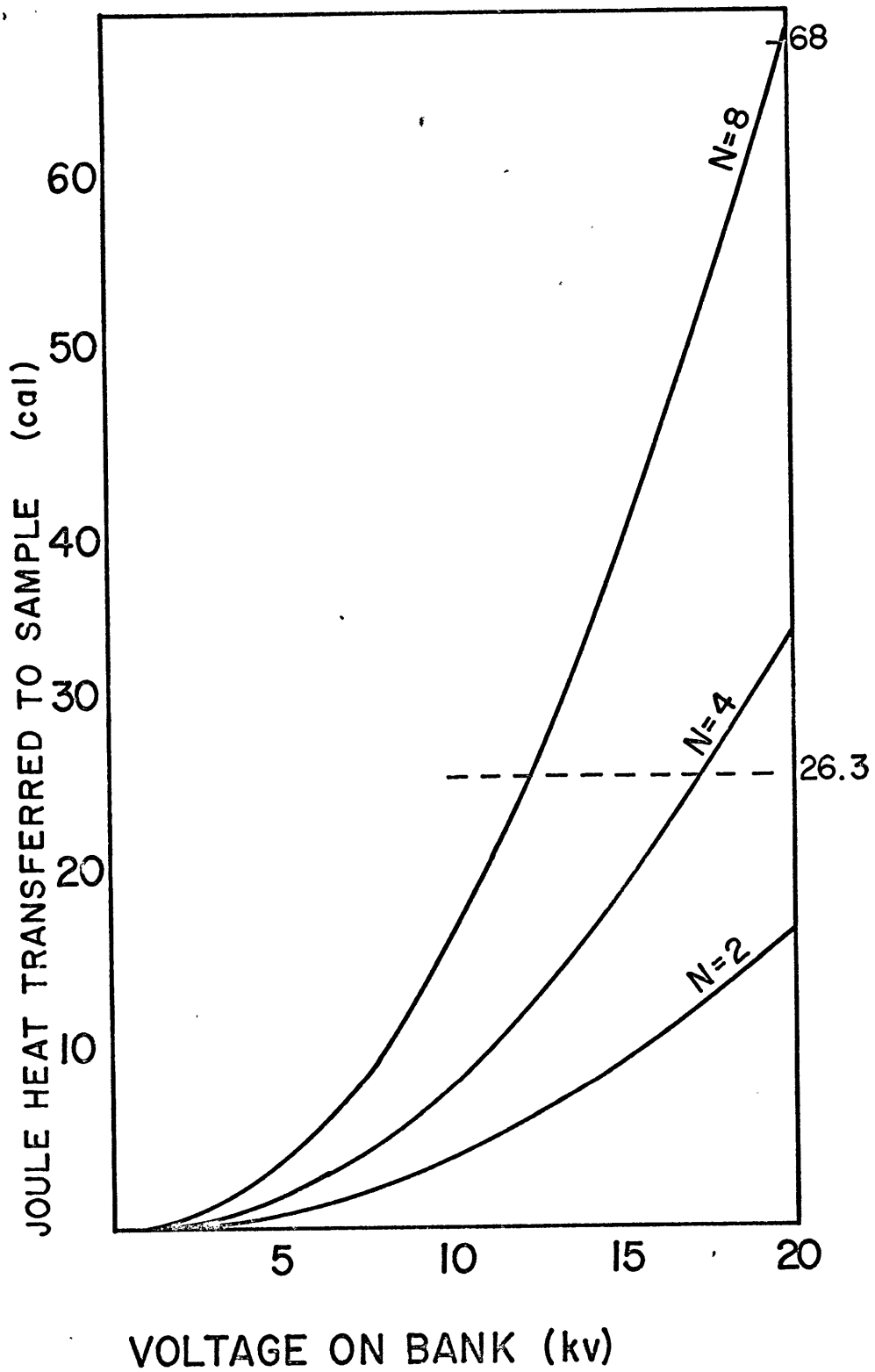
Fig. 2-9
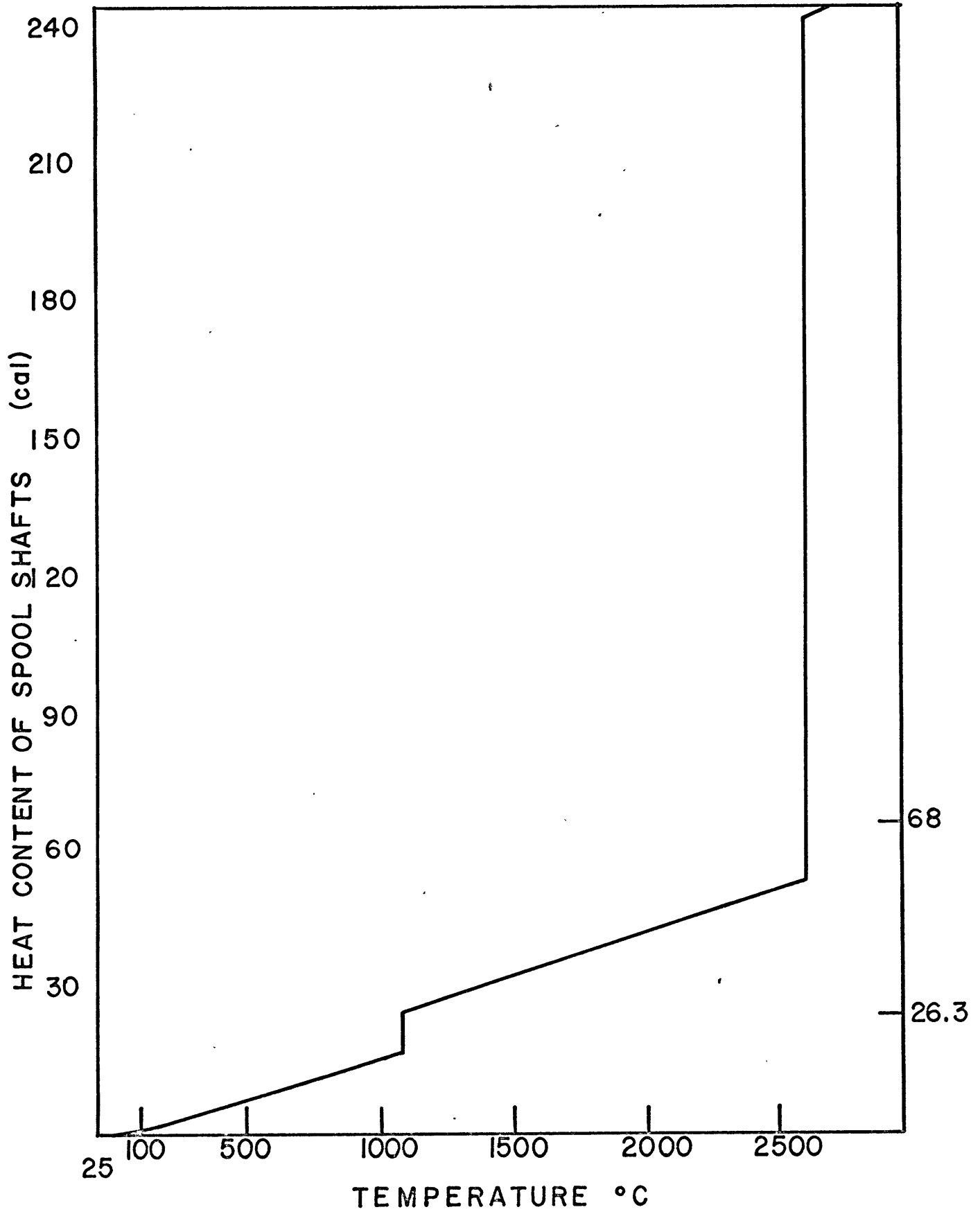
Fig. 2-10

from the CRC Handbook value for copper. The values given in figure 2-10 lack any pressure correction.

Comparison of figures 2-9 and 2-10 suggests that the spools will be destroyed when four capacitors are employed at voltages greater than 17.4 kV. This agrees very well with observation. It is also clear that joule heating cannot vaporize the spools.

It is important to note that although the copper spool may be heated to over 2000 °C, the sample will not get hot during the time that the pinch is applied. This is a consequence of the relatively long time scale of thermal convection. The radial temperature distribution in a rod of uniform composition is governed by the equation

$$\frac{d^2T}{dr^2} + \frac{1}{r}\frac{dT}{dr} = \frac{1}{\alpha^2}\frac{dT}{dt} ,$$

in which $\alpha = \sqrt{K/c\,\rho_m}$ (K = thermal conductity, c = specific heat, and ρ_m = mass density). The solutions to this equation are Bessel functions;

$$T = \sum_n A_n J_0(k_n r/\alpha)\, e^{-k_n^2 t} + T_o.$$

Let r_o be the sample diameter. We take the following boundary conditions:

$$T = 0 \text{ for } r < r_o, \quad t = 0$$
$$T = T_o \text{ for } r \geq r_o, \quad t \geq 0,$$

so that

$$\sum A_n J_0(k_n r/\alpha) = -T_o. \tag{2.41}$$

The values of A_n which satisfy equation (2.41) are given by Hildebrand (1962),

p. 231. The first ones are

$$A_1 = -1.602 \, T_o$$

$$A_2 = 1.065 \, T_o$$

$$k_1 = 2.405 \, \alpha/r_o$$

$$k_2 = 5.520 \, \alpha/r_o.$$

The values of α for the materials in the spools (ceramic or sample material) were in the range $.4 \pm .3$ cm/sec$^{\frac{1}{2}}$. Thus, k_1 is in the range $1.2 \pm .9$ sec$^{-\frac{1}{2}}$. Therefore, the range of charcteristic times, even for these pessimistic approximations, were

$$t_1 = \frac{1}{k_1^2} = .007 \begin{array}{c} + .1 \\ - .004 \end{array} \text{sec.}$$

The pinch pressure was only applied for about 10 μ sec, thus, the sample could not be heated by conduction during the time the pinch pressure was applied. However, when thermal equilibrium was reached between the sample and the spool, the sample may have become very hot. Some experimental results pertinent to this subject are given in section 4.1.

III. EXPERIMENTAL INVESTIGATIONS

3.1 Quartz

3.11 High pressure data on quartz

It is well known that fused quartz can be irreversibly densified by application of high pressure. However, the magnitude and cause of this effect are still subjects of controversy; figure 3-1 is a compilation of most of the published data.

The densification of quartz glass was first observed by Bridgman and Simon (1953). Using uniaxial compression, they measured the average density of solid quartz discs after pressure was applied. Above a threshold of about 100 kilobars, the quartz specimens were irreversibly densified. Cristiansen et. al. (1962) also employed unaxial stress on solid quartz discs. They found a threashold of only 40 kilobars. MacKenzie (1963) reported a threashold of about 60 kilobars. He employed solid samples in a belt apparatus; it turned out that the magnitude of the increase in refractive index, n, depended on the material out of which the apparatus was constructed. MacKenzie and Laforce (1963) and Saaka and MacKenzie (1969) used these results and a rather dubious interpretation of the data of Christiansen and Roy and Cohen to conclude that the densification of quartz is soley a function of shear stress, and would not occur in a truly hydrostatic pressure chamber.

Cohen and Roy (1965) used a unaxial press to study densification of ground fused quartz at various temperatures. It was found that elevated temperature caused the densification to take place at lower pressure, and that there was a maximum possible value of n for each temperature. They concluded that: "...at each temperature and pressure there is an equilibrium (metastable)

structure of the glass which is attained in a few minutes and then persists in-
definately at room temperature and atmospheric pressure." This conclusion
is directly opposed to that of MacKenzie. The indices of refraction observed
after quench from pressure were in a range ± .005 to ± .008. Roy and
Cohen proposed the hypothesis that the increase in density comes about by
rearrangement of basic structural units, most likely tetrahedral in shape.

Bridgman, Christiansen and MacKenzie measured densities. How-
ever, we have used the linear relationship between density and refractive index
(Cohen & Roy, 1962, MacKenzie, 1963) and the normal index of fused quartz
(1.460) to plot their data in figure 3-1 coordinates.

Wackerle (1962) has been the principal investigator of the effect of
shock waves on fused quartz. He found that below 98 kilobars the compression
was elastic. Material recovered from 250 kilobars was densified to 2.4 -
2.5 gm/cm^3 (n = 1.580 to 1.650). At 500 kilobars, the recovered material was
ordinary amorphous quartz. Shock waves in crystalline quartz resulted in the
formation of ordinary glass at pressures of 300 to 600 kilobars (DeCarli and
Jameison, 1959). Therefore, it appears that permanent densification of quartz
glass is produced by shock pressures in the range 98 to 300 kilobars.

It is not possible to predict whether pinch pressure can produce
high pressure crystalline polymorphs of quartz. Although coesite is stable
at only 21.5 kilobars (room temperature) (Bell & Boyd, 1968), it has never
been recovered from laboratory shock experiments on fused or crystalline
quartz. Traces of stishovite can be produced by only 75 kilobars in static
apparatus (Sclar et. al., 1963), and by much higher shock pressures in cry-
stalline quartz (DeCarli and Milton, 1965). Both coesite and stishovite can
form in natural impact events (Chao et. al., 1960, Chao et. al., 1962). Since
a glass-like phase is formed as an intermediate stage in high pressure quartz

FIG.3-1 THE EFFECT OF PRESSURE ON THE INDEX OF REFRACTION OF FUSED SILICA, 25°
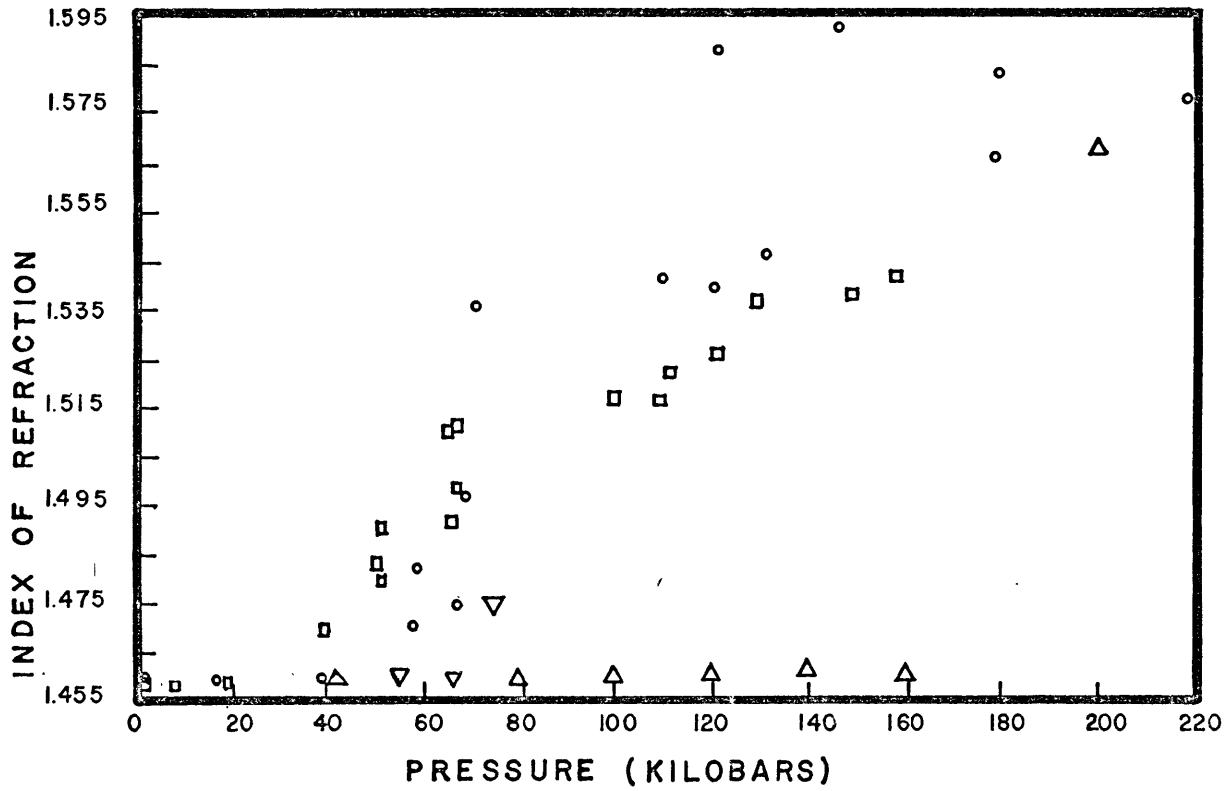
o CHRISTIANSEN ET AL, 1962

□ COHEN & ROY, 1962

△ BRIDGEMAN & SIMON, 1953

▽ MAC KENZIE, 1963

phase transitions (Dachille et. al., 1963, Chao, 1963), coesite or stishovite may be produced during pinch experiments on fused quartz. If they are, they should be recovered, since coesite is very stable at atmospheric pressure, even at 1400°C (Dachille et. al., 1963). Various accounts of the stability of stishovite have been reported - complete : reversion to glass in five minutes at 600°C (Dachille et. al., 1963), vrs. partically no reversion in 8000 minutes at 600°C (Skinner & Fahey, 1963).

We have subjected quartz glass to pinch pressures of 37 to 250 kilo-bars. Consideration of the preceding data leads us to seek answers to the following questions:

1) How is the index of refraction of quartz glass related to pinch pressure? Will an irreversible increase occur, as in static experiments, or will there be no change, as in some shock experiments? Will the relatively small amount of shear result in a lower index than in opposed anvil experiments? What will the threashold pressure for densification be?

2) Can coesite or stishovite form under pinch conditions, where the pressure is barely in their stability ranges, but of slightly longer duration than in shock waves?

3) Can a pinch pressure scale be based on the change in n as a function of P_p?

3.12 Pinch experiments on fused quartz

Four experiments were done with powdered fused quartz; the grain sizes were .061 to .044 mm. The powder was tapped into 1mm holes drilled through the axis of 4 and 6 mm diameter spools, as shown in figure 3-2a. The spools were made from OFHC copper and molybdenum. The shots were numbered GQ1 through GQ5, and the shot parameters are given in Appendix A1.
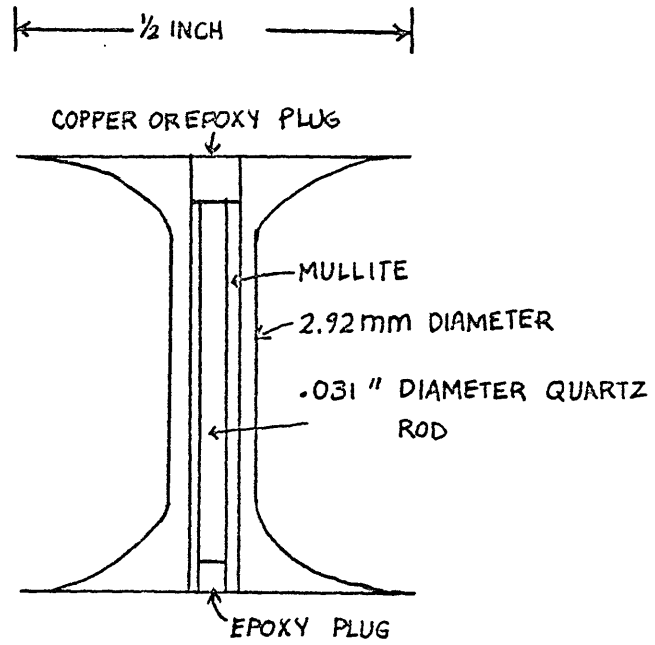
|← ½ INCH →|

COPPER OR EPOXY PLUG

MULLITE

2.92 mm DIAMETER

.031" DIAMETER QUARTZ ROD

EPOXY PLUG

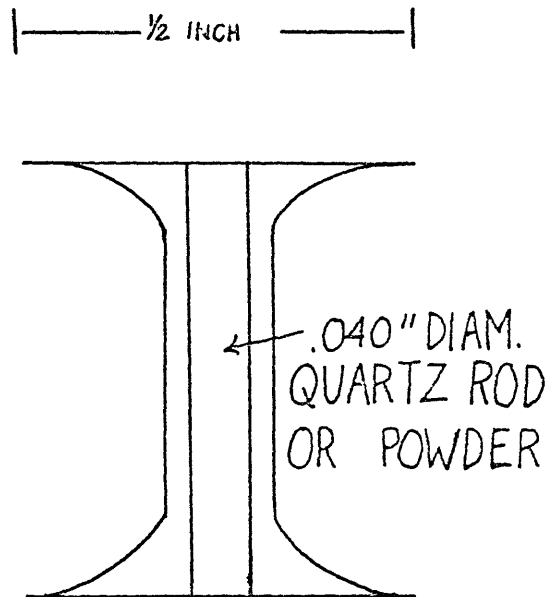FIG. 3-2b

|← ½ INCH →|

.040" DIAM. QUARTZ ROD OR POWDER

FIG. 3-2a

Even when the spools could not be recognized after the discharge, dissolving all the fragments in acid revealed a compacted quartz rod. The recovered quartz rods were white and fibrous in appearance; usually they could be easily crushed, but sometimes they contained a hard core. Diffractometer scans were made on several of the rods, but no evidence of crystalline phases was obtained. Oil immersion techniques were used to determine refractive indices. The difficulties of these measurements are discussed in Appendix A5. A unique index could not be recognized, and many of the grains were optically anisotropic. Blue and green incursions were present which had indices higher than 1.624. Observed indices of uncolored grains varied from that of the initial material to a maximum. The highest maximum which was obtained was 1.478 ± .002, at P_p = 51 kilobars. These data are plotted as crosses in figure 3-3 (an accident prevented measurements on GQ3). The failure of the index to increase monotonically with P_p may be attributed to the great strength of molybdenum and the fact that the powder was rather loosly packed into the spools. In hopes of improving the data, solid rods were tried in smaller diameter copper spools.

Four more experiments were done with the sample design of figure 3-2a and solid fused quartz rods which were center-less ground to 1mm diameter. Shots QR1 through QR4 were done with this configuration. Again many of the recovered grains were blue colored. The maximum measured n for these shots are also plotted in figure 3-3. Only clear regions of the grains were used for the index maxima. Although it is plausible that the blue coloring came from copper ions in the quartz grains, it is difficult to propose a mechanism for their placement. For example, in QR1 and QR3 it appeared that only the skin layer of the copper spools had melted, yet many of the quartz grains were blue colored.
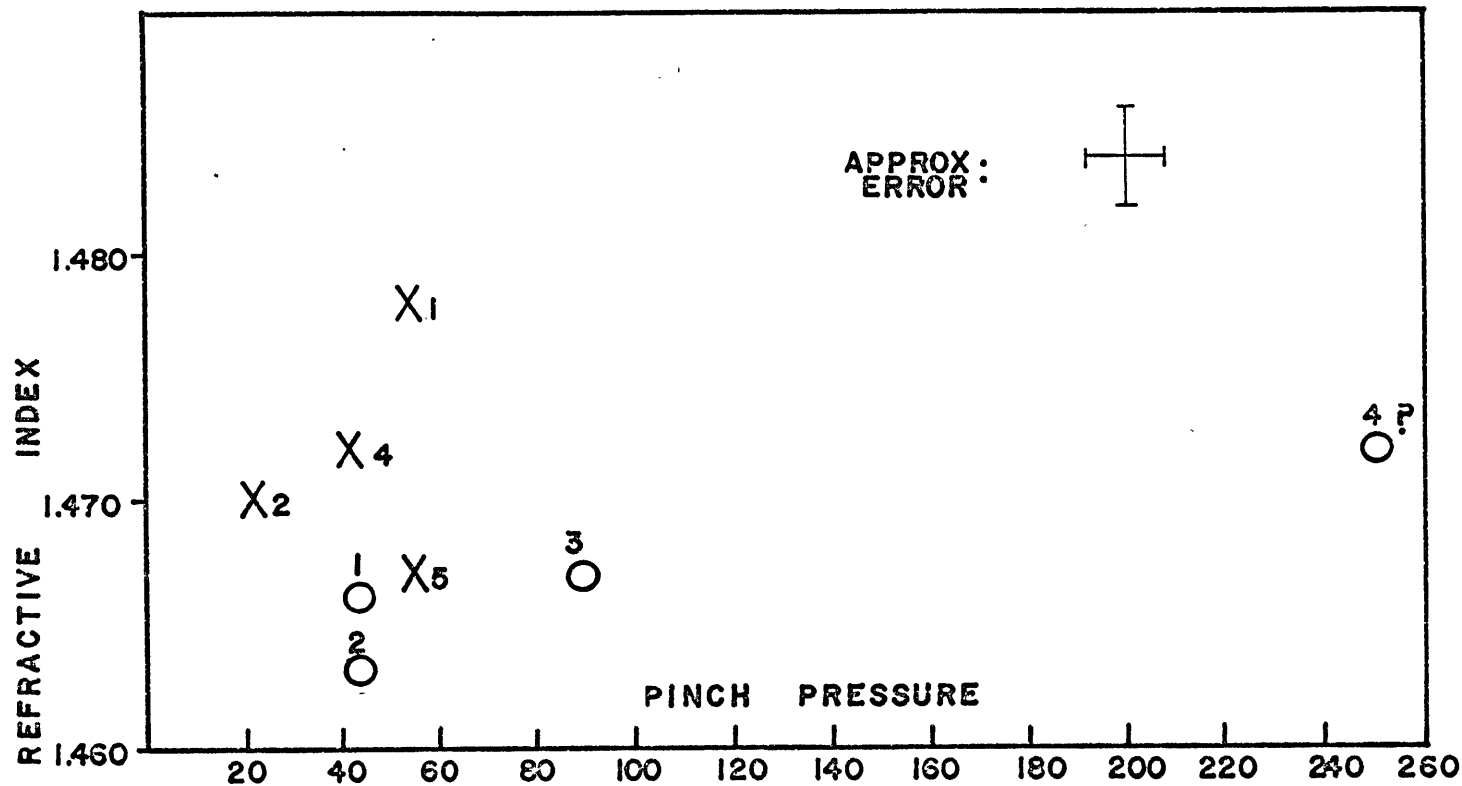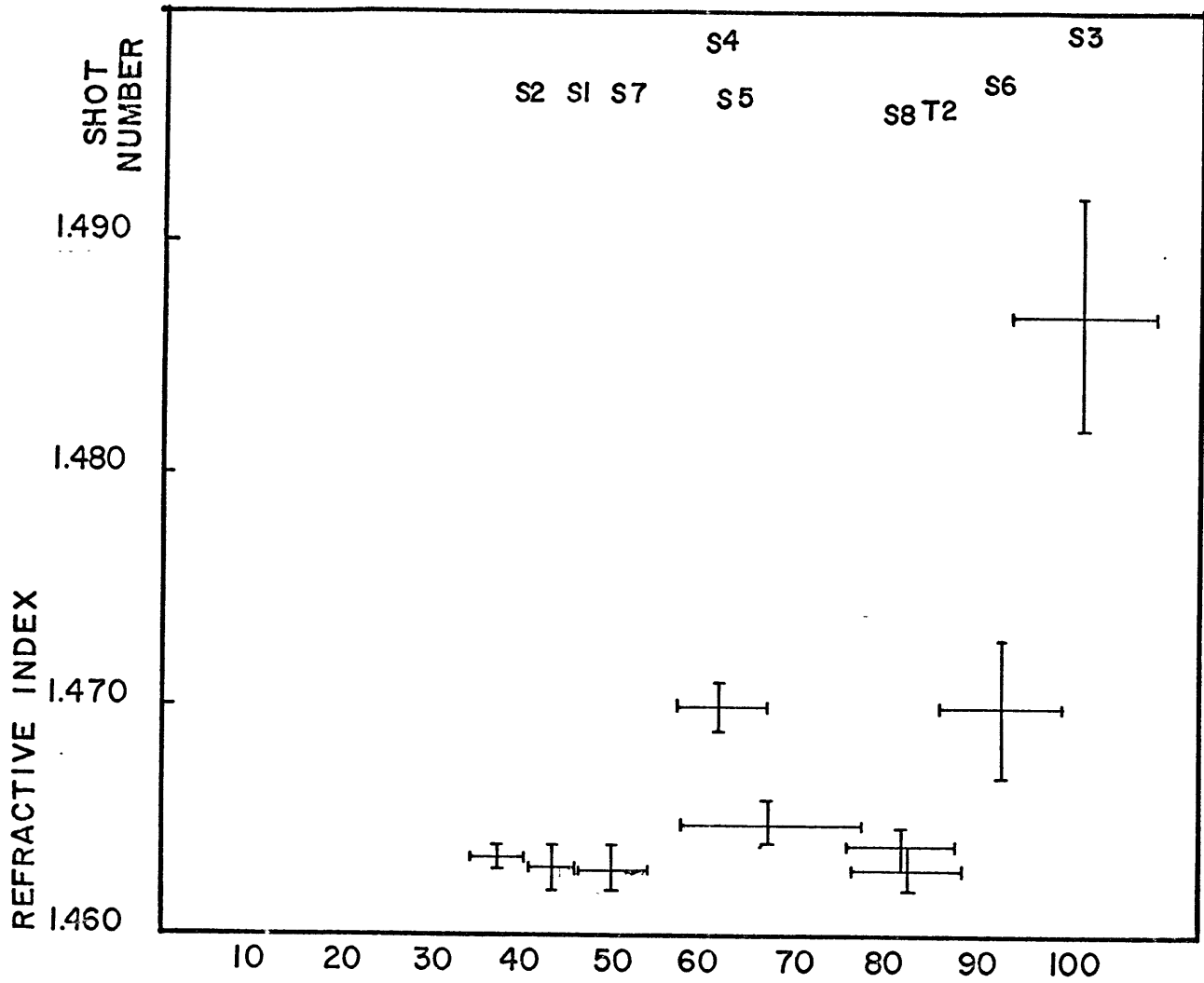
FIG.3-3 RESULTS OF FUSED QUARTZ EXPERIMENTS , SAMPLE AS SHOWN
IN FIG.3-2a
X- GROUND GLASS (SHOTS GQI-5)
O- SOLID RODS (SHOTS QRI-4)

FIG. 3-4 REFRACTIVE INDEX DATA - SOLID QUARTZ RODS - INSULATED SAMPLE (Fig 3-26)

(Initial refractive index was 1.460 ± .001 .)

The QR data are also plotted in figure 3-3. The pressure indicated for shot QR4 may be in error for two reasons: (1) After this shot, it was observed that the mylar insulation was cracked (see figure 2-2). Thus, the spool may have been short circuited. (2) The spool shaft was only partially destroyed. Reference to figure A-4, which is for 2.92 mm diameter spools (instead of 3mm, as in QR4) suggests that the spool shaft of QR4 should have been completely destroyed. The voltage at which spools are normally partially destroyed (at N = 6) is 14 to 15 kV, which corresponds to P_p = 132 to 168 kilobars.

In order to isolate the quartz rods from the copper spools, the sample design shown in figure 3-2b was used. The quartz rods were .031 inch diameter and ground from American Fused Quartz Co. spectrosil grade quartz, which does not contain air bubbles. The experiments done with these samples are labelled S1 through S8 and T2 in the appendix. As before, there was a large range of observed indices; the details of the index measurements for each shot are given in appendix A5. The maximum value of n for each shot (determined by a process descussed in appendix A5) are plotted in figure 4-4. The scatter in the data is less than observed by Christiansen et. al. (1962), and about the same as in the data of Cohen and Roy (1962) and Bridgman and Simon (1953). Sample S3, which had the largest index change, was analysed by the Debye-Scherrer technique. The resulting film contained no evidence for any crystalline phases of quartz. In these experiments, the recovered quartz was never blue colored.

Some experiments were done with Los Lunos obsidian in place of quartz. Shot G1 produced P_p = 135 kilobars. An X-ray powder film of the recovered material contained clear lines of α quartz (an alumina isulator was used). A powder film of the original contained only an extremely broadened strongest line of α quartz and a dozen or so unidentified lines. Index of

refraction measurements on obsidian could not be made because the black

obsidian grains could not be distinguished from the opaque granules of copper

mullite, and epoxy with which they were mixed.

3.13 Conclusions from pinch data

Our data show that quartz glass can be densified by pinch pressure,

but there is too much scatter to use the effect for pressure calibration. We

observed a low threashold for densification, as did Christiansen et. al.;

however, the index values we observed are lower than theirs and closest to

those of MacKenzie. Our results also suggest that slightly higher indices re-

sult from compression of fused quartz which has been ground to a fine powder;

the results of Roy and Cohen support this inference. Cohen and Roy had esta-

blished that equilibrium can be attained in less than a few minutes in their

experiments; from pinch results, it appears that only a few microseconds are

necessary. The failure to produce high pressure crystalline polymorphs of

quartz indicates that the relevant reactions are too slow to take place under

pinch conditions.

3.2 Boron Nitride

3.21 High pressure phases of boron nitride
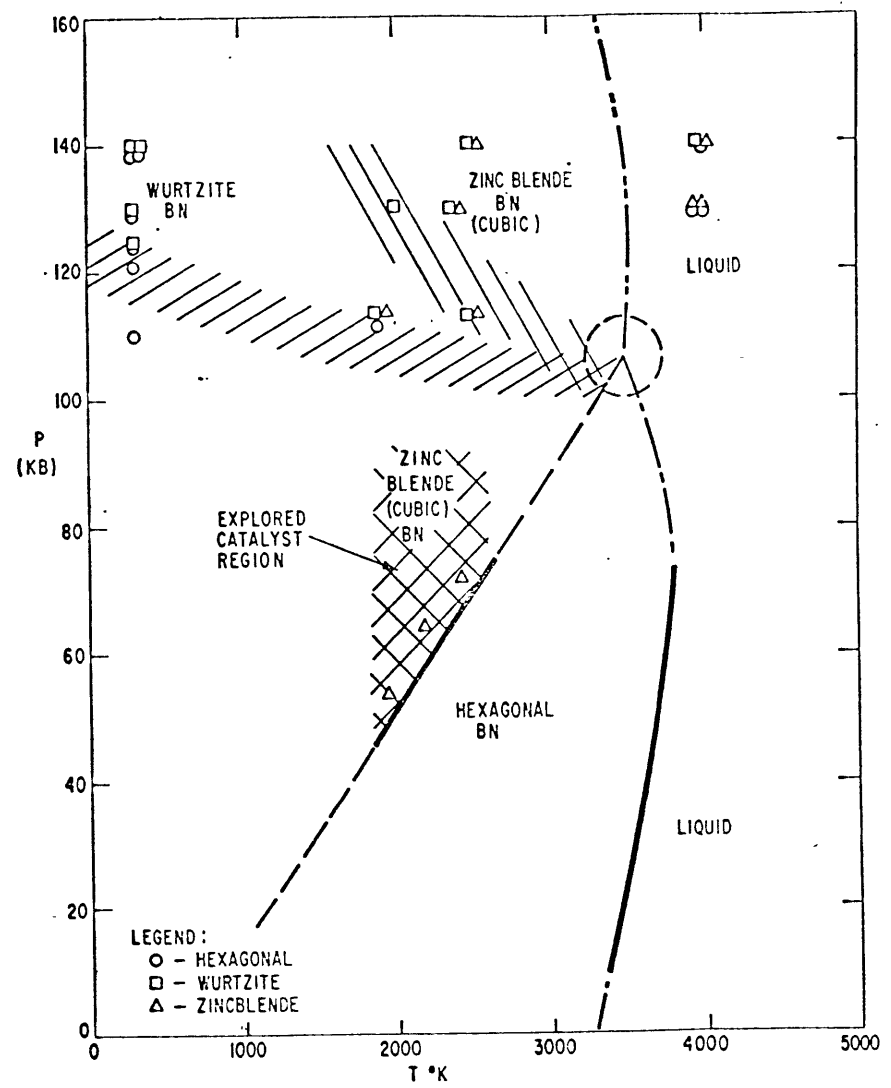
Figure 3-5   Phase diagram of boron nitride (after Bundy & Wentorf, 1963).

Bundy and Wentorf (1963) reported the high pressure phase diagram of boron nitride shown in figure 3-5. Ordinary hexagonal boron nitride transforms to a zincblende or wurtzite structure at about 130 kilobars. Al'tshuler (1967) has produced zincblende BN in shock waves, although pressures greater than 130 kilobars were apparently required. The zincblende phase could be recovered from both static and shock experiments. Bundy and Wentorf reported thw following d-spacings for the high pressure forms:

Table 1 - d-spacings for high pressure BN forms (from Bundy and Wentorf, 1963).

	wurtzite		zinclende
d	Intensity	d	Intensity
2.21	ms	2.09	s
2.10	m	1.81	w
1.96	m	1.28	m
1.52	mw	1.086	mw
1.275	mw	.904	w
1.185	m	.832	w
1.09	mw		

Bless (1968) reported attempts to produce high pressure forms of BN by pinch pressure. He used one inch long copper and stainless steel enclosed BN rods. P_p in his experiments was always less than 130 kilobars, and because of copper contamination, a definative statement on the formation of zincblende BN could not be made.

Because BN high pressure polymorphs have been produced and recovered in static and shock wave experiments, and the results of earlier low-pressure pinch experiments were ambiguous, it was decided to subject BN to very high pinch pressure utilizing the low inductance spool design described in section 2.11.

3.22 BN experiment

In order to eliminate the possibility of copper contamination, an aluminum spool was constructed and stainless steel connecting discs were used. A pinch pressure of 182 kilobars was produced by $N = 7$, $V = 17.5$ kV. The spool was destroyed, and fragments were collected and analysed with a diffractometer. The results are given in table 2:

Table 2 - d-spacings and indentification from BN experiment

observed d	observed intensity	indentification
3.28	15	BN (3.33)
3.04	50	
2.87	10	β Al_2O_3 (2.80) ?
2.70	7	β Al_2O_3 (2.68) ?
2.50	7	
2.34	7	Al (2.34)
2.26	7	β Al_2O_3 (2.27) ?
2.24	7	β Al_2O_3 (2.26) ?
2.09	25	zincblende BN
2.04	15	Al (2.024)
1.899	7	

There were no recognizable peaks below d = 1.899. Except for d = 3.04, the only clear line which could not be accounted for was 2.09; this corresponds exactly with the strongest line of zincblende BN reported by Bundy and Wentorf. The only possible contaminates which have reflections at d = 2.09 are copper and B_2O_3. Copper contamination was made very unlikely be constructing the sample and connecting discs out of other materials. B_2O_3 could not have been present, for a strong line at 2.78 $\overset{\circ}{A}$ is missing.

It is therefore concluded that high pressure zincblende BN has been produced by pinch pressure of 210 kilobars. This result is consistent with previous static and shock wave data.

3.3 Cadmium Sulfide

3.31 Cadmium sulfide high pressure polymorphs

Cadmium sulfide at STP possesses two stable structures, zincblende (cubic) and wurtzite (hexagonal). Many investigators have reported that a high pressure phase transition occurs in CdS between 20 and 30 kilobars. Samara and Drickamer (1962) and Miller et. al. (1966) observed an increase in electrical conductivity of at least five orders of magnitude at the transition. That the high pressure phase has the NaCl structure has been verified by Miller et. al. (1966), Corll (1964), Smith and Martin (1963), Jayaraman et. al. (1963), and Rooymans (1963). The high pressure phase can be quenched by cooling under pressure when the CdS has been precipitated from a chloride solution (Miller et. al., 1966, Corll, 1964).

Miller et. al. also reported that the quenched high pressure phase is still a semiconductor, and that if the material is held under pressure for 48 hours, the conductivity returns to nearly the normal value. They suggested that the sharp increase in conductivity observed at the transition is some sort of grain boundary effect. Miller et. al. found that with static pressures and temperatures below 150°C several weeks were required to approach equilibrium. With oscillating shear stresses, several hours were required. All authors reported hysterisis of about 10 kilobars in pure CdS. In view of these observations, it is somewhat surprising that Kennedy and Benedict (1966) reported that the reaction goes to completion in shock waves at a pressure of about 30 kilobars. (It is not clear whether or not they measured an increase in resistance. They report that it occurs, referring to a future publication which apprently never appeared.) Miller et. al. discovered a high temperature
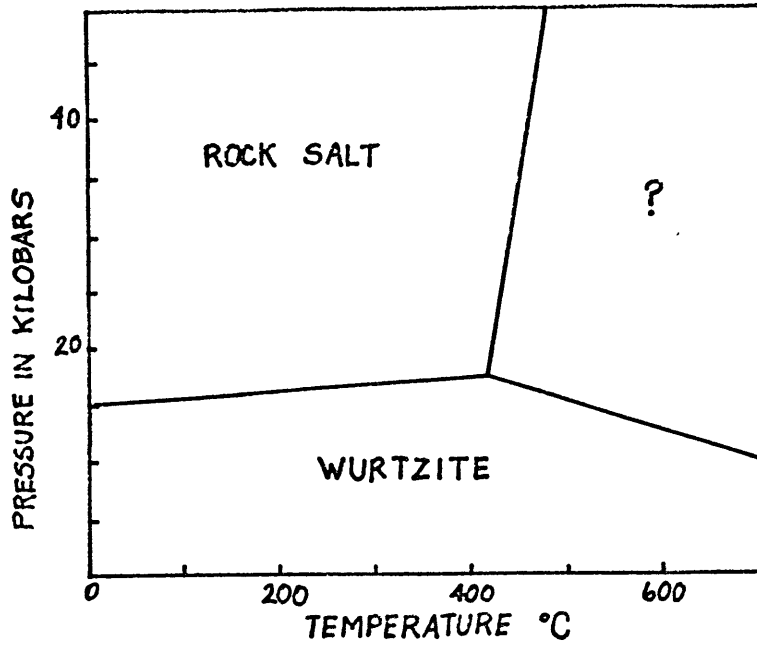
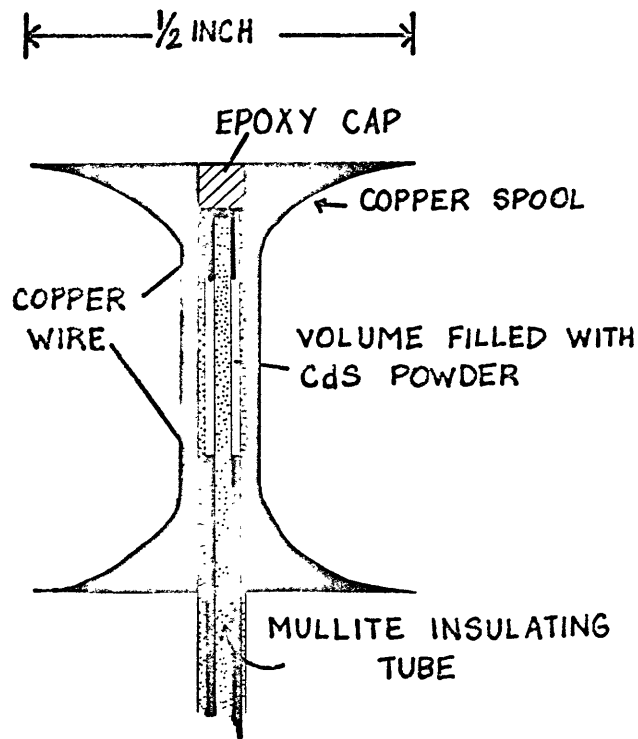FIG. 3-6 PHASE DIAGRAM
OF CdS (AFTER MILLER
ET AL , 1966)

FIG 3-7 SAMPLE FOR
MEASURING RESISTIVITY
OF CdS

phase of CdS which could not be quenched to STP but was recognized by the red color of the final material. Figure 3-6, the phase diagram of CdS, is reproduced from their paper.

3.2 Pinch experiments with cadmium sulfide

Quite a few rather difficult experimental problems required solution before the resistivity of CdS could be measured during the pinch. During the experiment, points adjacent to the sample were raised to thousands of volts, the volume available for instrumentation was very small, and the usually fragile sample had to be assembled among massive and clumsy clamp blocks and anvils. The cadmium sulfide used was Fisher Certified powder; Debye-Scherrer analysis indicated that it had the zincblende structure.

Figure 3-7 illustrates the sample design finally adopted (sometimes with small modifications). Two- holed mullite thermocouple insulation tubes served as pressure chambers; the hole diameters were 1/64 inch. The holes were filled with cadmium sulfide by means of a standard metallographic press and special adapter; 10,000 psi was used. It was necessary to add water to the CdS powder - a mixture of paste consistency usually worked well. After filling, the sample was baked at about 150°C for one-half hour or more. Weighing before and after heat treatment assured that all the water was eliminated.

The diameter of the lower contact wires was slightly less than that of the ceramic holes. In some cases, the wires were cemented into place with epoxy; then the volume occupied by the powder could be calculated and the density figured from the weight gain. The average density of the CdS powder in these samples was 3.14 gm/cm^3. Since the density of crystalline CdS is 4.82 gm/cm^3, the average porosity was 35%.

a) for measuring voltage across sample = Vs
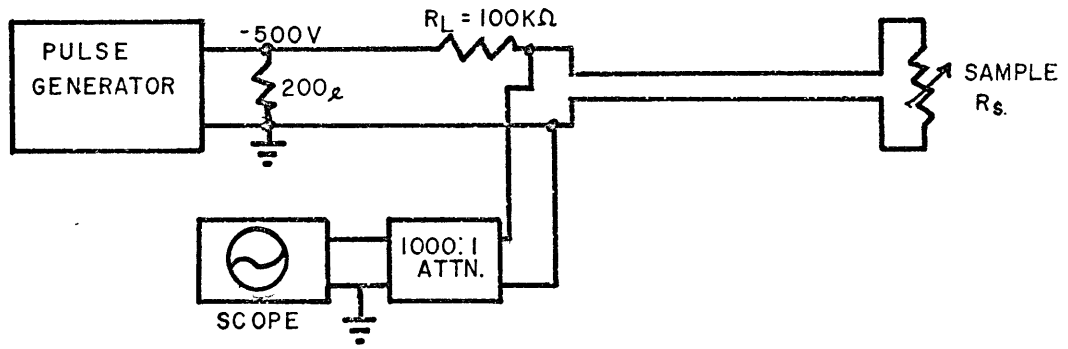
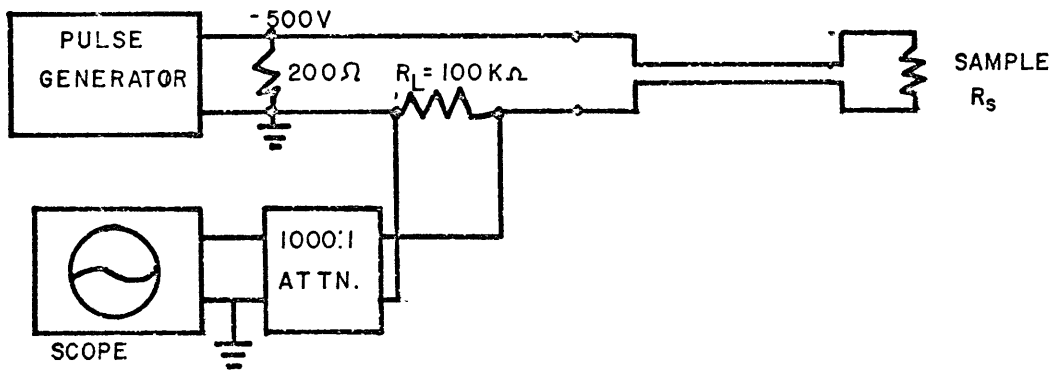b) for measuring voltage across 100 kΩ resister

FIG. 3-8 CIRCUIT USED FOR MEASURING RESISTANCE
OF CdS SAMPLES

The initial resistance of these samples was greater than expected. From

$$R = \rho \ell / \pi r^2 ,$$

the resistance of the CdS in figure 3-7 is 40 megaohms (using $\rho = 10^{-7} \Omega^{-1} m^{-1}$).

In practice, the resistance was always so high that it caused no deflection on a six volt multimeter. No improvement resulted from baking in a reducing atmosphere in order to eliminate the oxide coating on the copper wires. The excess resistance must arise from a poor connection between the loosly packed powder and copper connecting wires. During the pinch it should vanish since the contact is made within the region of maximum pressure.

Figure 3-8 illustrates the circuit used to measure resistivity. The lead wires running to the sample were either RG62 cable or tightly twisted magnet wires. The signal could always be boosted well above noise levels, since the initial voltage across the sample could be made as high as -2 kV by means of a Velonix high power high voltage pulse generator. Transient voltages were avoided by starting the experiments 150 μsec after the beginning of a 200 μsec pulse. Voltages were always measured via a 1000:1 Tektronix attenuator, in order to protect the oscilloscopes. The elements to the left of the leads were placed in a shielded enclosure. The resistance of the sample was high enough that there was no danger of heating from preliminary pulse generator pulses.

If the sample resistance changes by a factor f, e.g.

$$R_s \rightarrow f R_s ,$$

then V_s, the voltage across R_s, becomes

$$V_s \rightarrow \frac{f (R_s + R_L)}{f R_s + R_L} V_s ,$$

and V_L, the voltage across R_L, becomes

$$V_L \rightarrow \frac{R_s + R_L}{f R_s + R_L} \ V_L \ .$$

Notice that V_L is more sensitive to small f, and V_s is more sensitive to large f. Figure 3-9 gives measured values of V_s or V_L in CdS experiments in which data was obtained; the curves were obtained by tracing oscillographs. Figure 3-10 gives results for some test cases on inert samples.

In the experiments in which the copper spool was not completely destroyed, microscopic analysis showed that the powder was still in place. Photo 5 is a photomicrograph of sample E24, taken after the pinch. The largest dimension of the CdS filled cavity is about 75% of the diameter of the original hole. The color of the recovered CdS was yellow, thus it is unlikely that the phase labelled III in figure 3-6 was present.

Theoretical trace
sample becomes con-
ducting at first pres-
sure peak
sample destroyed by
second

V_s

-100
-200

2 μsec

V_s

100V
0
-200V
-400V

E3

$P_p = 95\,kb$

2 μsec

V_s

100V
0
-100V
-200V

E5

$P_p = 32.3\,kb$

2 μsec
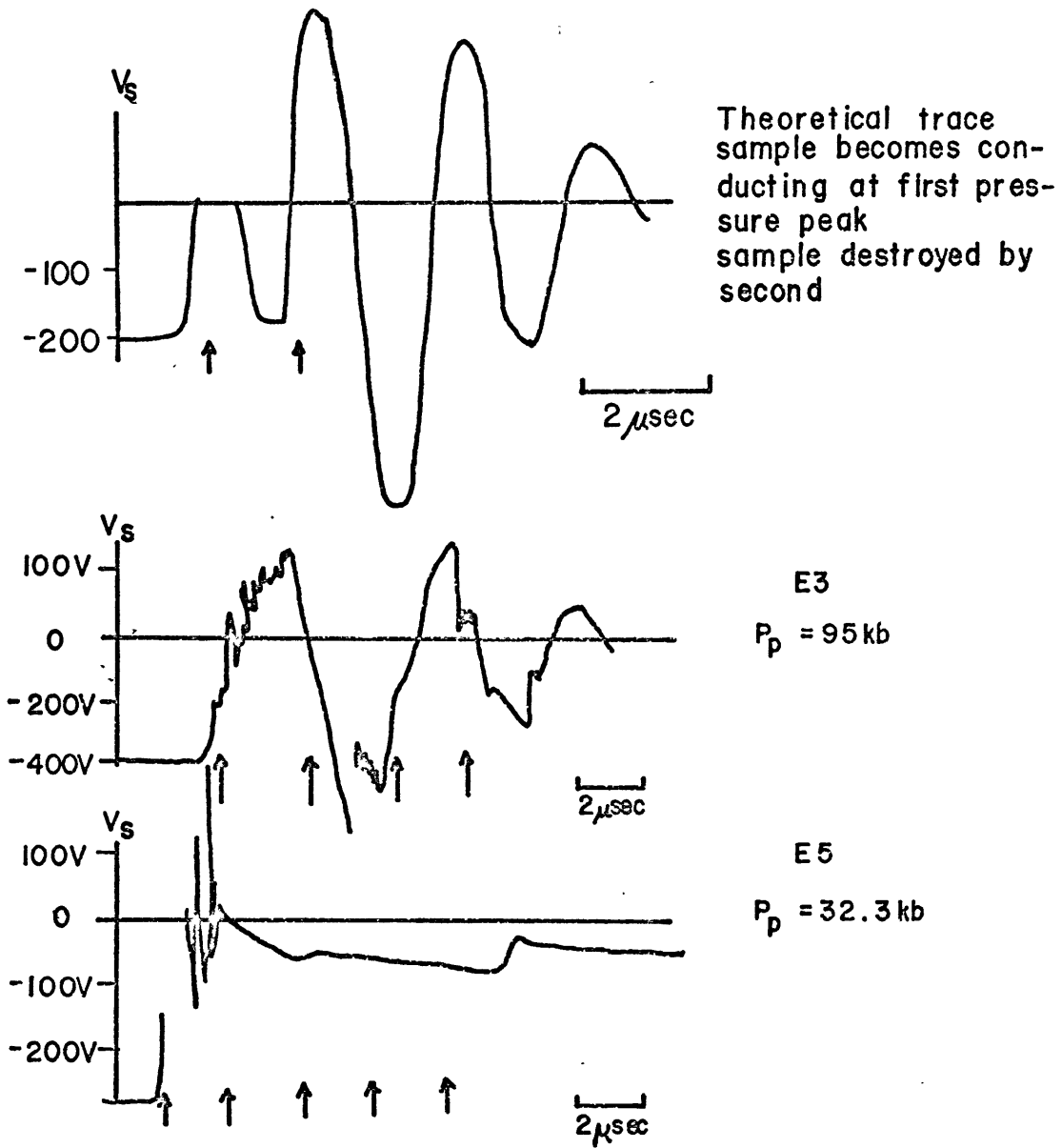
FIG. 3-9 OSCILLOSCOPE RECORDS FROM CdS EXPERIMENTS.
SAMPLE DESIGN IS SHOWN IN FIG 3-7. CIRCUIT IS DIA-
GRAMED IN FIG 3-8. ARROWS INDICATE TIMES OF CURRENT
MAXIMA. MORE DETAILS OF THESE EXPERIMENTS ARE
GIVEN IN APPENDIX AI.
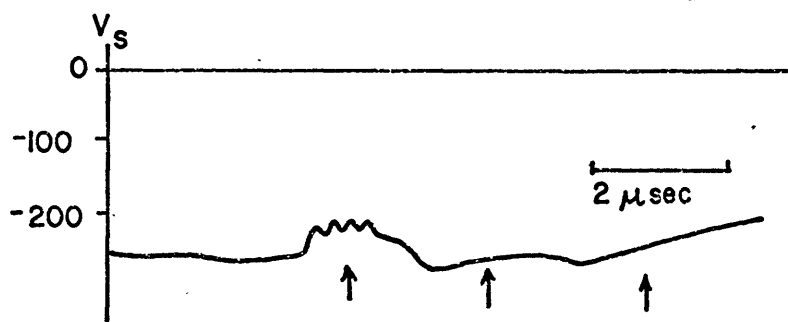
FIG 3-9 CONT'D

E7
$P_p = 27\,kb$
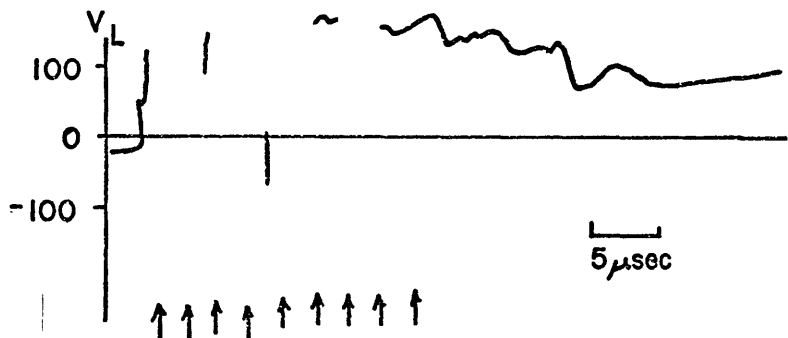
E15
$P_p = 29.5\,kb$

E17
$P_p = 51\,kb$
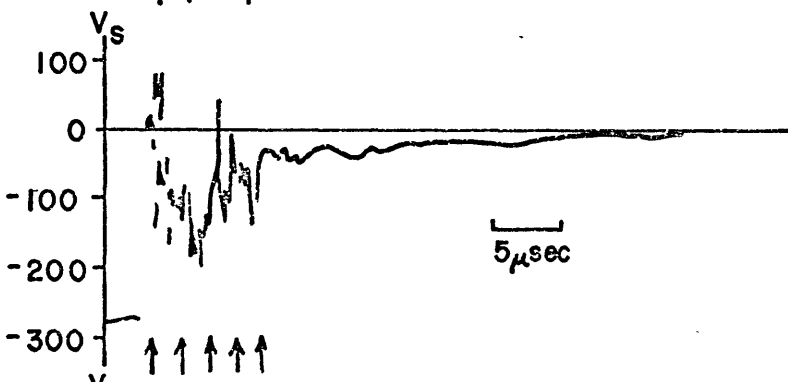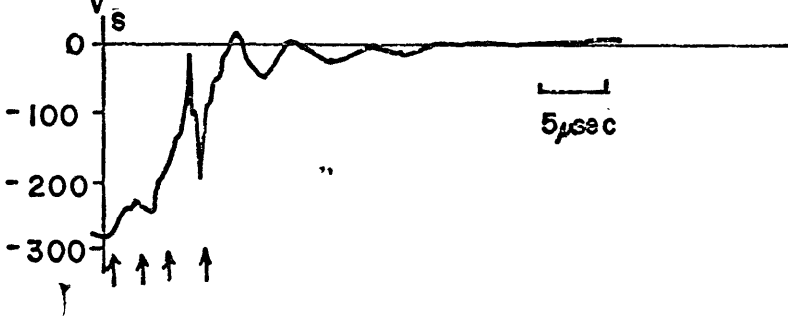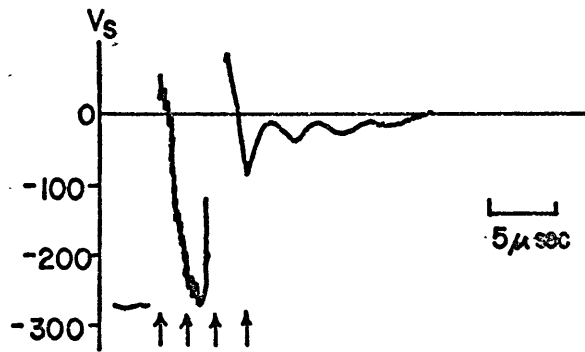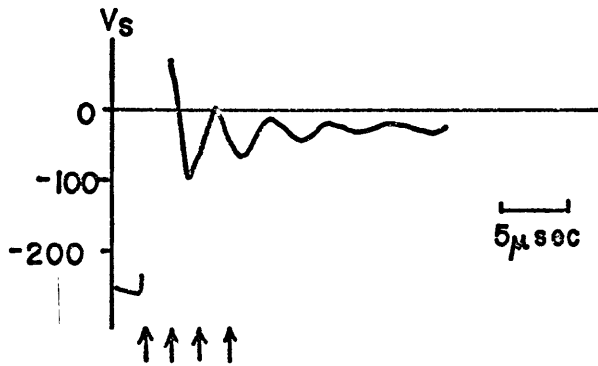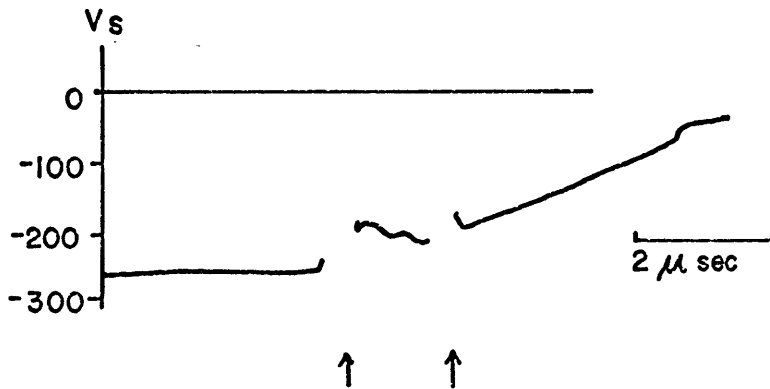
E18
$P_p = 42.5\,kb$

FIG 3-9   CONT'D

FIG. 3-9 CONT'D
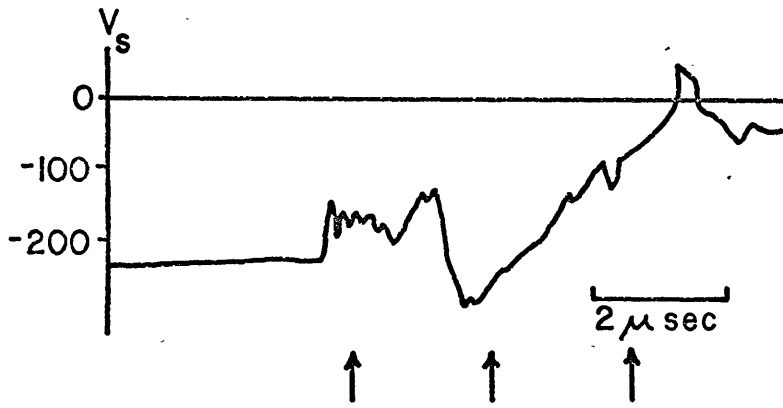
E 22
$P_p = 51$ kb
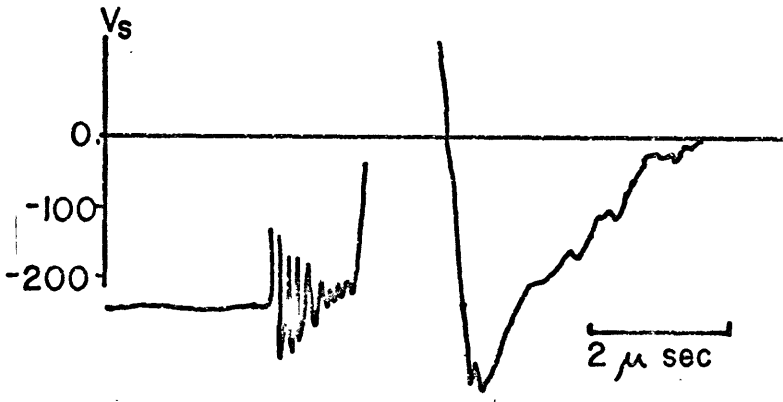
E 23
$P_p = 97$ kb
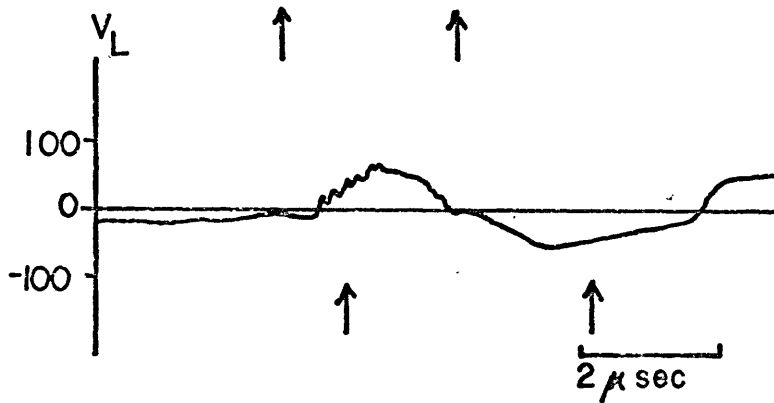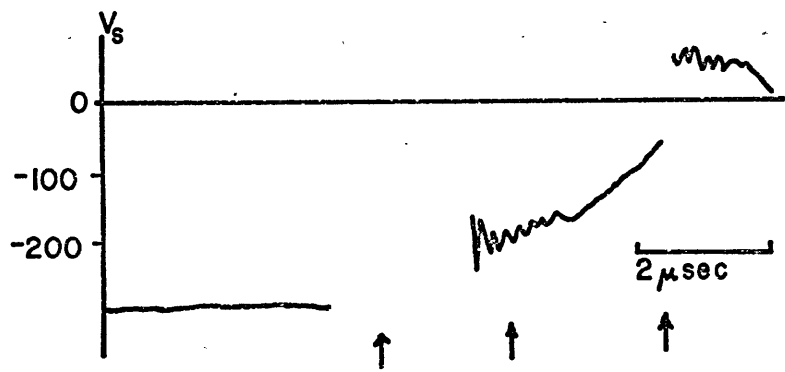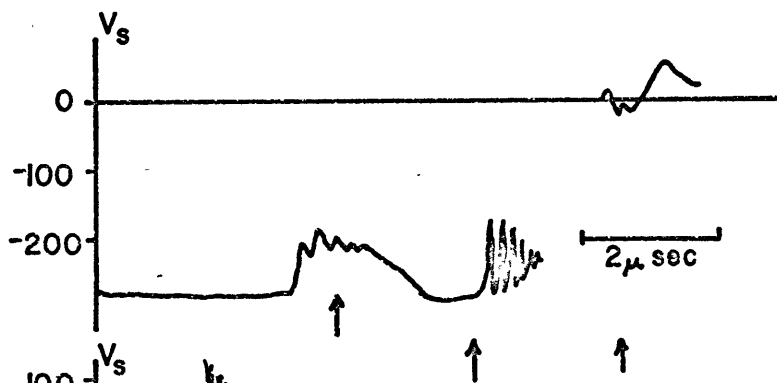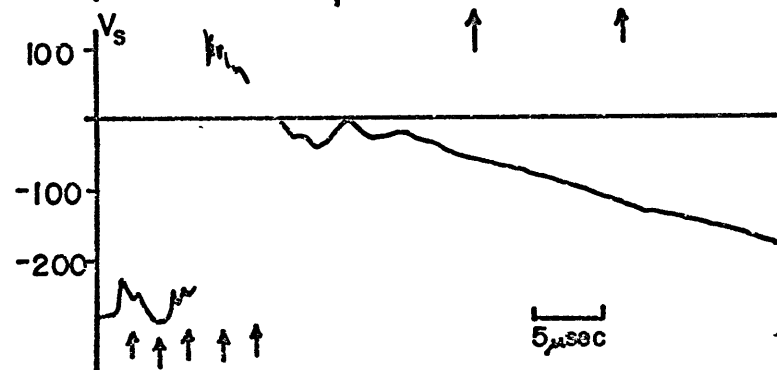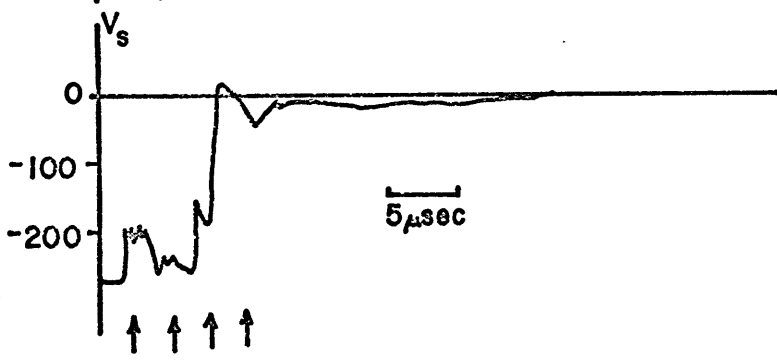
E 24
$P_p = 96$ kb

FIG. 3-10 OBSERVATIONS FROM EXPERIMENTS IN WHICH SAMPLES WERE FILLED WITH INERT MATERIALS.

3.33 Interpretation of pinch experiments

The first drawing in figure 3-9 illustrates the ideal case: The pinch pressure causes the CdS to become conducting during the first current peak. Consequently, R_s becomes much less than R_L, and $V_s \rightarrow 0$. Shortly afterward V_s is disturbed by several mechanisms, such as cracking of the ceramic in the region of high shear stress or where it emerges from the spool, or destruction of the spool by joule heating.

The ideal behaviour is obscured by two kinds of noise. The first is evident in shots E3, E5, E15, E19, E20, and E5 and E10 in figure 3-10. It is distinguished by a very fast and large positive excursion of V_s. This is caused by failure of the ceramic insulator. It was later found that about half of the samples tested could not hold off more than 10 to 15 kV. (The other half were okay to 20 kV.)
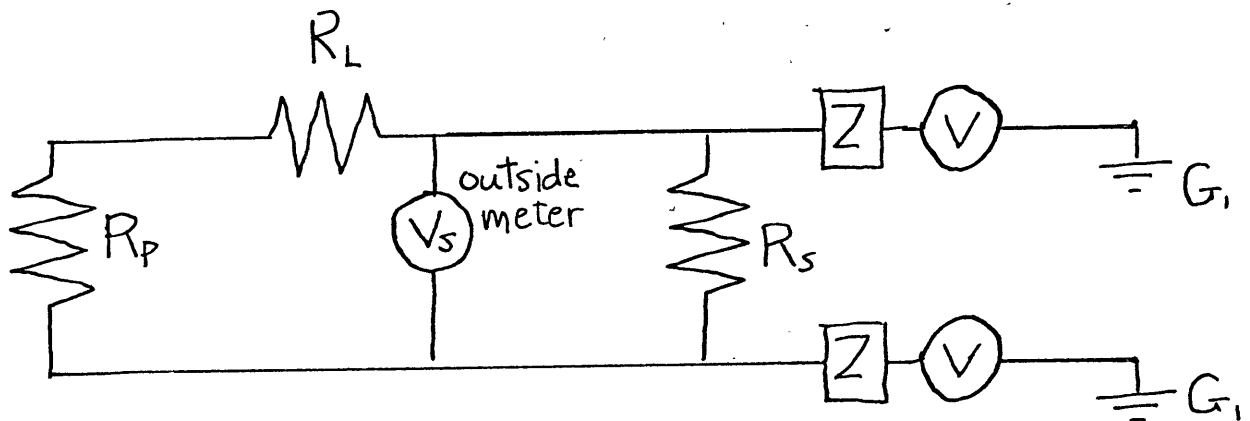
Fig. 3-11 Diagram to explain the origin of initial voltage drop in $|V_s|$ and $|V_L|$.

The other kind of noise signal was an increase of about +100 volts in V_s or V_L during the first half cycle. It occurred in SiO_2 filled as well as CdS filled samples; examples are E7, E18, E21, E22, E24, and E9 and E10. The origin of this noise signal can be explained by capacitive coupling. Referring to figure 3-11,

$$V = i_n (Z + R_L + R_p), \text{ since } R_s \gg R_L + R_p$$

V is the potential relative to ground of the base of the copper spool, Z is the "leak" impedance, and Rp is the imput impedance of the power supply $(200 \, \Omega)$. Let V_{nL} and V_{ns} be the noise additions to V_L and V_s. It is clear from the circuit (figure 3-8) and $R_p \ll R_L$ that $V_{nL} = V_{ns}$, and

$$i_n = \frac{V_{ns}}{R_L + R_p} \approx 10^{-3} \text{ amps.}$$

So that

$$Z \cong \frac{V}{i_n} - R_L \cong 10^7 - 10^5 = 10^7 \text{ ohms.}$$

Z must be capacitive, since

$$Z = 1/2 \pi f C = 10^7$$

implies that the leak capacitance, C, is 10^{-13} f, which agrees well with the capacitance of the lower lead wires shown in figure 3-7 as they emerge from the spool, estimated by

$$C \cong \frac{2 \pi \epsilon \ell}{\log b/a} = 5 \times 10^{-12} \text{ f}$$

(ℓ = 2cm, $\epsilon \sim 57.6 \times 10^{-12}$ f/m, b/a = 4.16). The resistive leak was be shown to be negligible:

$$R = \frac{\epsilon}{\sigma C} \quad \text{(see, for example, Harnwell, 1949, p. 101)}$$

$$\cong 10^{17} \text{ ohms.}$$

The conclusion is: if the CdS powder became conducting, V_s should have jumpted about $+100$ volts. This definately did not occur in shots E7, E18, E21, E22, and E24. Therefore, $R_s \gg R_L = 10^5$ ohm throughout the first pressure peak. The conductive phase transition in CdS did not take place.

3.34 Discussion of results

In the preceding section it was concluded that the cadmium sulfide resistance was always much greater that 10^5 ohms. Thus, the great increase in conductivity often observed at the phase transition did not occur. There are three possible explanations for this negative result: (1) The phase transition could not even begin to take place in so short a time. (2) The phase transition happened, but the grain boundary conduction mechanism did not operate. (3) The pressure was not felt by the CdS because of its porosity and the strength of the mullite insulator. First we discuss the last possibility.

The compressive strength of mullite, according to the manufacturer, (Omega Engineering Company) is 10^5 psi $= 6.8$ kilobars. If this is correct, the CdS powder should have been easily compacted. Reference to Photo 4 shows that this was the case.

If the mullite remained elastic, we can calculate the contraction of the CdS filled hole, assuming no strength for the powder. From equation A6.8, with $E_2 = 0$,

$$\zeta_r = \frac{2(1 - \nu^2) P R_1^2 R_2}{E(R_1^2 - R_2^2)}$$

(in this equation, R_1 is the radius of the mullite, R_2 is the radius of a concentric inner CdS filled cylinder, ν and E are the Poisson's ratio and Young's modulus of the mullite. The Young's modulus of the CdS is set equal to zero.)

We evaluate ζ_r by assuming the maximum probable values for E and ν, 500 kilobars and 1/2. We also let $P = 100$ kilobars and $R_1 = 2R_2$.

$$\zeta_r > 2R_2/5.$$

Therefore, even if the mullite remains elastic, the CdS will be easily compacted by the pinch pressure.

The compressibility of CdS powder under pressure was measured by Cline and Stephens (1965) to be about 2×10^{-3} (kilobars)$^{-1}$. This is probably greater than the compressibility of mullite. It can be seen from equation A6.9 that for $E_{CdS} \geq E_{mullite}$, the pressure experienced by the CdS is equal to or greater than the pressure on the mullite. It follows that in many of the shots for which data was obtained, the pressure applied to the CdS was above the recognized transition pressure.

In section 3.11, it was remarked that the CdS phase transition is very sluggish under static pressure. Thus, the likely explanation for the failure to observe the resistance change is that the shock data of Kennedy and Bennedict are wrong, and the transition cannot take place in only a few microseconds. It is also possible that the high pressure phase formed, but the grain boundary conduction mechanism was suppressed by the pinch pressure. This might happen if the pinch pressure, which was usually over twice the transition pressure, greatly altered the surface electronic states of the grains.

3.4 Carbon

3.41 High pressure polymorphs of carbon

The graphite-diamond transition in carbon is one of the best known and one of the few commercially important high pressure processes. However, although a great deal of work has been done, many details of the PT phase diagram of carbon remain obscure. Figure 3-12 is a compendium of most of the high pressure data on carbon. It can be seen that there are definately two high pressure polymorphs, "hexagonal" and cubic diamond. There may also be a third, called " δ carbon". Figure 3-12 shows established phase boundaries and the stable phases at various (P, T) points. Probably much more data has been taken, but is not included in published reports. The numbers in the figure refer to the references discussed below.

(1) Aust and Drickamer (1963). Samples of single crystal graphite apparently underwent a phase transition when subjected to static pressure of about 150 kilobars. The transition was marked by an increase in resistance of about four times. Formation of the high pressure phase was favored by high temperatures. The transition was not observed in powdered graphite. Some of the new phase could be recovered at zero pressure, where it was stable even at 450°C. An X-ray diffraction pattern showed the material was cubic, with an estimated density of 2.803 gm/cm^3. We call this material δ carbon, after Bundy, 1967.

(2) Alder and Christian (1961). Shock wave measurements on carbon revaled two changes in the slope of the Hugoniot, which were interpreted as partial and sudden complete conversion to diamond. The uppermost point on the diamond liquid boundary was not in this paper, but was attributed to the authors

by Bundy (1963). Alder and Christian also reported a transition to a metallic

state at 600-900 kilobars, but their data in this region are disputed by Pavlov-

skii and Drakin (1966).

(3) DeCarli and Jamieson (1961). When carbon was shocked to 300

kilobars, small crystals of diamond were recovered. The material used was

a commercial graphite that probably contained some rhombohedral graphite.

Diamond could not be recovered from silmilar experiments using pure graphite.

(4) Bundy (1963). ·Using static pressure and pulse heating, the

graphite diamond transition was studied at high pressure and temperature, and

the results connected with earlier work in which the metastable graphite-dia-

mond boundary was explored by means of catalysts.

(5) Bundy (1967). A new hexagonal form of carbon named "hexagonal

diamond" was reported. Its precise P-T stability range was not delineated

because most samples were only partially converted and contained both kinds

of diamond. The conditions under which the hexagonal diamond polymorph

formed were very similar to those of Drickamer's δ carbon phase - the

resistivity increased several times and the high pressure phase was stabilized

by high temperatures greater than 1000°C. (Bundy was never able to observe

the X-ray lines of δ carbon, and he quotes Drickamer as saying that his δ

carbon results may have been spurious.) Hexagonal diamond could only be

produced by applying pressure parallel to the c axis of sinal crystal or alligned

pyrolytic graphite. The great strength of graphite perpindicular to the c axis

may explain this result. During flash heating, the hexagonal transition was

observed to occur in milliseconds. A Debye-Scherrer pattern was reported;

the density of the hexagonal diamond was the same as cubic diamond (3.51 gm/

cm^3). It was pointed out that the atom movements to go from graphite to hex-

agonal diamond are simpler than those required to transform graphite to cubic

diamond (3.51 gm/cm^3). It was pointed out that the atom movements to go from graphite to hexagonal diamond are simpler than those required to transform graphite to cubic diamond. Bundy also quoted a Dutch Dupont patent, which reported that when graphite is finely dispersed in a metallic plate and shocked to pressures of 700 to 1400 kilobars, diamonds are produced which are 30% to 50% hexagonal. Evidence for the natural occurrance of shock produced hexagonal diamond was obtained by X-ray analysis of a Canyon Diablo meteorite fragment (see also Hanneman et. al., 1967).

(6) Bundy (1963b). Using flash heating at high pressure, the melting curve of graphite was determined. The heat of fusion was about 25 kcal/mole. The onset of melting was recognized by a decrease in electrical resistance. It was found that different types of graphite melted at the same temperature.

.3.42 Pinch experiments on graphite

Figure 3-3 illustrates the construction of the graphite pinch sample. Graphite powder was pressed into a mullite tube with 12000 psi. The inner diameter of the tube was 1/32 inch (.793 mm). The tube fitted snugly into the inner hole of a 2.92 mm diameter copper spool. Epoxy or ambroid cement was used to seal the ends so that powder could not leak out during handling.

FIG.3-12 PHASE DIAGRAM OF CARBON

◇ CUBIC DIAMOND
▢ HEXAGONAL DIAMOND
O GRAPHITE
△ δ - CARBON
   (NUMERS REFER TO
    REFERENCES IN TEXT)

CUBIC DIAMOND

HEXAGONAL DIAMOND

LIQUID

METASTABLE GRAPHITE

GRAPHITE
METASTABLE DIAMOND

PRESSURE IN KILOBARS

TEMPERATURE °K

500
400
300
200
100

1000   2000   3000   4000   5000

FIG.3-13   GRAPHITE SAMPLE

COPPER SPOOL

MULLITE INSULATOR

GRAPHITE POWDER

EPOXY PLUG

PAGES (S) MISSING FROM ORIGINAL

84

iron oxides.

<u>D1b material left from etching impact blocks:</u> Definately contained Al_2O_3. Some evidence for mullite. No evidence for graphite, copper, SiO_2, iron, or iron oxides.

<u>D2 recovered material:</u> Definately contained copper, Cu_2O, and Al_2O_3. Perhaps contained β quartz; no evidence for graphite, CuO, iron, or iron oxides.

All three powder patterns contained the two broad lines at d = .865 and .840 which were present in the original graphite powder. The evidence for presence of high pressure carbon polymorphs is presented in table 3:

Table 3 - Comparison of d-spacings of high pressure carbon polymorphs with those observed in pinched graphite.

δ carbon

(Aust & Drickamer, 1963)

d	D1a	D1b	D2
3.208 w	-	-	obsc. (Cu_2O)
2.770 m	-	-	2.81 mw
2.467 m	obsc. (CuO)	-	obsc. (Cu_2O)
1.844 w	obsc. (Cu)	1.80 mw	-
1.600 w	obsc. (mullite)	obsc. (Al_2O_3)	obsc. (Al_2O_3)
1.485 w	-	-	1.487 vw

hexagonal diamond (Bundy, 1967)

error in d: ± .01 - .02   (*line common with cubic diamond)

d	D1a	D1b	D2
2.19 s	-	2.18 w	2.19 w
2.06* s	obsc. (Cu)	2.07 m	obsc. (Cu)
1.92 m	-	-	1.905 vw
1.50 w	obsc. (Al_2O_3)	-	1.491 vw
1.26* ms	-	1.275 mw	1.265 vw
1.17 m	-	-	-
1.075* m	-	1.09 mw	1.105 vw
1.055 w	-	1.04 w	-
.855 w	obsc. (stock)	obsc. (stock)	obsc. (stock)
.820* w	-	-	-

cubic diamond (ASTM data)

d	D1a	D1b	D2
2.060*s	obsc. (Cu)	2.07 m	obsc. (Cu)
1.26* w	-	1.275 mw	1.265 vw
1.075* w	-	1.09 mw	-
.892 vw	obsc. (Al_2O_3)	-	-
.818* w	-	-	-

It can be seen in table 3 that there is slight evidence for δ carbon in D2, and good evidence for hexagonal diamond in D1b and D2. There is some agreement for cubic diamond, but the lines observed also arise from hexagonal diamond, and the intensities agree better with hexagonal diamond.

The confidence with which hexagonal diamond is observed in D2 is calculated as follows: Bundy gives his error as between .01 and .02 Å . The accuracy of the D2 film - judging from the closeness of fit with copper and Al_2O_3, is about ± .01 (slightly better for lower d values). Between 6.0 Å and .99 Å there were 29 unidentified lines. (This film was read without knowledge of the position of the diamond lines, so the observations were not biased.) If we consider a line within ± .02 of an observed line to be a good fit, then there is .04 x 29 = 1.14 Å of length which results in correspondance to observed lines. In other words, the probability that one randomly chosen value of d will correspond with an observed line is approximately 1.16/5.01 = .22. The chance that the two strongest lines of a randomly chosen material will correspond to two unidentified lines is approximately .04. Therefore, the statement that hexagonal diamond was produced in shot D2 carries about 96% confidence. For D1, a similar level of confidence is implied by the data. Given that hexagonal diamond was present, it can not be determined from the data whether or not cubic diamond was also present.

In order to obtain agreement between δ carbon lines and D2, we must assume an error range of ± .04 between Drickamer's data and ours. According to the preceding arguments, the confidence with which δ carbon can be identified in sample D2 is 79%. However, there is no way to justify such a large error range. We consider the evidence for presence of δ carbon to be very marginal.

Our conclusion that hexagonal diamond was produced by pinch pressure is consistent with the published high pressure data on carbon. As discussed in section 3.61, shock waves in graphite have been reported to produce both types of diamond, and production of diamond is favored when there is some rhombohedral graphite present. In static experiments, hexagonal (or cubic)

diamond is only produced by pressure parallel to the c axis of aligned crystals. However, the pinch pressures used here are higher than the static pressures required for the diamond transition, so that the transverse strength effect may be overcome. It is also plausible that as the graphite powder is compacted by the pinch pressure, the grains rotate so that the weaker c axis points in the direction of maximum pressure.

3.5 Albite

3.51 High pressure instability of albite

Figure 3-14

Stability field of albite
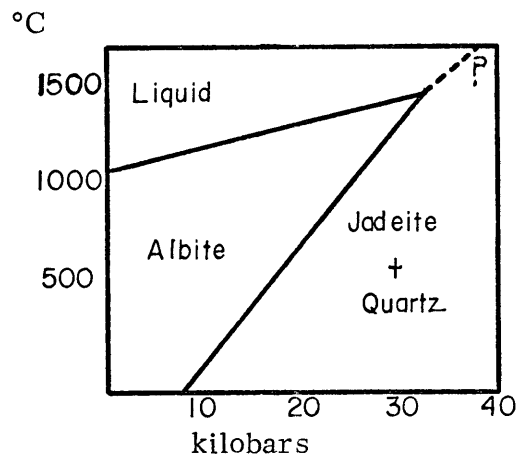
Albite is known to decompose under pressure to jadeite and quartz:

$$NaAlSi_3O_8 \text{ (albite)} \quad \rightleftarrows \quad NaAlSi_2O_6 \text{ (jadeite)} \quad + \quad SiO_2 \text{ (silica glass)}.$$
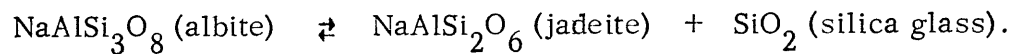
This reaction has been studied by Birch and LeCompte (1960), who found that the phase boundary could be described by P(kilobars) $= 6 + .2\,T\,(°C)$. Melting of albite has been studied by Birch and LeCompte (1960), Boyd and England (1963) and Bell and Rosenbloom (1965). These authors all agree that the melting curve of albite intersects the albite-jadeite phase boundary at about 33 kilobars. These data on albite are summarized in figure 3-14.

When liquid albite was quenched, its index of refraction turned out to be a function of the pressure (Boyd and England, 1963). The relationship was linear, starting at n = 1.488 and extending to n = 1.518 at 30 kilobars.

The transformation of albite to jadeite and silica glass has not been observed in shock waves (Short, 1968). However, shock loading to 300 kilobars of plagioclase similar in composition to albite resulted in complete transformation to a dense glass called maskelynite (Milton & DeCarli, 1963). The threashold pressure for formation of maskelynite may be only 150 kilobars (Ahrens and Rosenberg, 1968). Natural occurrances of maskelynite also indicate shock origin (Bunch et. al., 1967).

Pinch experiments on albite were undertaken with the objective of determining the effect of transient pressure and temperature of slightly longer duration than in shock waves. This type of information is required for under-standing the distinction between impact and metamorphic structures in nature (see, for example, Chao, 1968).

3.52 Pinch experiments with albite

The sample configuration for the albite experiments was the same as described in the section on graphite. At least 10,000 psi was used to press a slurry of 325 mesh albite powder into mullite tubes. After filling, the samples were heated above 100°C until they stopped losing weight. (Shot A4 was an exception; see below.) The density in three test samples was determined to be 1.6 gm/cm^3, which is equivalent to a porosity of 39% ($\pm 5\%$). Four experiments were done; all employed 2.92 mm diameter spools with epoxy reinforcement. Further details are given below:

Shot A1: N = 2, V = 17.5 kV, P_p = 32.6 kb. The spool was made of coin silver. The material which was recovered was obtained by dissolving the

silver from a short section of the spool shaft which remained intact.

Shot A2 : $N = 4$, $V = 16$ kV, $P_p = 109$ kb. This spool was partially melted by the pinch current; it is shown in photo 8.

Shot A3 : $N = 4$, $V = 16.5$. An attempt was made to quench this sample before it could get very hot: a 1/8 inch hole was drilled through all sample assembly parts beneath the spool. A 1000 ml water filled beaker was placed under this hole to catch ejected material. Unfortunately, the material was ejected with such force that the beaker shattered and nothing was recovered for analysis.

Shot A4 : $N = 2$, $V = 18$, $P_p = 47$ kb. The spool used in this experiment was like the one in figure 3-2b. An attempt to quench the sample was again made, replacing the beaker with a steel pan. Since the sample was being quenched in water, baking to eliminate the initial water in the powder was dispensed with. Apparently the spool shaft and its contents were ejected, for nothing was left in the guard ring, and the pan contained a great deal of debris. Photo 6 shows a sample of the material caught in the pan. (The bottom of the pan was dented to a degree that only a very small increase in projectile energy would have punctured it.)

3.53 Results of pinch experiments

All of the recovered material was photographed in a Debye-Scherrer X-ray camera. Some microscopic examinations were also made. The albite recovered was always "low albite", never the "high" form sometimes recovered after prolonged heating at high temperature (Smith, 1968). The details of the observations for each shot follow:

Shot A1 : The X-ray pattern showed virtually all the lines of albite and mullite (A.S.T.M. values). No lines of "mw" intensity or stronger were unidentified. There was no trace of jadeite, crystalline quartz, copper, copper oxides, or Al_2O_3.

Shot A2: The X-ray observations for this shot were the same as shot A1. The index of refraction of this material was studied by oil immersion. There were two characteristic types of grains - one was opaque and one was relatively transparent. It was assumed that the clearer grains were albite; they were optically anisotropic, with indices in the range 1.526 to 1.530. This includes the index values for crystalline albite.

Shot A4: The X-ray lines were dramatically stronest on this film; albite and mullite and copper were readily identified. There was no trace of jadeite, copper oxides, or Al_2O_3. Microscopic examination of the powder again revealed many clear grains, but their indices were above 1.562. which is much higher than any form of albite.

From these observations it can definately be concluded that albite did not decompose to jadeite and quartz under pinch pressure. Moreover, the strength of the albite lines and the refractive indices measured in A2 suggest that the albite was not melted, even though the copper spools were partially liquified.

3.6 Mullite

In the quartz, albite. and graphite experiments. the insulating tubes were made of mullite, $Al_6Si_2O_3$. Mullite is an artifical refractory made by decomposing one of the polymorphs of Al_2SiO_3. In many of the shots with mullite tubes, Debye-Scherrer patterns of recovered material were made. In the highest pressure shots, no lines of mullite were observed, but X-ray lines of Al_2O_3 were present. Thus, it appears that under exteme pinch pressure mullite can decompose into alumina and amorphous silica. The relevant data are reviewed below:

Shot	P_p	mullite present?	alumina present?
Al	32.6	yes	no
A4	47	yes	no
S3	102	yes	yes
A2	109	yes	no
D2	195	no	yes
Dla	300	yes	yes
Dlb	300	no	yes

McQueen's (1968) shock wave data also indicates a phase transition in this region.

IV. CONCLUSIONS

4.1 P-T History of Samples

During an experiment the sample is subjected to a series of decreasing pressure waves. After the currend has stopped the sample will begin to heat by conduction. This is illustrated schematically in figure 4-1.

The sample is heated nearly adiabatically by the pinch compression, e.g.

$$T = T_o \exp - \int_{V_o}^{V} \frac{\gamma}{V} \, dV.$$

In our experiments, this effect is negligible. However, the copper spool surrounding the sample is joule heated to a temperature which can be determined from figures 2-9 and 2-10. This temperature is plotted in figure 4-2. In the figure, the maximum values of P_p and N to which various sample materials were subjected is also plotted. The condition of the recovered material was consistent with the calculated temperature in every case. This point is further discussed below:

a) SiO_2: In the experiments with uninsulated quartz rods, P_p was greatest in shot QR4 (250 kilobars). In the insulated experiments, it was greatest in S3 (102 kilobars). In both cases, $T_m < 1665\,°C$, the melting temperature for SiO_2 glass (taken from G.E. fused quartz data). However, the glass temperature of SiO_2 is only 1200 °C, and that is the temperature above which some annealing would be expected (Saaka and MacKenzie, 1968). Among the published reports on stability of densified glass, there is no agreement on annealing effects of temperature at one atmosphere. It is probable that some of the divergence between our results and those of other investigators

Figure 4-1   P-T history of sample.
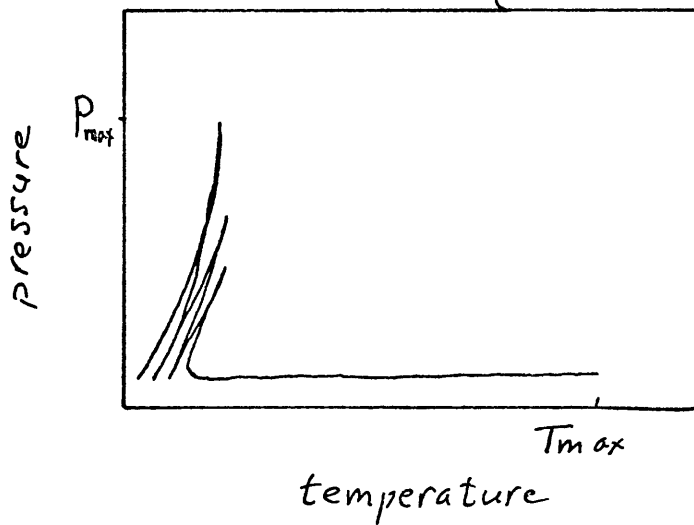
Figure 4-2
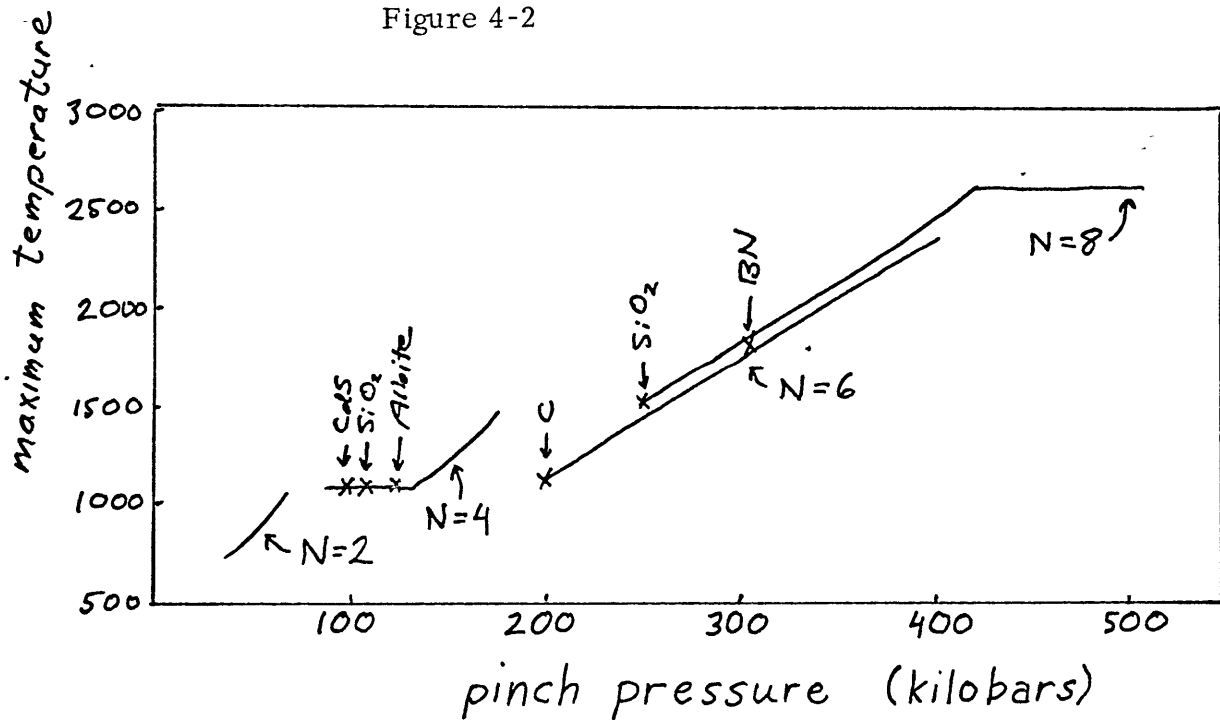
The theoretical maximum temperature of spools from Joule heating.

Data points are the maximum N and P_p for various sample materials.

is due to temperature annealing after the pinch.

b) CdS: It is doubtful that any of the CdS melted, since the specimens were still powder after the experiment. Thus, T_m < 1750°C (the CRC Handbook value of the melting temperature of CdS).

c) C: Bundy (1967) does not discuss the one atmosphere temperature stability of hexagonal diamond. However, it is certain that T_m was less than the melting temperature of graphite, 4000°C (Bundy, 1963b).

d) Albite: As discussed in section 3.5, the albite sample did not melt, and therefore T_m < 1100°C.

4.2 Recapitulation

There are many important geophysical problems concerning the lower mantle and core which seem unlikely to be solved by present high pressure technology. However, there are several characteristics of magnetic pinch compression, viz. pressures to one megabar or more, high temperatures available, and adiabatic compression lasting a few microseconds, which suggest that the pinch may be of much assistance in solving these problems.

The present apparatus produces pinch pressure by discharge of a 120 μf low inductance capacitor bank through cylindrical conductors. The pinched samples are enclosed in copper spools of varying diameter. A Rogowski coil situated around the spools allows measurement of pinch current. The measured currents agree well with those predicted by consideration of circuit inductance and resistance, although there is some variation due to variable spark gap inductance.

The pinch pressure produced by the capacitor discharge is inversely proportional to the square of the square of the sample diameter and directly proportional to the square of the initial charge on the capacitors. Because of uncertainties in the exact current path, the calculated pinch pressure must be considered an approximate lower bound. Although there is little doubt that pressures of several megabars can be produced by pinch techniques, they are not practically useful. In 2.92 mm diameter spools, the greatest pinch pressure which can be non-destructively produced is about 100 kilobars; the pressure felt by the sample, however, may be twice this high.

When the copper spools were filled with fused quartz, an irreversible densification resulted from application of pinch pressure. This is consistent with static experiments, and with additional data may form the basis

for a pinch pressure scale.

When boron nitride was subjected to the pinch, traces of the zinc-blende high pressure phase were produced. This indicates a pressure of at least 130 kilobars.

A research program was undertaken which resulted in the capability of measuring order of magnitude changes in electrical conductivity of materials during the pinch. CdS was studied by this technique; no evidence of its conducting high pressure phase transition was observed. There are several possible explanations, the most likely being that the conduction mechanism could not operate under the pinch conditions.

When graphite powder was pinched to 200 kilobars and above, traces of hexagonal diamond were produced. The static pressure required for formation of this material is not well determined, but is definately greater than 100 kilobars.

The stability of albite was studied under pinch pressure. It did not decompose to jadeite; nor were "high albite", albite glass, or maselynite produced. Using these results, we predict that albite will be stable in many natural "impact metamorphism" events.

It was discovered that mullite can decompose under pinch pressure to alumina and amorphous silica.

In terms of P_p, the observations can be summarized:

1) graphite goes to hexagonal diamond at $P_p \leq 195$ kilobars

2) hexagonal boron nitride goes to zincblende BN at $P_p \leq 195$ kilobars

3) albite is stable at $P_p \leq 110$ kilobars.

4) mullite decomposes at $P_p \approx 100$ kilobars

5) the index of refraction of silica glass increases with pressure, being about 1.487 at $P_p = 100$ kilobars

4.3 Suggestions for Future Work

The conclusion of this paper is that many high pressure effects can be studied by a magnetic pinch. However, quantitative measurement of the actual sample pressure and properties under pressure have not been possible. If the pinch technique is to become a useful pressure device, this difficulty must be overcome. There are basically to possible ways to proceed:

1) <u>Recovery experiments</u>: One can concentrate on recovery of high pressure polymorphs and modifications. Interesting results a propos to the subject of shock metamorphism should result from this approach.

Unfortunately, it will not be simple to calibrate P_p by this method. Since phase transformations seldom go to rapid completion in static experiments, the threashold pressure for a transition will often be difficult to recognize. Moreover, in the interesting region above 200 kilobars, samples will be heated to over 2000°C; this will inhibit recovery of high pressure phases. Below 200 kilobars, other investigators using Bridgman type anvils are doing a quite adequate job of investigating quenchable high pressure phases.

A solution to this dilemma may be found by cooling the sample. It will never be possible to cool the sample during the pinch, for the cooling rate is proportional to $1/r$ and the heating rate is proportional to $(r \log \frac{1}{r})^{-1}$. However, at low pressures, the quenching method used in shot A4 may prove satisfactory. At very high pressures, perhaps heat conduction to the sample can be prevented by directing a high velocity water jet at the spool.

2) <u>Real time measurement of pressure parameters</u> :   Alternatively,

one can attempt measurements of electrical properties during the pinch.   In

the present apparatus, this can be done only to order of magnitude accuracy.

This is sufficient to detect many phase changes which involve transitions from

semi-conducting to metallic states (see, for example, Doran, 1966).   It is also

conceivable that volume can be measured as a function of pinch pressure -

either by making the sample the core of a cylindrical capacitor, or by laser

reflection from the surface of the spool (Bless, 1968, has already reported

some preliminary experiments in this direction).

Programs such as these will be difficult to implement because of

capacitive and magnetic coupling between the measurement and discharge cir-

cuits.   Statistical analysis may be a means of averaging out spurious signals.

Unfortunately, we found that experiments in which electrical parameters were

measured extremely time consuming.

To pursue these ideas, one would proceed as follows: a) Use large

resistance discontinuities to accurately calibrate P_p.   b) If P_p turns out to

be reproducible, phase changes in geophysical materials in the range 500 to

1000 kilobars can be sought.   c)   After a method of measuring compressibility

has been developed, equation of state data can be obtained.

An additional possible method of studying materials under mega-

bar pressure and extremely high temperature is development of a theoretical

model for destruction of the spools (such as the one for imploding liners dis-

cussed in section 1.32.).

In conclusion, there is little doubt that the magnetic pinch can and

should become a useful high pressure research tool for operation in the 500

kilobar to one megabar region.   The task will be relatively inexpensive in terms

of equipment and overhead.   However, we estimate the effort will require several

years of diligent work by a team of experienced scientists.

V. ACKNOWLEDGEMENTS

VI. APPENDICES

A1. Complete Data for all Shots

This section contains complete data for all experiments performed with the sample assembly described in section 2.2. They are presented chronologically in table 4. These data form the basis for various statistical results presented in section A2.

In table 4, the following abreviations are employed:

column 1: code name for shot

column 2: section of this paper which contains more information about shot

column 3: diameter of spool in mm

column 4: number of capacitors employed

column 5: voltage on capacitors in kV

column 6: measured period of discharge in μ sec; usutally $\pm$ .2.

column 7: pinch pressure, calculated from equation (2.31).

column 8: contents of spool

column 9: type of reinforcement around spool. The coating usually did not completely fill the space between the spool shaft and guard ring. The materials used were: Devcon aluminum epoxy (ae), Atlas Epoxy Bond (eb), Hysol Epoxy Patch (ep), EE Cummings Stycast 2850FT (sty), saureisen cement (sc), and Donsel's EZ Plastic Mount (EZ). Of these, the epoxy patch was the strongest, but the stycast had the best resistance to thermal shock.

column 10: spool damage: Little = only outer surface melted, Destroyed = nothing of shaft could be recognized after shot, Great = in between "little" and "destroyed". Photos 7, 8, and 9 illustrate examples.

Table 4 - Data for all experiments. (See text for explanation of abreviations.)

column 1	2	3	4	5	6	7	8	9	10	11
shot	sec.	$\tilde{d}$	$\underline{N}$	$\tilde{V}$	$\tilde{T}$	P_p	sample	armour	damage	remarks
GQ1	3.12	4	4	15	4.8	55.3	ground quartz	none	destroyed	
GQ2	"	6	4	15	5.2	21	"	"	little	see photo 7
GQ3	"	4	4	15	4.4	63.5	"	ae	great	
GQ4	"	4	4	15	5.6	52.3	"	none	destroyed	molybdenum spool
GQ5	"	6	6	17.5	5.6	55.3	"	ep	destroyed	"
QR1	"	4	4	15	-	-	1mm quartz rod	ep	little	
QR2	"	4	4	15	6.0	35.3	"	none	destroyed	
QR3	"	4	6	16.2	6.1	90	"	ep	little	
QR4	"	3	6	18.3	5.5	250	"	ep	great	mylar may have failed T ± .3
BNS1	3.22	3.73	7	17.5	5.8	182	BN rod	ep (thin)	destroyed	aluminum spool
R3		2.92	4	15	-	-	CdS powder	ep	destroyed	hole under spool
R4		"	4	15	5.4	82	"	ep	little	"
R6		"	3	17.5	4.7	82.7	"	ep	great	"

column 1 shot	2 sec.	3 $\tilde{d}$	4 $\underline{N}$	5 $\tilde{V}$	6 $\tilde{T}$	7 $\underline{P}_p$	8 sample	9 armour	10 damage	11 remarks
E1	3.32	2.92	2	15	4.4	30.9	CdS powder	sc	little	hole under spool
E2	"	"	4	14.3	-	-	"	none	little	" , prefire
E3	"	"	4	15	5.0	95	"	ep	little	"
E4	"	"	2	11	-	-	"	EZ (thin)	little	" , prefire
E5	"	"	2	15	4.3	32.3	"	EZ	little	"
E6	"	"	2	14	4.3	28.2	"	EZ	little	"
E7	"	"	2	14	4.4	27	"	EZ	little	"
E8	"	"	2	14	4.4	27	300 mesh alumina	EZ	little	" , thick flange
E9	"	"	2	16	4.7	30.1	CdS powder	ep	great	"
E10	"	"	2	15	5.0	24	"	EZ	little	" , $\tilde{T} \pm .3$
E11	"	3.18	2	15.3	4.9	21.8	"	EZ	little	" "
E12	"	2.92	4	15.3	5.5	77	fused silica	EZ	destroyed	" "
E13	"	"	4	15.9	4.8	116	"	ep	great	" "
E15	"	"	2	15	4.5	29.5	NaCl	EZ	little	" "
E17	"	"	2	17.5	4.0	51	CdS powder	ep	great	" "

column 1	2	3	4	5	6	7	8	9	10	11
shot	sec.	$\tilde{d}$	N	$\tilde{V}$	$\tilde{T}$	P_p	sample	armour	damage	remarks
E18	3.32	2.92	2	16	4.0	42.4	CdS powder	ep	great	hole under spool, $\tilde{T} \pm .3$
E19	"	"	2	18	4.0	54	"	EZ	destroyed	" "
E20	"	"	2	17.5	4.0	51	"	EZ	destroyed	" "
E21	"	"	2	17.6	4.0	51.3	"	EZ	destroyed	" "
E22	"	"	2	17.5	4.2	46	"	sty	destroyed	" "
E23	"	"	4	17	5.0	97.2	"	sty	destroyed	" "
E24	"	"	4	15	5.0	96	"	sty	great	" "
E25		"	6	16	5.6	195	iron wires	none	destroyed	T measured between 2nd & 3rd peaks
E26		"	6	16	5.0	244	"	none	destroyed	"
E27		"	6	16	5.3	218	"	none	destroyed	"
E28	A3	"	6	16	6.4	144	"	ep	destroyed	hole under spool
E29	"	"	8	16	6.4	256	"	sty	destroyed	" , silver spool
E30	"	"	8	16	6.4	256	"	sty	destroyed	"
A1	3.52	"	2	17.5	5.0	32.6	albite powder	eb	destroyed	silver spool
T1		"	4	15	5.8	71.3	copper wire	sty	great	hole under spool
T2	3.12	"	4	15	5.4	82	quartz rod	ep	little	"

column 1	2	3	4	5	6	7	8	9	10	11
shot	sec.	$\tilde{d}$	$\underline{N}$	$\tilde{\underline{V}}$	$\tilde{\underline{T}}$	$\underline{P}_p$	sample	armour	damage	remarks
A2	3.52	2.92	4	16	5.0	109	albite powder	eb	great	see photo 8
D1	3.42	"	8	16	6.0	300	graphite powder	sty	destroyed	
G1	3.12	"	6	15.2	6.4	135	obsidian rod	eb (thin)	destroyed	hole under spool
D2	3.42	"	6	17.6	-	-	graphite powder	none	destroyed	see photo 9
T3		"	6	15	6.2	195	quartz rod	sty	destroyed	hole under spool
A3	3.52	"	4	16.5	4.8	125	albite powder	sty	destroyed	
S1	3.12	"	2	15	3.7	43.5	quartz rod	none	little	
S2	"	"	2	15	4.0	37.4	"	sty	little	mylar may have failed
A4	3.52	"	2	18.1	4.3	47	albite powder	ep	destroyed	hole under spool
S3	3.12	"	4	16	5.1	102	quartz rod	ep	destroyed	
S4	"	"	2	17.5	3.6	62.1	"	ep	little	
S5	"	"	2	19.2	3.8	67.5	"	ep	destroyed	
S6	"	"	4	14.5	5.3	79.5	"	ep	little	
O1	"	"	2	17	4.5	37.5	obsidian rod	ep	destroyed	
S7	"	"	3	15	5.2	49.8	quartz rod	ep	destroyed	silver spool
S8	"	"	4	15	5.4	82.3	"	sty	great	

A2. Characteristics of the discharge

The measured discharge periods listed in table 4 are in qualitative

agreement with those calculated in section 2.14. The number of times that

various periods were observed is plotted in figures Al through A3, in which

the theoretical values are also indicated. For the case N = 4 (the most com-

mon case), the mean of all measurements was 5.14 with a standard deviation

of .45. At higher voltages, the periods were somewhat shorter; taking only

the four shots above 15.5 kV, the mean and standard deviation are 4.85 and

.08. This trend is also apparent in the other graphs. Only a small fraction

of the variations in $\tilde{T}$ can be due to instrumental error. The unpredictability

of $\tilde{T}$ in general must be due to the variations in the current path through the

spark gaps.

Bless (1968) found it convenient to summarize the effect of the dis-

charge on one inch 4mm diameter rods by means of a N vrs. $\tilde{V}$ plot. He found

that above a certain energy (which was about four times the energy required for

melting) the rods were destroyed. Furthermore, there was never enough

energy for vaporization. Figure A4 is a similar plot of the present data (taken

from table 4). The relative values of melting and vaporization energy are dif-

ferent than those observed by Bless for straight rods: only 26.3 calories was

required to melt the spool shafts; using $U = \frac{1}{2} N C_o V^2$, this corresponds to

$\tilde{V} = 2.7$ when N = 2. The energy required for vaporization was 246 calories,

or $\tilde{V} = 38$. at N = 8. In other words, compared to the straight rods employed

by Bless (1968), the spools were much better able to survive high energy dis-

charges; the reason for this is probably that destruction of the rods began pre-

maturely at the sharp corners (as occurs in exploding wires). The threshold

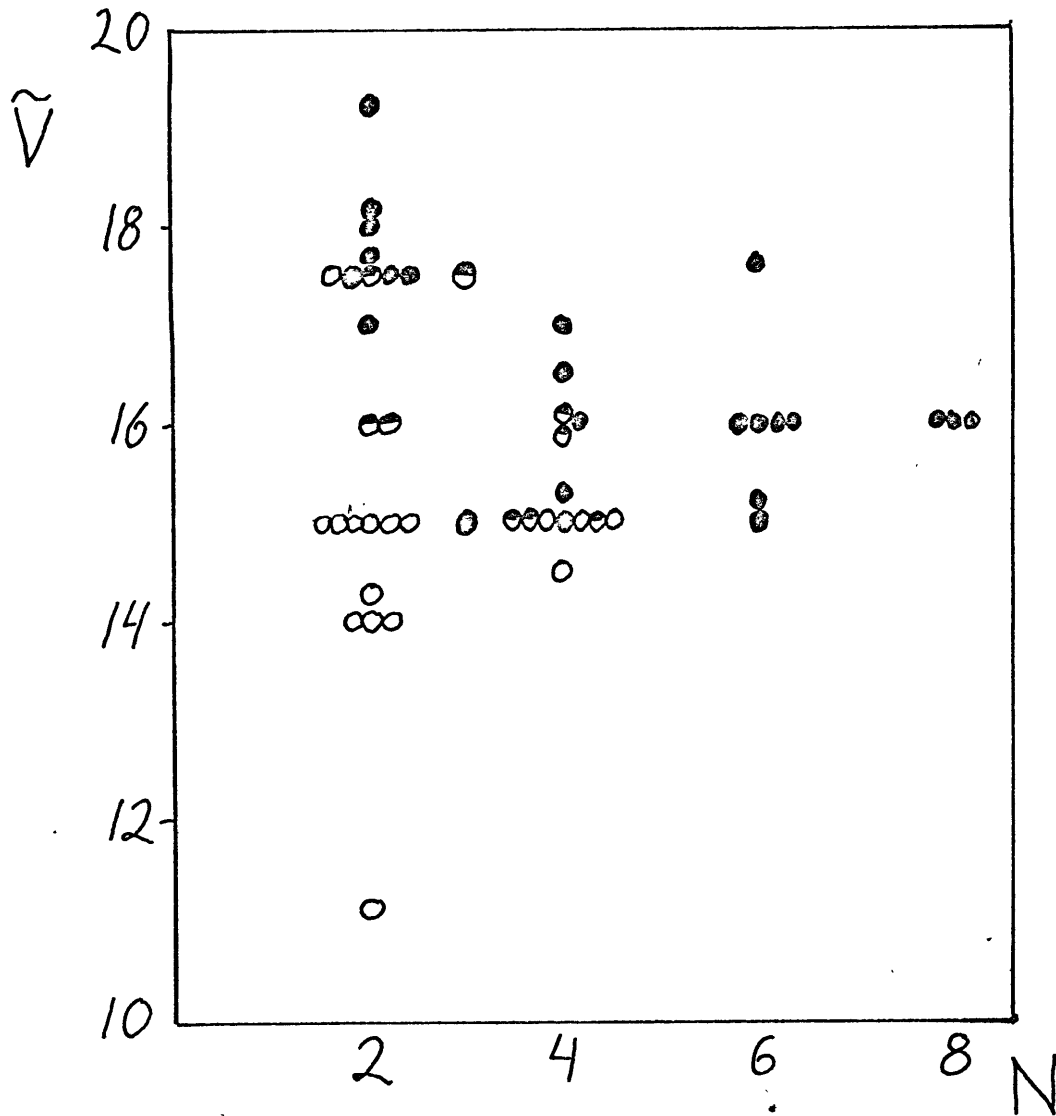above which the spools are destroyed agrees rather will with the calculations

FIG A-1   T̃ vrs. Ṽ for N=2

FIG A-2
T̃ vrs. Ṽ
for N=4

FIG A-3
T̃ vrs. Ṽ
for N= 6
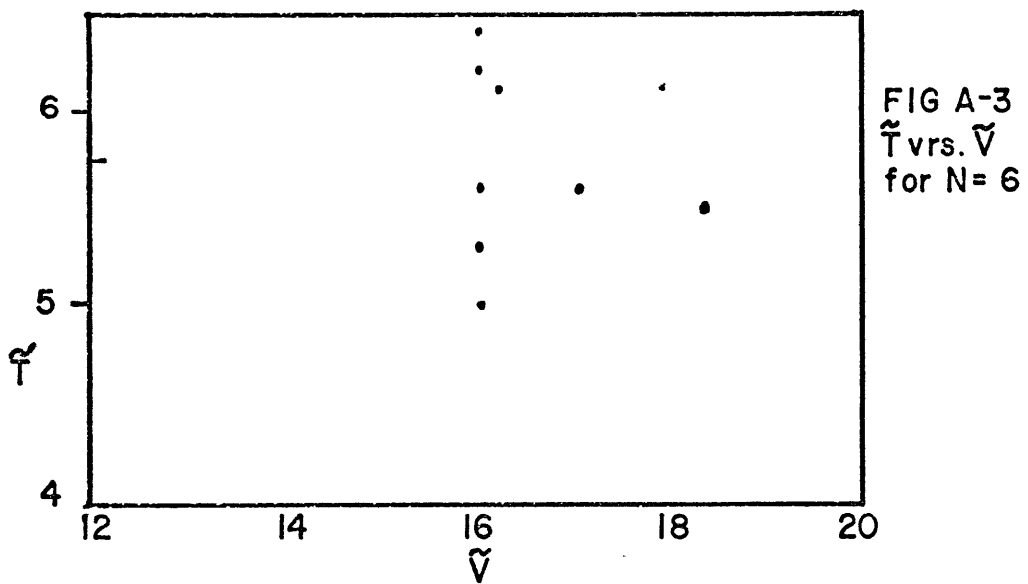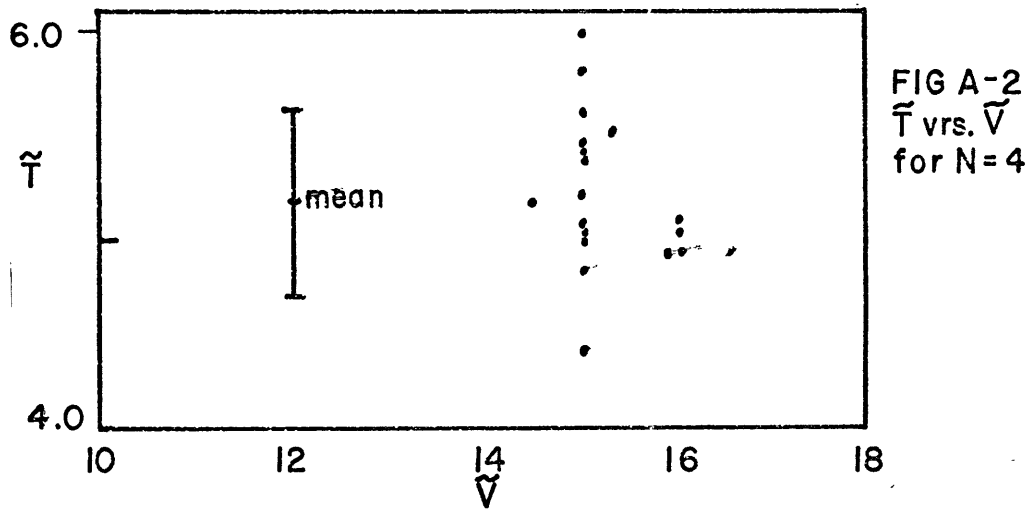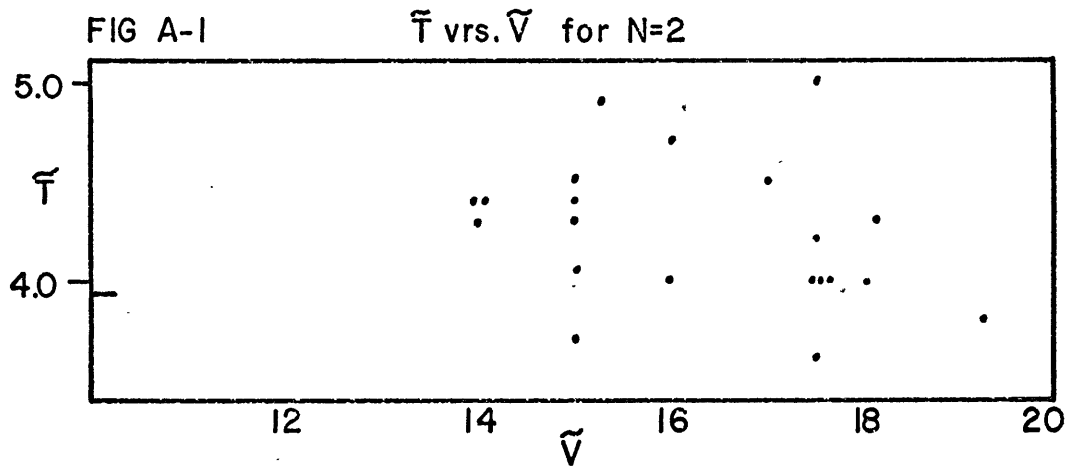
Figure A-4

Response of 2.92 mm diameter spools:

    O   little damage (shaft intact)

    Ø   great damage (shaft broken)

    ●   spool shaft completely destroyed

(horizontally adjacent points refer to same N, $\tilde{V}$)

of section 2.22, which are baaed on the resistance of the spool relative to the rest of the circuit.

A3. Pinch Experiments on Iron

The high pressure properties of iron have been studied by many investigators: The 130 kilobar $\alpha \rightarrow \epsilon$ transition has been seen in shock waves by Johnson et. al., 1962, Smith and Fowler, 1961, and Sclar, 1969. Drickamer and Balchan (1962) and Bundy (1965), using static equipment, have reported that the resistivity of iron increases about three times at the transition. Bless (1968) also reported production of ϵ iron; by magnetic pinch pressure; his conclusion was based on indirect evidence in the change of microstructure of iron cycled through high pressure.

The present experiments on iron were initiated because the change in resistivity at the phase transition had been over-estimated by a factor of 100. The sample design was similar to that shown in figure 3-7, except that iron wire, drawn until it just fitted the insulator holes, was substituted for the CdS powder and copper leads. R_L was also changed to 220 Ohm. Experiments were done at 145 kilobars and 178 kilobars (shots E28, E29, and E30). All that could be observed was that the resistivity of the iron under pinch pressure was not more than 100 times its normal value.

Unfortunately, it was not possible to perform an experiment capable of resolving a 3X increase in resistance of an iron wire. The reason is that a sample could not be constructed with a resistance greater that about 1 ohm. The maximum current which the high voltage pulse supply could produce was

about 10 amps; thus, the largest signal which could be hoped for was 30 volts. Subtraction of the oscillograph records of shots E29 and E30 gives a measure of the irreproducible noise in a 178 kilobar shot. The mean difference between the two traces during the first half cycle is about 300 volts. Thus, unless a 3X increase in sample resistance could be transformed to a voltage greater than 300 volts, there is little chance of observing it with the present apparatus. (However, plug-in units are available for the high voltage pulser which produce 10^3 amps for shorter times.)

In conclusion, the pinch experiments with iron only indicated that the iron remains a metallic conductor under pinch pressure of 178 kilobars. Modifications of the high voltage pulse circuit (which are beyond our present resources) are required to enable measurement of the 3X increase in iron resistivity associated with the $\alpha \rightarrow \epsilon$ transition.

A4. Variation of Pinch Pressure Within Copper Spools

P_p as defined in equation (2.31) only approximately gives the pressure applied to the sample. P_p is obtained by evaluating

$$P = \frac{\mu_o I_b^2}{8\pi^2 r_o^2} \equiv P_M$$

which is the magnetic pressure at the surface of the spool. However, the pressure inside the spool is governed by the relation

$$\frac{\partial}{\partial r}\left[P + \frac{B^2}{2\mu_o}\right] + \frac{B^2}{\mu_o r} = 0 \qquad (A4.1)$$

(see Spitzer, 1962, for a derivation of this equation in e.m. units). Since (A4.1) implies

$$\frac{\partial}{\partial r}\left[P + \frac{B^2}{2\mu_o}\right] < 0,$$

the total pressure increases inward.

The magnitude of this effect depends critically on the current distribution. Unfortunately, due to Joule heating, the resistivity varies with radius, and the current distribution will not have a simple exponential form. The general behavior of solutions to equation (A4.1) can be obtained by analysis of a linear current distribution,

$$I = \frac{I_o}{s}(r - r_o + s) = \frac{I_o}{s}(r - r') \qquad (A4.2)$$

where

$$r' = r_o - s$$

and r_o is the radius of the spool.

This current distribution is approached when Joule heating has caused the resistivity of the skin layer to increase significantly. Continuing,

$$B^2 = \frac{\mu_o^2 I_o^2}{4\pi^2 r^2 s^2} (r^2 - 2rr' + r'^2)$$

$$P + \frac{B^2}{2\mu_o} = -\frac{\mu_o I_o^2}{4\pi^2 s^2} \int (\frac{1}{r} - \frac{2r'}{r^2} + \frac{r'^2}{r^3}) \, dr \quad (r < r_o)$$

$$= -\frac{\mu_o I_o^2}{4\pi^2 s^2} (\log r + \frac{2r'}{r} - \frac{r'^2}{2r^2}) + C.$$

In order to match the boundary condition:

$$P + \frac{B^2}{2\mu_o} = P_M \quad \text{at } r = r_o,$$

we demand

$$P + \frac{B^2}{2u_o} - P_M = -\frac{\mu_o I_o^2}{4\pi^2 s^2} \left[\log \frac{r}{r_o} + 2(\frac{r'}{r} - \frac{r'}{r_o}) \right.$$

$$\left. + \frac{1}{2}(\frac{r'^2}{r_o^2} - \frac{r'^2}{r^2}) \right] \quad (r < r_o)$$

(A4.3)

The behavior of equation (A4.3) as $s \to 0$ can be determined from l'Hopital's Rule:

$$\underset{s \to 0}{\text{Lim}} \frac{\log \frac{r_o - s}{r_o} + 2(1 - \frac{r_o - s}{r_o}) + \frac{1}{2}\left[\frac{(r_o - s)^2}{r_o^2} - 1\right]}{s^2}$$

$$= \lim_{s \to 0} \quad - \frac{r_o}{2s(r_o - s)} + \frac{1}{2r_o s} + \frac{1}{2r_o^2}$$

$$= 0 \quad \text{(by partial fractions)}.$$

The exponential skin depth is about $r_o/10$. For $s = r_o/10$ and $r = r'$, the right hand side of equation (A4.3) becomes

$$-200\, P_M\, (-1.054 + 2.000 - .0950) = .078\, P_M.$$

For $s = r_o/50$, it becomes $.015\, P_M$, and for $s = r_o/5$, $.16 P_M$. Thus, we conclude that P_p, which is obtained by evaluating P_M, only represents the pressure inside the spool when the skin depth is vanishingly small.

The solution of equation (A4.1) for exponential current variation is considerably more complicated:

$$I = I_o\, e^{(r - r_o)/s}$$

$$B^2 = \frac{\mu_o^2\, I_o^2}{4\pi^2 r^2}\, e^{2(r - r_o)/s}.$$

Then,

$$- \frac{1}{\mu_o} \int B^2\, dr = - \frac{\mu_o I_o^2\, e^{-2r_0/s}}{4\pi^2 r_o^2} \int \frac{1}{x^3}\, e^{2xr_o/s}\, dx,$$

where $x = r/r_o$. Evaluation of the integral gives

$$- \frac{1}{\mu_o} \int B^2\, dr = -P_M\, e^{-2r_o/s} \left[- \frac{e^{2xr_o/s}}{x^2}\left(1 + 2\frac{xr_o}{s}\right) + \right.$$

$$\frac{4 r_o^2}{s^2} \left(\log x + \sum_{n=1}^{\infty}{}' \frac{(2 x r_o)^n}{s^n} \frac{1}{n\,n!} \right) \Bigg]$$

We now have a solution of the form

$$P + \frac{B^2}{2 \mu_o} = -F(r) + \text{Constant} \qquad (r < r_o)$$

When we impose the boundary condition

$$P + B^2/2 \mu_o = P_M \qquad \text{at } r = r_o,$$

we obtain the solution

$$P + B^2/2\mu_o - P_M = - \left[F(r) - F(r_o) \right] = \Delta$$

$$\Delta = - P_M\, e^{-2r_o/s} \left[(1 + \frac{2r}{s})(e^{2r_o/s} - \frac{e^{2r/s}}{x^2}) \right.$$

$$\left. + \frac{4 r_o^2}{s^2} (\log x + \sum_{n=1}^{\infty} \frac{r^n - r_o^n}{s^n} \frac{2^n}{n\,n!}) \right] \quad (A4.4)$$

Δ evaluated at $r = r_o - s$ gives the amount that the pressure in the spool exceeds the nominal value, P_p. We evaluate Δ for the typical conditions:

$$s = .2 \text{ mm}$$

$$r_o = 1.5 \text{ mm}$$

The series in equation A4.4 converges very slowly. We find

$$\sum_{n=1}^{n=19} \frac{r^n - r_o^n}{s^n} \frac{2^n}{n\,n!} = 168,760 ,$$

and the 19th term is 8,965. Since ther terms n = 15 through 19 drop by about 2000 each, we approximate the total sum by 178,000. Evaluation of the other terms in equation (A4.4) gives

$$\Delta = -30.61 \times 10^{-8} \, P_M \, (-.4698 + .5162) \times 10^8$$
$$= .9 \, P_M .$$

Therefore, an exponential current distribution approximately doubles the pressure in the spool.

The actual current distribution will be somewhere in between a linear and exponential decrease, since the resistivity is greater (and hence the skin depth is greater) in the outer regions of the spool. This effect may explain the observations of Bless (1968) on pinched iron and boron nitride. He obtained evidence for 130 kilobar phase transitions in both of these materials, even though P_p was only about 100 kilobars. Now it is clear that the pressure produced in the center of his samples could have been as high as $2P_p$.

A5. Details of Refractive Index Measurements

The refractive indices of fused silica samples were measured by the Becke line and oblique illumination techniques (see, for example, Mason and Berry, 1968). In many cases, these measurements were complicated by a number of problems:

a) When the spool was destroyed, the quartz grains comprised only a small fraction of the recovered material, so that only a little data was available.

b) Often the quartz was contained in clumps of very small particles in which the Becke line was very hard to see.

c) Often a range of indices was present, occasionally even in the same grain. Most of the grains were optically isotropic, but some were birefringent.

d) It was sometimes difficult to obtain an objective measure of the distribution of indices because there were many small grains with lower indices and only a few large grains with higher indices. Also, each time the powder was shaken onto a slide, a different sample of the powder was obtained; thus, in some instances, repeated measurements in the same liquid failed to converge. In S8, for example, both of these problems occurred, making an objective determination of n very difficult.

The measurements on the insulated quartz rods are described in detail because they were the most carefully done. We define f as the fraction of material which has n less then the index liquid. f vrs. n is plotted in figure A5.

The index liquids used were .002 apart. Because of the temperature dependence of n, some of the plotted points are only .001 apart. f was calculated by weighting the observations according to the following scheme:

a) Unamibiguous determination by either Becke line or oblique ilumination = 1.

b) Unambiguous determination by both methods = 2.

c) Uncertainty in n or in identification of grain as quartz = $\frac{1}{2}$.

These weights are also given in figure A5. f is computed from

$$f = \frac{\text{weight of observations less than reference liquid}}{\text{total weight}}$$

In a couple of cases, when there were many small grains, the weights were somewhat subjective because time was not taken to double check each grain by both methods.

For each sample, an attempt was made to take enough data to make n increase monotonically with f. (Since all observations are reported, in some instances one must ignore the points with relatively less weight.) The data points in figure 3-4 were determined from the observations in figure A5 by the following algorithm:

a) Lower boundary of error bracket where f definately is above .7.

b) Upper boundary of error bracket were f definately is above .9.

c) Data point placed in middle of error bracket.

d) No error bracket smaller than .001.
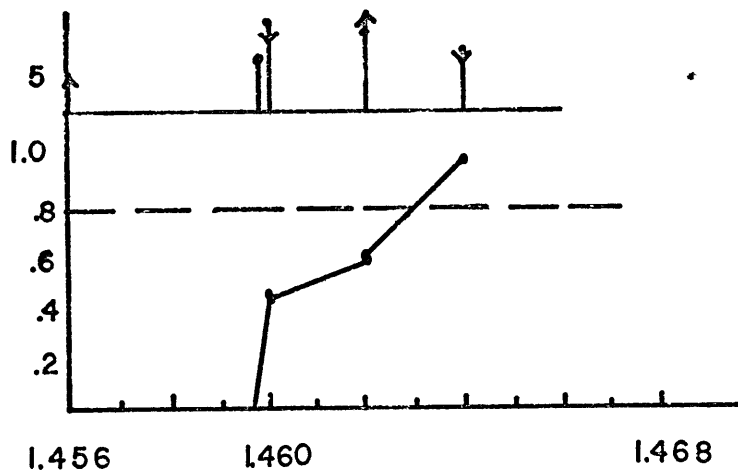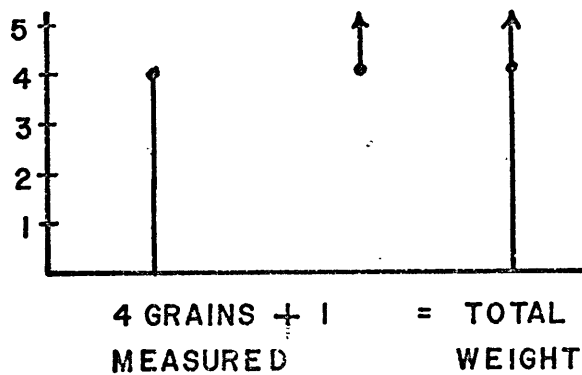
FIGURE A-5   REFRACTIVE INDICES MEASUREMENTS.

$$f = \frac{\text{weight of observations with refractive index less than n}}{\text{total weight}}$$

(the method of weighing observations is explained in the text.)

VERTICAL LINES OVER DATA POINTS GIVE NUMBERS
OF GRAINS AND WEIGHTS.

for   example:

4 GRAINS + I   = TOTAL
MEASURED   WEIGHT

SHOT SI

N = 2 , V = I5

P_p = 43.5 kb

1.456   1.460   1.468

FIG. A-5 CONT'D

SHOT T2
N=4 V=15
P_p =82 kb

SHOT S2
N=2 V=15
P_p = 37.4 kb
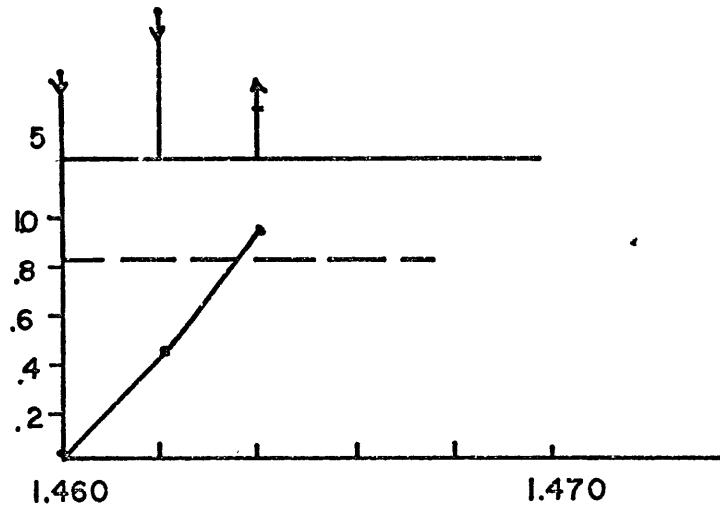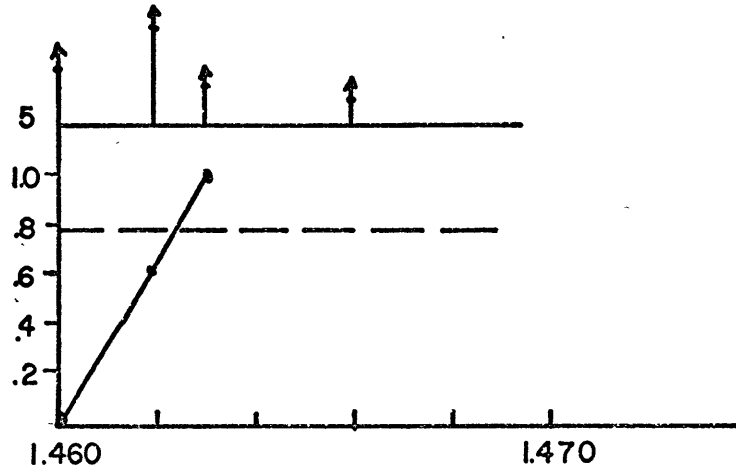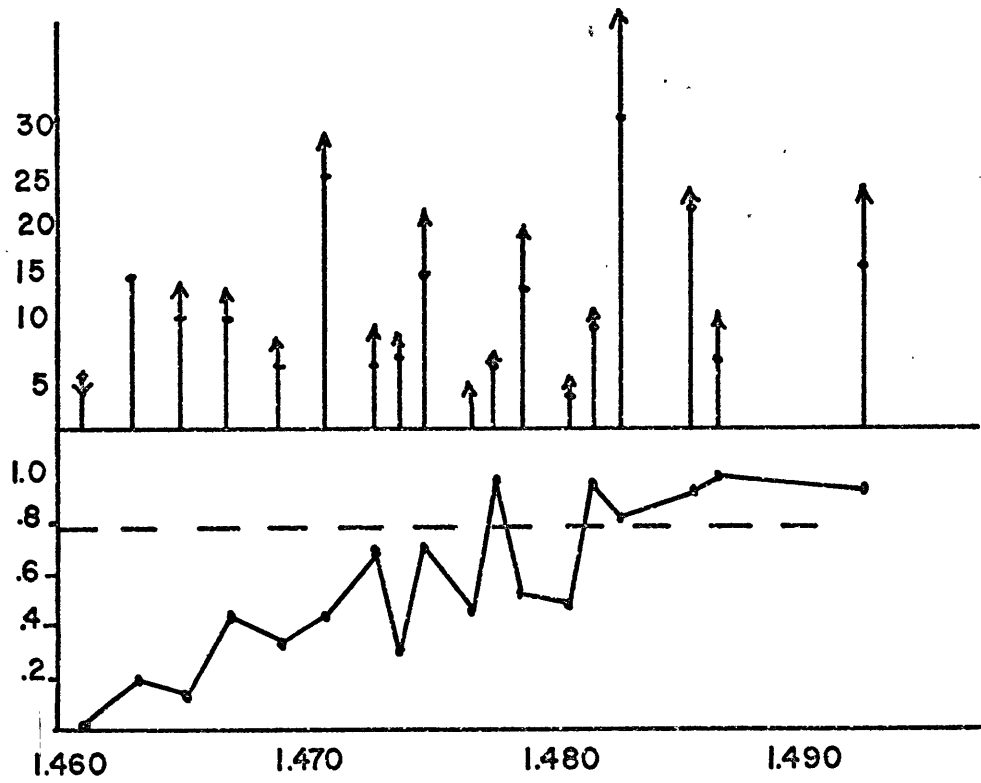
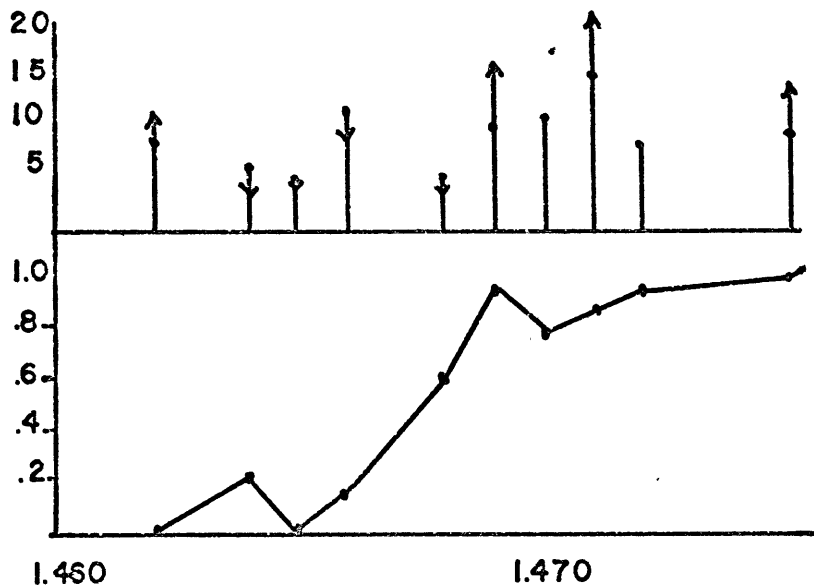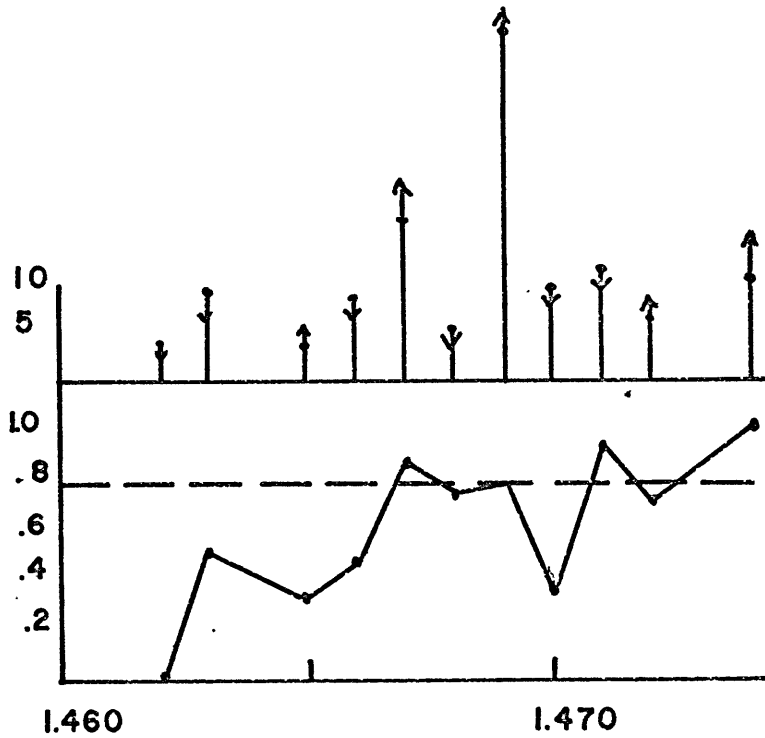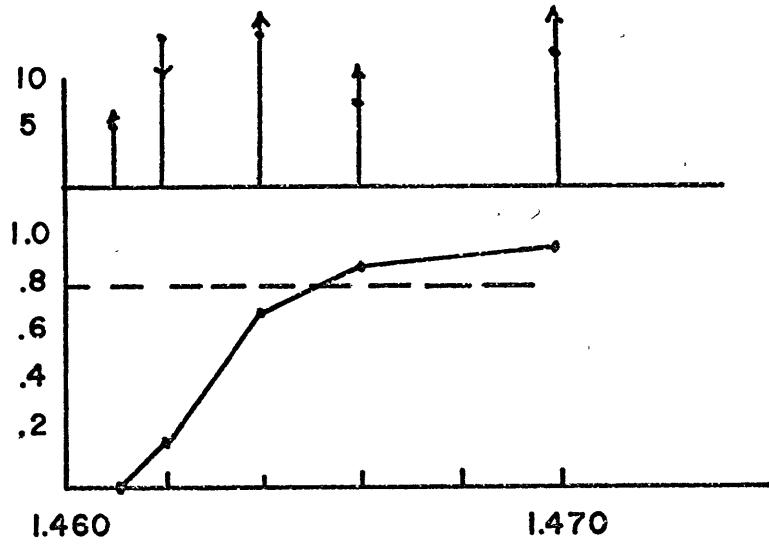ABOVE: S3   N= 4, V =16 , P_p= 112 kb

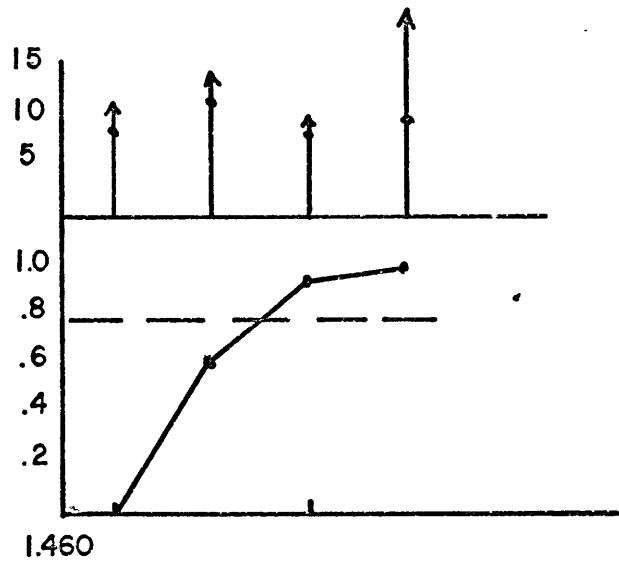S4   N=2 , V=17.5 , P_p= 62.1 kb

FIG A-5 CONT'D

S5   N = 2, V = 19 $\pm$ .2 , P_p = 67.5 kb

S6   N = 4, V = 14.5 P_p = 93 kb

FIG A-5 CONT'D

S7   N=3, V=15 , P_p= 49.8 kb

1.460   1.470

1.460
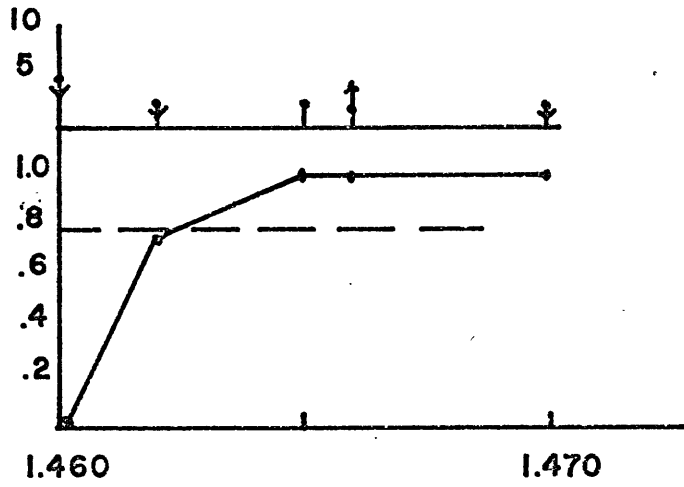
S8   N = 4, V = 15 P_p= 82.3 kb
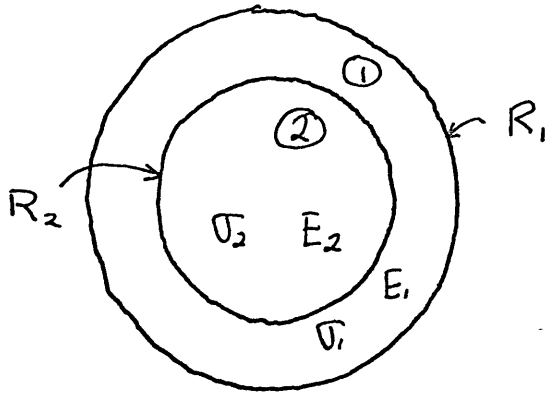
A6. Stress and Strain within Samples

Figure A6 -

Geometry for stress calculation

and indentification of symbols.

Figure A6 represents two concentric cylinders and explains the symbols used in this section. From Fung, 1966, we can write the stress for axial-symmetric problems as

$$\sigma_{rr} = \frac{A}{r^2} + B(1 + 2 \log r) + 2C$$

$$\sigma_{\theta\theta} = -\frac{A}{r^2} + B(3 + 2 \log r) + 2C$$

$$\sigma_{r\theta} = 0.$$

The displacements for the case of plane stress are:

$$\varsigma_r = \frac{1}{E} \left[-\frac{(1+\nu) A}{r} - B(1 + \nu) r + 2B(1 - \nu - 2\nu^3) \right. $$
$$\left. r \log r + 2C(1 - \nu - 2\nu^2) r \right] + \alpha \sin \theta + \gamma \cos \theta$$

$$\varsigma_\theta = \frac{4 B r \theta}{E} (1 - \nu^2) + \alpha \cos \theta - \gamma \sin \theta + \varsigma r .$$

(All of these symbols are defined in the Symbol Table.) We seek solutions
for which $\zeta_\theta = 0$. Therefore, B, α, γ, and β are zero. The terms which
remain are

$$\left. \begin{array}{l} \sigma_{rr} = \dfrac{A}{r^2} + 2C \\[3mm] \sigma_{\theta\theta} = -\dfrac{A}{r^2} + 2C \\[3mm] \zeta_r = \dfrac{1}{E}\left[-\dfrac{(1+\nu)A}{r} + 2C(1-\nu-2\nu^2)r \right] \end{array} \right\} \quad (A6.1)$$

Let the superscripts (1) and (2) represent the value of quantities in
regions (1) and (2), respectively. Since $\sigma_{rr}^{(2)}$ is finite at $r = 0$, we may take
it to be in the form

$$\sigma_{rr}^{(2)} = 2D \qquad (A6.2)$$

Thus,

$$\zeta_r^{(2)} = \frac{2D}{E_2}(1-\nu_2)r \qquad (A6.3)$$

and

$$\sigma_{rr}^{(1)} = \frac{A}{r^2} + 2C$$

$$\zeta_r^{(1)} = \frac{1}{E_2}\left[-\frac{(1+\nu_1)A}{r} + 2C(1-\nu_1-2\nu_1^2)r \right]$$

The boundary conditions are

$$\sigma_{rr}^{(1)}(R_1) = P_o \qquad (A6.4)$$

$$\sigma_{rr}^{(1)}(R_2) = \sigma_{rr}^{(2)}(R_2)$$

$$\zeta_r^{(1)}(R_2) = \zeta_r^{(2)}(R_2).$$

or,

$$D \frac{2}{E_2}(1 - \nu_2 - 2\nu_2^2) R_2 \quad + A \frac{1+\nu_1}{E_1 R_2} \quad + C \frac{2}{E_1}(1 - \nu_1 - 2\nu_1^2)R_2 \quad = 0$$

$$A \frac{1}{R_1^2} \quad + 2C \quad = P_0$$

$$-2D \quad + A \frac{1}{R_2^2} \quad + 2C \quad = 0$$

$$(A6.5)$$

Equations (A6.5) can be solved by determinants. We are only interested in the value of D. Evaluation of the determinant quotient gives:

$$D = -\frac{P_0 \left(2 \frac{1+\nu_1}{R_2 E_1} + 2(1 - \nu_1 - 2\nu_1^2)/R_2^2 E_1\right)}{\frac{2}{E_2}(1 - \nu_2 - 2\nu_2^2) R_2 \left(\frac{2}{R_1^2} - \frac{2}{R_2^2}\right) - 2\left[\frac{2(1 - \nu_1)}{E_1 R_2}1 + \frac{2(1 - \nu_1 - 2\nu_1^2)}{E_1 R_1^2}1\right]R_2}$$

Equation (A6.6) can be substituted into equation (A6.2) and reduced to yield the stress in the inner cylinder:

$$(A6.7)$$

$$\sigma_{rr}^{(2)} = \frac{2 P R_1^2 (E_2/E_1)(\nu_1^2 - 1)}{(R_1^2 - R_2^2)(2\nu_2^2 + \nu_2 - 1 + \nu_1(E_2/E_1)) - (E_2/E_1)(R_1^2 + R_2^2) + 2(E_2/E_1)\nu_1^2 R_2^2}$$

Similarly, the strain is obtained by substituting equation (A6.6) into equation (A6.3):

$$\zeta_r^{(2)} =$$

(A6.8)

$$\frac{2 P_o R_1^2 (v_1^2 - 1) (1 - v_2 - 2v_2^2) \ r}{(R_1^2 - R_2^2) \left[E_1(2v_2^2 + v_2 - 1) + E_2 v_1^2 \right] - E_2(R_1^2 + R_2^2) + 2 E_2 v_1^2 R_2^2}$$

It is easily verfied that A6.7 and A6.8 display the proper behavior in various limiting cases, such as

$$v_1 = v_2; \ E_1 = E_2 \ \text{makes} \ \sigma_{rr}^{(2)} = P_o \ .$$

$$R_1 = R_2 \ \text{makes} \ \sigma_{rr}^{(2)} = P_o.$$

$$E_1 \to \infty \ \text{makes} \ \sigma_{rr}^{(2)} \to 0 \ \text{and} \ \zeta_r^{(2)} \to 0.$$

$$E_2 = 0 \ \text{makes} \ \sigma_{rr}^{(2)} = 0.$$

To obtain a quantitative estimate of the stress within the sample, we evaluate equation (A6.7) with the approximations:

$$v_1 = v_2 = v$$

$$v^2 \ll v.$$

Then,

$$\sigma_{rr}^{(2)} = \frac{2P_o}{3(1 - v)} \frac{E_2}{E_1} \ . \tag{A6.9}$$

Usually,

$$\frac{2}{3(1 - v)} \cong 1.$$

Therefore, when $E_2 > E_1$, the pressure in medium (2) will usually be greater than in medium (1).

VII. REFERENCES

T.J. Ahrens, D.L. Anderson, and E.A. Ringwood, "Equation of State and Crystal Structure of High Pressure Phases of Shocked Silicates and Oxides", Rev. Geophys. 7, 667-708, 1969

T.J. Ahrens and J.T. Rosenberg, "Shock Metamorphism Experiments on Quartz and Plagioclase", in Shock Metamorphism of Natural Materials, B.M. French and N.M. Short, eds., Mono Book Corp., 1968

S. Akimoto and Y. Ida, "High Pressure Synthesis of Mg_2SiO_4 Spinel", Earth and Plan. Sci. Let. 1, 358-359, 1966

B.J. Alder and R.H. Christian, "Behavior of Strongly Shocked Carbon", Phys. Rev. Let. 7, 367-69, 1961

L.V. Al'tshuler, "Peculiarities of Phase Transitions in Compression and Rarefaction Shock Waves", Sov. Phys. JETP 25, 260-65, 1967

S. Archambeau, E.A. Flinn, and D.G. Lambert, quoted by A.E. Ringwood, 1969

R.B. Aust and H.G. Drickamer, "Carbon - A New Crystalline Phase", Science 140, 817-819, 1963

W.A. Bassett, T. Takahashi, and P.W. Stook, "X-Ray Diffraction and Optical Observations on Crystalline Solids up to 300 Kbar", Rev. Sci. Inst. 38, 37-42, 1967

P.M. Bell and F.R. Boyd, "Phase Equilibrium Data Bearing on the Pressure and Temperature of Shock Metamorphism", in Shock Metamorphism of Natural Materials, B.M. French and N.M. Short, eds., Mono Book Corp., 1968

F.D. Bennett et. al., "Resistance Changes Caused by Vaporization Waves in Exploding Wires", in Exploding Wires Vol. 3, W.G. Chace and H.K. Moore, eds., pp. 65-88, Plenum Press, 1964

F. Birch & P. LeCompte, "Temperature-Pressure Plane for Albite Composition", Am. J. Sci. 258, 209-217, 1960

F. Bitter, "Histoire des Champs Magnetiques Intenses, et de Leurs Contributions a la Physique", in Les Champs Magnetiques Intenses (Paris: C. N. R. S.), 1967

F. Bitter, "Ultrastrong Magnetic Fields", Sci. Am. 213, 65-73, 1965

F. Bitter, S. J. Bless, and G. Fiocco, "Preliminary Experiments with a Fast Z-pinch Capacitor Discharge- The Generation of High Pressures in Solids", R. L. E. Quart. Prog. Rept. No. 86, pp. 53-57, M. I. T., 1967

S. J. Bless, "Production of High Pressures with a Magnetic Pinch", S. M. Thesis, M. I. T., 1968

S. J. Bless, "High Pressure Experiments with a Magnetic Pinch", R. L. E. Quart. Prog. Rept. No. 92, pp. 151-59, M. I. T., 1969a

S. J. Bless, "High Pressure Experiments with a Magnetic Pinch", (abstract) Trans. Am. Geophys. Union 50, p. 311, 1969b

F. R. Boyd & J. L. England, "Effect of Pressure on the Melting of Diopside, $CaMgSi_2O_6$, and Albite, $NaAlSi_3O_8$, in the Range up to 50 Kilobars", J. Geophys. Res. 68, 311-323, 1963

P. W. Bridgman & I. Simon, "Effect of Very High Pressure on Glass", J. Appl. Phys. 24, 405-413, 1953

T. E. Bunch, A. J. Cohen, and M. R. Dence, "Natural Terrestrial Maskelynite", Am. Min. 52, 249-253, 1967

F. P. Bundy, "Direct Conversion of Graphite to Diamond in Static Pressure Apparatus", J. Chem. Phys. 38, 631-643, 1963a

F. P. Bundy, "Melting of Graphite at Very High Pressure", J. Chem. Phys. 38, 618-630, 1963b

F. P. Bundy, "Pressure-Temperature Phase Diagram of Iron to 200 kbars, 900°C", J Appl. Phys. 36, 616-620, 1965

F.P. Bundy & J.S. Kasper, "Hexagonal Diamond- A New Form of Carbon", J. Chem. Phys. 46, 3437-46, 1967

F.P. Bundy & R.H. Wentorf, "Direct Transformation of Boron Nitride to Denser Forms", J. Chem. Phys. 38, 1144-49, 1963

E.C.T. Chao et. al., "First Natural Occurrence of Coesite", Science, 132, 220-22, 1960

E.C.T. Chao et. al. , "Stishovite, SiO2, a Very High Pressure New Mineral from Meteor Crator, Arizona", J. Geophys. Res. 67, 419-421, 1962

E.C.T. Chao, "Shock Effects in Certain Rock-Metamorphosed Minerals", Science, 156, 192-202, 1967

E.C.T. Chao, "Pressure and Temperature Histories of Impact Metamorphosed Rocks- Based on Petrographic Observations", in Shock Metamorphism of Natural Materials, B.M. French & N.M. Short, eds., Mono Book Corp., 1968

E.B. Christiansen et. al., "Irreversible Compressibility of Silica Glass as a Means of Determining the Distribution of Force in High Pressure Cells", J. Am. Cer. Soc. 45, 172-177, 1962

C.F. Cline & D.R. Stephens, "Volume-Compressibility of BeO and other II-VI Compounds", J. Appl. Phys. 36, 2869-2873, 1965

E.C. Cnare, "Magnetic Flux Compression by Magnetically Imploded Metallic Foils", J. Appl. Phys. 37, 3812-3816, 1966

H.M. Cohen & R. Roy, "Reply to 'Comments on 'Effects of Ultra High Pressure on Glass", J. Am. Cer. Soc. 45, 398-99, 1962

H.M. Cohen & R. Roy, "Densification of Glass at very High Pressure", Phys. Chem. Glasses 6, 149-161, 1965

J.A. Corll, "Recovery of the High-Pressure Phase of Cadmium Sulfide", J. Appl. Phys. 35, 3032-33, 1964

F. Dachille, R.J. Zeto, & R. Roy, "Coesite and Stishovite: Stepwise Reversal Transformations", Science 140, 991-93, 1963

P.S. DeCarli & J.C. Jamieson, "Formantion of Diamond by Explosive Shock", Science 133, 1821, 1961

P.S. DeCarli & J.C. Jamieson, "Formation of an Amorphous Form of Quartz under Shock Conditions", J. Chem. Phys. 31, 1675-1676, 1959

P.S. DeCarli & D.J. Milton, "Stishovite: Synthesis by Shock Wave", Science 147, 144-45, 1965

D.K. Doran & R.K. Linde, "Shock Effects in Solids", Solid State Physics Vol. 19, 229-90, 1966

H.G. Drickamer & A.S. Balchan, "High Pressure Optical and Electrical Measurements", in Modern Very High Pressure Techniques, R.H. Wentorf, ed., Butterworth, 1962

H.G. Drickamer et. al., "X-Ray Diffraction Studies of Lattice Parameters of Solids Under Very High Pressures", Solid State Physics Vol. 19, 135-229, 1966

G.E. Duvall & G.R. Fowles, "Shock Waves", in High Pressure Physics and Chemistry, R.S. Bradley, ed., 209-292, Academic Press, 1963

C.M. Fowler, W.B. Garn, & R.S. Caid, "Production of Very High Magnetic Fields by Implosion", J. Appl. Phys. 31, 588-594, 1960

C.M. Fowler et. al., "Flux Compression by Implosion", in High Magnetic Fields, H. Kolm et. al., eds., M.I.T. Press, 1962

R. Fowles & R.F. Williams, "Plane Stress Wave Propagation in Solids", J. Appl. Phys. 41, 360-363, 1970

F.B.A. Frūngel, High Speed Pulse Technology, Vol. I, Part A, Academic Press, 1965

Y.C. Fung, Foundations of Solid Mechanics, Prentice Hall, section 9.3 1965

J.J. Gilvarry, "Lindemann and Gruneisen Laws and a Melting Law at High Pressure", Phys. Rev. Lett. 16, 1089-91, 1966

M. Guillot, "Production de champs magnétiques transitoire très intenses par augmentation de la densité de flux au moyen d'une feuille métallique Comprimé par decharge de condesnateur", C.R. Acad. Sc. Paris 267, 1398-1401, 1968

B. Gutenberg, Physics of the Earth's Interior, Academic Press, New York, 1969

R.E. Hanneman, H.M. Strong, and F.P. Bundy, "Hexagonal Diamonds in Meteorites: Implications", Science 155, 995-97, 1967

G.P. Harnwell, Principles of Electricity and Magnetism, McGraw Hill, N.Y., 1949

R. Hide, "Free Hydromagnetic Oscillations of the Earth's Core and the Theory of the Geomagnetic Secular Variation", Phil. Trans. Roy. Soc. Lon. Ser. A 259, 615-650, 1966

F.B. Hildebrand, Advanced Calculus for Applications, Prentice Hall, 1962

A. Jayaraman, W. Klemet Jr. and G.C. Kennedy, "Melting and Polymorphic Transitions for Some Group II-VI Compounds at High Pressures", Phys. Rev. 130, 2277-82, 1963

P.C. Johnson et. al., "Temperature Dependence of Shock-Induced Phase Transformations in Iron", J. Appl. Phys. 33, 557-61, 1962

R.N. Keeler, private communication, 1970

K.H. Kelly, "High Temperature Heat-Content, Heat-Capacity, and Entropy Data for the Elements and Inorganic Compounds", U.S. Bur. Mines #584, 1960

J.D. Kennedy & W.B. Benedick, "Shock Induced Phase Transition in Single Crystal CdS", J. Phys. Chem. Solids, 27, 125-127, 1966

G.C. Kennedy & R.S. Vaidya, "The Effect of Pressure on the Melting Temperature of Solids", J. Geophys. Res. 75, 1019-1022, 1970

L. Knopoff, "The Melting of Metals", paper presented at Francis Birch Symposium on Solid Earth, Cambridge, Mass., 1970

E.A. Kraut & G.C. Kennedy, "New Melting Law at High Pressures", Phys. Rev. Let. 16, 608-9, 1966

H.G. Latal, "Seed Field Diffusion Through Liners", Acta Physica Austriaca, 284-295, 1966

H.G. Latal, "Theory of the Cnare Effect", Ann. Phys. 42, 352-64, 1967

J.D. Lewin & P.F. Smith, "Production of Very High Magnetic Fields by Flux Compression", Rev. Sci. Instr. 541-48, 1964

H. Lipson & A.R. Stokes, "The Structure of Graphite", Proc. Roy. Soc. A 181, 101-105, 1942

J.D. MacKenzie, "High-Pressure Effects on Oxide Glasses: I. Densification in Rigid State", J. Amer. Cer. Soc., 461-69, 1963

J.D. MacKenzie & R.P. Laforce, "High-Pressure Densification of Glasses and the Effects of Shear", Nature 197, 480-81, 1963

B. Mason & L.G. Berry, Elements of Minerology, Chapter 6, Freman & Co., 1968

K.L. McDonald, "Penetration of the Geomagnetic Secular Field Through a Mantle of Variable Conductivity", J. Geophys. Res. 62, 117-141, 1957

R.G. McQueen, S.P. Marsh, & J. Fritz, "Hugoniot Equation of State of Twelve Rocks", J. Geophys. Res. 72, 4999-5036, 1967

R.G. McQueen, "The Equation of State of Mixtures, Alloys, and Compounds", in Seismic Coupling, G. Simmons ed., VESIAC, Univ. Mich., 1968

R.O. Miller, F. Dachille, & R. Roy, "High-Pressure Phase-Equilibrium Studies of CdS and MnS by Static and Dynamic Methods, J. Appl. Phys. 37, 4913-4918, 1966

D.J. Milton & P.S. DeCarli, "Maskelynite: Formation by Explosive Shock", Science 140, 670-71, 1963

D.E. Munson & L.M. Barker, "Dynamically Determined Volume Relationships for Aluminum, Copper, and Lead", J. Appl. Phys. 37, 1952-1660, 1966

M.N. Pavlovskii & V.P. Drakin, "Concerning the Metallic Phase of Carbon", JETP Letters 4, 116-118, 1966

M.H. Rice, R.G. McQueen, & J.M. Walsh, "Compression of Solids by
Strong Shock Waves", in Solid State Physics Vol. 6, pp. 1-64,
1958

A.E. Ringwood, "Minerology of the Mantle", in Advances in Earth Sciences,
P.M. Hurley, ed., M.I.T. Press, 357-399, 1966

A.E. Ringwood, "Phase Transformations in the Mantle", Earth & Plan. Sci.
Let. 5, 401-412, 1969

A.E. Ringwood, "Phase Transformations in the Earth's Mantle and in the
Moon", paper presented at Francis Birch Symposium on the Solid
Earth, Cambridge, Mass. 1970

A.E. Ringwood & A. Major, "Synthesis of Mg_2SiO_4 - Fe_2SiO_4 Spinel Solid
Solutions", Earth Plan Sci. Let. 1, 241-245, 1966

J.K. Roberts & A.R. Miller, Heat and Thermodynamics , p. 551, Inter-
science Publ., 1951

C.J.M. Rooymans, "Structure of the High Pressure Phase of CdS, CdSe, and
InSb", Phys. Let. 4, 186-7, 1963

S. Saaka & J.D. MacKenzie, "High Pressure Effects on Glass", J. Non-Cryst.
Solids 1, 107-142, 1969

G.A. Samara & H.G. Drickamer, "Pressure Induced Phase Transitions in
Some II-IV Compounds", J. Phys. Chem. Solids 23, 457-61, 1962

C.B. Sclar, "Relationship of High-Pressure Transformations to Microstructure
in Iron", abstract, Trans. Am. Geophys. Union 50, No. 4, p. 228,
1969

C.B. Sclar, A.P. Young, L.C. Garrison, & C.M. Schwartz, "Synthesis and
Optical Crystallography of Stishovite, a Very High Pressure Poly-
morph of SiO_2", J. Geophys. Res. 67, 4049-54, 1962

J.W. Shearer, "Interaction of Capacitor-Bank-Produced Megagauss Magnetic
Field with Small Single-Turn Coil", J. Appl. Phys. 40, 4490-97,
1969

N.M. Short, "Experimental Microdeformation of Rock Materials by Shock
Pressures for Laboratory-Scale Impacts and Explosives", in
Shock Metamorphism of Natural Materials, N.M. Short & B.M.
French, eds., Mono Book Corp., 1968

F. Simon & G. Glatzel, "Bemerkungen zur Schmelzruckkurve", Z. Anorg.
    Alleg. Chem. 178, 309-316, 1929

B.J. Skinner & J.F. Fahey, "Observations on the Inversion of Stishovite
    to Silica Glass", J. Geophys. Res. 68, 5595-5604, 1963

C.S. Smith & C.M. Fowler, "Further Metallographic Studies of Metals after
    Explosive Shock", Response of Metals to High Velocity Deformation,
    P.G. Shewman & V.F. Zackey, eds., New York, 1961

J.V. Smith, "The Powder Patterns and Lattice Parameters of Plagioclase
    Feldspars, I. the Soda-Rich Plagioclases", Min. Mag. 31, 47-68,
    1956

P.L. Smith & J.E. Martin, "The High-Pressure Structures of Cadmium
    Sulfide and Cadmium Telluride", Phys. Let. 6, 42, 1963

L. Spitzer, Physics of Fully Ionized Gases, Intersicence, 1962

H.M. Strong, "High Temperature Methods at High Pressure", in Modern
    Very High Pressure Techniques, R.H. Wentorf, ed., 1963

M.N. Toksoz, M.A. Chinnery, & D.L. Anderson, "Inhomogeneities in the
    Earth's Mantle", Geophys. J. R. Astr. Soc. 13, 31-59, 1967

V.D. Urlin, "Melting at Ultra High Pressures in Shock Waves", Sov. Phys.
    JETP 22, 341-346, 1966